



The Henryk Niewodniczański
Institute of Nuclear Physics
Polish Academy of Sciences
in Krakow, Poland

Doctoral dissertation

**Modelling beam transport and
biological effectiveness to develop
treatment planning for ion beam
radiotherapy**

Leszek Grzanka

Supervisor:
prof. dr hab. Paweł Olko

Krakow 2013

*Clara est, et quæ numquam marcescit sapientia,
et facile videtur ab his qui diligunt eam, et invenitur ab his qui quæerunt illam.
Præoccupat qui se concupiscunt, ut illis se prior ostendat.
Qui de luce vigilaverit ad illam, non laborabit:
assidentem enim illam foribus suis inveniet.
Cogitare ergo de illa sensus est consummatus:
et qui vigilaverit propter illam, cito securus erit.
Quoniam dignos se ipsa circuit quærens,
et in viis ostendit se illis hilariter, et in omni providentia occurrit illis.
Initium enim illius verissima est disciplinæ concupiscentia.
Cura ergo disciplinæ, dilectio est: et dilectio, custodia legum illius est:
custoditio autem legum, consummatio incorruptionis est:
incorruptio autem facit esse proximum Deo.*

The Book of Wisdom, 6: 12-20

Acknowledgements

During the long and winding road to complete my PhD thesis I had the chance of meeting many inspiring persons, contributing to the presented work in many ways.

I would like to thank my Supervisors: Professor Paweł Olko and Professor Michael Waligórski for their knowledge, experience and guidance, and the time spent on valuable discussions and reading the many drafts of this thesis.

I am grateful to Dr. Steffen Greilich and Dr. Marta Korcyl with whom I have been working on the libamtrack library project. Considerable progress in this project was triggered by my cooperation with the German Cancer Research Center (DKFZ) in Heidelberg. I am especially grateful to Dr. Steffen Greilich for enormous amount of support and knowledge sharing and also to the administrative director of DKFZ, Prof. Josef Puchta for financial support during my stays in Heidelberg.

This project has been supported by a three-year doctoral scholarship program *Doctus*, co-funded by the European Social Fund. The necessary financial support was also provided by the Institute of Nuclear Physics of the Polish Academy of Sciences (IFJ PAN). I am grateful to both these institutions for financing my Ph.D. project. Part of the computing within this project was performed using the Cracow Cloud infrastructure at the IFJ PAN and at the Academic Computer Centre ACK Cyfronet AGH.

In parallel to work on the thesis project, I had the opportunity of participating in the TOTEM experiment at CERN, Geneva. I thank Hubert Niewiadomski and the whole TOTEM collaboration for sharing many ideas, resources needed to conduct scientific research and for covering expenses related to my stays at the CERN laboratory.

Let me also express my gratitude to all my friends, especially those encountered during the period of my PhD studies, for their support, patience and time spent together. I also thank my family, especially my Parents. When I was a child they helped me to develop my curiosity, which is still guiding me.

Contents

Streszczenie	1
Abstract	2
Introduction	3
Aim and scope of work	9
Chapter 1. The physics and radiobiology of track structure	11
1.1. Particle Track Physics	11
1.1.1. Stopping power and Linear Energy Transfer	12
1.1.2. Dose and fluence	15
1.1.3. Scattering and energy straggling	16
1.1.4. The Bragg peak	16
1.2. Radiobiology and biophysical models of cellular survival	17
1.2.1. Cell survival and Relative Biological Effectiveness	18
1.2.2. Biophysical models of cellular survival	20
Chapter 2. Evaluation of elements of track structure models	24
2.1. The libamtrack software library	24
2.2. Electron energy-range relationships	25
2.3. Radial Dose Distribution formulae	27
2.4. Comparison of $D(r)$ formulae with experiment	29
2.5. Radial integration of $D(r)$ and LET	30
2.6. Conclusions	32
Chapter 3. The Katz model of cellular survival	35
3.1. Principles of the Katz model	35
3.2. The extended target radial dose distribution	37
3.3. Probability of inactivation — the m-target formula	37
3.4. Inactivation cross-section	38
3.5. The ion-kill and gamma-kill modes of inactivation	41
3.6. Algorithm of the integrated version of the Katz model	41
3.7. Algorithm of the scaled version of the Katz model	43
3.8. Comparison between Scaled and Integrated versions of the Katz Model	44
3.9. Fitting Katz model parameters from cell survival data	45
3.10. Mixed-field calculations	48
3.11. Conclusions	49
Chapter 4. Modelling the Transport of Carbon Beams	51

4.1. Monte-Carlo simulations and energy-fluence spectra.	51
4.1.1. Monte-Carlo simulations of carbon ion beams.	51
4.1.2. The energy-fluence spectra database in the libamtrack library — SPC files	52
4.1.3. Algorithm for interpolation of the energy-spectrum data files.	55
4.1.4. A sample calculation of energy-fluence spectra	55
4.2. Optimization of dose vs. depth distributions	56
4.2.1. The depth-dose profile optimization algorithm	56
4.2.2. A sample calculation of a flat dose vs. depth profile	58
4.3. Conclusions	59
Chapter 5. Modelling the Depth Distribution of Cellular Survival . . .	63
5.1. Calculation of cellular survival in a mixed ion field	64
5.2. Calculation of survival vs. depth profile	65
5.2.1. The optimization algorithm	65
5.2.2. A sample calculation of a flat survival vs. depth profile	66
5.3. Comparison with a cell survival vs. depth experiment	69
5.4. Comparison with LEM-based survival vs. depth calculations	70
5.5. Dependence of survival vs. depth on beam entrance dose	71
5.6. Dependence of survival vs. depth on cell oxygenation status	73
5.7. Conclusion	75
Chapter 6. Discussion and conclusions	78
6.1. Discussion	78
6.2. Summary and conclusions	84
6.3. Future Work	86
Appendix A (Radial Dose distribution and Electron range models) . .	88
Delta electron range formulae	88
Formulae of Geiss and Scholz	88
Formula of Butts and Katz	88
Formula of Waligórski	88
Formula of Tabata	89
Radial dose distribution formulae	89
Formula of Zhang	89
Formula of Katz	89
Formula of Geiss	90
Formula of Cucinotta	90
Appendix B (Extended target calculations)	91
Appendix C (Software)	92
libamtrack	92
fitting-katz-cell-survival	93
spc	93
carbon-sobp	93
Bibliography	95
List of Tables	101
List of Figures	102

Streszczenie

Radioterapia z użyciem wiązki jonów węgla jest nową techniką, mającą szczególne zastosowanie w leczeniu radioopornych guzów o trudnej lokalizacji. Planowanie leczenia, gdzie na podstawie zaleceń klinicznych fizyk medyczny dokonuje optymalizacji przestrzennego rozkładu inaktywacji komórek nowotworowych przez odpowiednie napromienienie objętości leczonej, jest jedną z podstawowych procedur radioterapii. Zasadniczą trudnością w planowaniu leczenia wiązkami jonowymi jest konieczność prawidłowego uwzględnienia zmian względnej skuteczności biologicznej jonów (WSB) w obszarze poszerzonego piku Bragga. W przypadku radioterapii jonowej, inaczej niż w radioterapii konwencjonalnej prowadzonej wiązkami fotonów i elektronów, uzyskanie jednorodnego rozkładu dawki w obszarze leczonym nie oznacza, że uzyskano jednorodny rozkład inaktywacji komórek nowotworowych, z powodu zmian WSB dla dawek promieniowania jonowego.

W ramach tej pracy opracowany został algorytm mający zastosowanie w systemach planowania leczenia radioterapii jonami węgla. Algorytm ten składa się z części radiobiologicznej, odpowiedzialnej za obliczenie rozkładu dawki i inaktywacji komórek, oraz z modelu transportu wiązki jonów węgla, opartego o symulacje metodą Monte Carlo. Do obliczeń rozkładu inaktywacji komórek zastosowany został model struktury śladu (model Katza), pozwalający opracować wydajną obliczeniowo metodę przewidywania przeżywalności komórek w zadanym mieszanym polu jonów węgla i cząstek wtórnych. Model Katza wraz z modelem wiązki zostały użyte w procedurze optymalizacji wejściowego spektrum energii-fluencji wiązki węglowej w taki sposób aby na wybranym obszarze otrzymać zadany rozkład dawki lub przeżywalności.

Poprawność przewidywań przy pomocy przygotowanego algorytmu została została zweryfikowana przez porównanie z opublikowanych danych przeżywalności komórek jajnika chomika chińskiego (CHO) naświetlanych in-vitro wiązką jonów węgla.

Systemy planowania leczenia używane obecnie w radioterapii jonami węgla oparte są o model efektu lokalnego (LEM). Zastosowanie modelu Katza daje możliwości porównania planów leczenia opracowanych przy pomocy różnych modeli. Otwartość implementacji przygotowanych rozwiązań stwarza możliwości do rozwoju i szerokiej współpracy z innymi grupami badawczymi pracującymi nad tematyką radioterapii jonowej.

Abstract

Radiation therapy with carbon ions is a novel technique of cancer radiotherapy, applicable in particular to treating radioresistant tumours at difficult localisations. Therapy planning, where the medical physicist, following the medical prescription, finds the optimum distribution of cancer cells to be inactivated by their irradiation over the tumour volume, is a basic procedure of cancer radiotherapy. The main difficulty encountered in therapy planning for ion radiotherapy is to correctly account for the enhanced radiobiological effectiveness of ions in the Spread Out Bragg Peak (SOBP) region over the tumour volume. In this case, unlike in conventional radiotherapy with photon beams, achieving a uniform dose distribution over the tumour volume does not imply achieving uniform cancer cell inactivation.

In this thesis, an algorithm of the basic element (kernel) of a treatment planning system (TPS) for carbon ion therapy is developed. The algorithm consists of a radiobiological part which suitably corrects for the enhanced biological effect of ion irradiation of cancer cells, and of a physical beam transport model. In the radiobiological component, Katz's track structure model of cellular survival is applied, after validating its physical assumptions and improving some aspects of this model. The Katz model offers fast and accurate predictions of cell survival in mixed fields of the primary carbon ions and of their secondary fragments. The physical beam model was based on available tabularized data, prepared earlier by Monte Carlo simulations. Both components of the developed TPS kernel are combined within an optimization tool, allowing the entrance energy-fluence spectra of the carbon ion beam to be selected in order to achieve a pre-assumed uniform (flat) depth-survival profile over the SOBP region, assuring uniform cancer cell inactivation over the tumour depth.

Implementations of all the relevant codes developed in this thesis are contained in the freely available libamtrack code library.

The developed TPS kernel is successfully benchmarked against a published data set of CHO (Chinese Hamster Ovary) cell survival curves, after irradiation of these cells in-vitro by carbon ion beams.

The developed 1-dimensional kernel of a carbon ion therapy planning system could be expanded to a realistic full-dimensional system, also for proton radiotherapy. Application of Katz's radiobiological model in this kernel offers an interesting alternative to the presently used ion planning systems based on the Local Effect Model, due to the robustness and simplicity of the Katz model and to the efficient computational techniques applied. Open-source coding and the general availability of the libamtrack library may stimulate other research groups to cooperate in further development of results obtained in this thesis.

Introduction

Among the three basic techniques of treating primary cancers, *radiotherapy* is applied most frequently, alone or in combination with surgery or chemotherapy. Applying a high dose of ionizing radiation sterilises the rapidly multiplying cancer cells and stops their further multiplication. Since healthy cells surrounding the tumour volume will also be sterilised (or inactivated) by this high absorbed dose, optimising radiotherapy relies on delivering the prescribed dose precisely and uniformly to the tumour volume while sparing to the extent possible the neighbouring healthy tissues. In modern *tele-radiotherapy* external conventional beams of megavolt X-rays or electrons, generated by medical linear accelerators, are applied to treat the tumour volume located at some depth within the patient's body. Careful adjustment of the beam direction, beam collimation and accurate calculations of beam transport and dose deposition in the patient's body are necessary to optimally deliver the therapeutic dose. Dedicated computer software systems, so-called *Treatment Planning Systems* (TPS) are used for this purpose. The role of the TPS is to enable the medical physicist to properly adjust the energy, directions and collimation of the X-ray or electron beams to achieve conformal distribution of the medically prescribed dose to the tumour (target) volume. As input, the conventional TPS incorporates *accelerator-specific data* (reference dosimetry related to the physical specifications of the medical accelerator, such as beam energy, beam orientation and geometry, or beam modification by collimator settings, etc.), and *patient-specific data* (three-dimensional volume representations of patient's tissues and of the treated volumes, together with their local density specifications). Patient-specific data are usually obtained from a series of computed tomography (CT) images of the relevant part of the patient's body, including respective volume distributions of Hounsfield numbers which enable locally deposited dose in these volume elements to be calculated. The TPS incorporates a *physical model of beam transport* through the patient's body, where, basing on the patient data, absorbed dose deposited locally in the treated area and in the target volume can be calculated. In these calculations, local variation of absorber density (e.g., in bone, lung or in soft tissues) and superposition of the effect of applying the beams from several angles, can be accounted for. Advanced therapy planning systems are also able to use "inverse planning" techniques which seek an optimum dose distribution in the target volume, satisfying some pre-set conditions for this optimisation.

In conventional radiotherapy where megavolt photon or electron beams are applied,

uniform distribution of dose absorbed in the tumour volume implies a uniform level of inactivation of tumour cells in this volume. Because tumour cells rapidly proliferate, they are often deprived of oxygen supply, making them more radioresistant than the neighbouring healthy tissues (through the so-called *oxygen effect*). Application of fractionated schemes of conventional radiotherapy (where, typically, some 60 Gy is delivered to the tumour volume in 30 daily fractions of 2 Gy each) allows better sparing of the healthy tissues against tumour cells, due to radiobiological considerations. By performing treatment planning using several beam shaping techniques, such as multi-leaf collimators, irradiation from many angles or applying intensity modulation of the photon beam fluence (IMRT) and advanced “inverse planning” techniques, accurate conformation of the dose delivered to the tumour (target) volume can be achieved, however with some enhancement of dose to the neighbouring regions.

In 1946 Robert Wilson [Wilson et al., 1946] drew attention to the possibility of applying beams of protons or of heavier ions in cancer radiotherapy. There are two main advantages to this proposal: the well-defined proton range and the dramatic increase of dose deposited at its distal range, known as the *Bragg peak*. In the case of ions heavier than proton, apart from these two advantages, the other important advantages are in the possibility of achieving an enhancement of the biological effect per deposited dose, known as the enhanced *Radiobiological Effectiveness* (RBE) of such ions. Additionally, heavier ions may have the capability of eliminating the oxygen effect, i.e. are able to effectively sterilise, on a per dose basis, also the oxygen-deprived or radio-resistant cancer cells. A general feature distinguishing between X-ray or electron beams and beams of protons or of heavier ions is their different stopping power, or Linear Energy Transfer (LET). Thus, beams of photons or electrons are “low-LET” radiations, while beams of protons or heavier ions are called “high-LET” radiations, to underscore the importance of ionisation density in evaluating differences between the radiobiological properties of X-ray or electron beams and of ion beams.

In the 1950’s the technique of culturing cell lines (*in vitro*) [Puck and Marcus, 1956] was developed, which enabled detailed studies to be undertaken of the radiobiological properties of “high-LET” ion beams, mainly in terms of the cellular survival biological endpoint. In parallel, biophysical models of radiation action on cells were developed. Based on microdosimetry considerations [ICRU, 1983], cellular survival versus dose of low-LET (X-ray) radiation became described by an exponential expression with terms linear and quadratic with dose (the so-called “alpha-beta” or linear-quadratic description), where a purely exponential survival (with an “alpha” term only) dose dependence could be observed for some high-LET radiations. Within this formalism, the RBE could then be introduced and defined (see Chapter 1). RBE was found to be a complicated function of ion LET, of the survival level and of the intrinsic radiosensitivity of the cellular system. LET alone was found not to be a good general predictor of RBE over a range of ion species. In particular, ions of different charges and of the same LET values showed different RBE values, indicating the importance of track structure in these considerations. However, representations of individual cell lines by their linear-quadratic parameters and by their alpha/beta ratios were also found to be useful in predicting the outcome of fractionated conventional low-LET radiotherapy and in describing early and late effects in tissues irradiated by photon and electron

beams [Fowler, 1989], [Fowler, 2010] and thus became commonly accepted in clinical radiotherapy, though for reasons other than high-LET RBE modelling considerations.

To exploit the properties of high-LET radiations in radiotherapy, beams of *fast neutrons* were developed and applied clinically in the 1960's [Wambersie et al., 1994]. Also, at that time, radiotherapy using beams of heavy ions, up to xenon, began at the Bevalac accelerator in Berkeley (USA) [Pirruciello and Tobias, 1980]. While these early trials were not entirely successful, they paved the way for the development of modern ion radiotherapy, indicating that energetic carbon ions (of some 300 MeV/amu) may be the most convenient “heavy” ion beam for radiotherapy applications, from clinical and radiobiological considerations. The alternative “light” ion beams for radiotherapy are beams of protons of energy of about 260 MeV. As illustrated in Fig. 1, such energies of these ion beams, resulting in their range in water of about 25 cm in water, allow tumour volumes to be reached in all parts of the patient's body, demonstrating advantageous depth-dose characteristics against conventional megavolt X-ray radiotherapy.

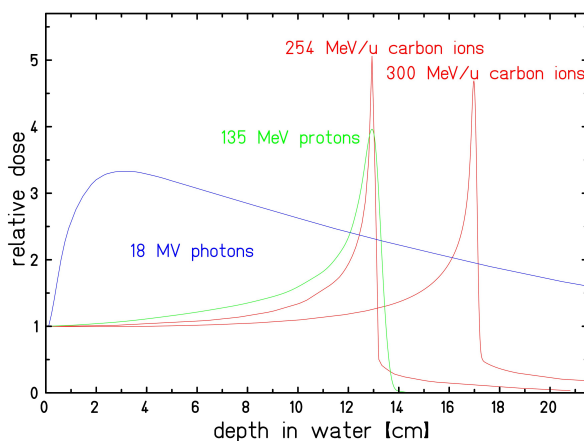


Figure 1. Relative depth-dose profiles of photons, protons and carbon ions. The Bragg peak of proton and carbon beams is clearly visible. Note that all dose profiles have been normalized to the same entrance dose. Reprinted from Haettner [Haettner, 2006].

Since the width of the Bragg peak is usually much less than the size of the tumour volume, techniques of spreading-out of the Bragg peak have to be employed [Russo, 2007]. A non-trivial superposition of several Bragg peaks of beams of a range of energies is required for this purpose, as may be seen in Fig. 2, different for proton and carbon beams. Notable in this figure is the difference in the depth distributions of the “physical depth dose” and of the “biological depth dose”, which represents here a measure of cellular survival with depth and which arises from the enhanced RBE of the ion beams, being higher for the carbon beam. This implies that the ion beam treatment planning system has also not only to contain the physical dose component, but also to include a radiobiology component in order to represent the overall biological effect (e.g., via RBE) of the spread-out ion beam composition. Notably, as seen in Fig. 2, achieving a uniform distribution of physical dose over the tumour volume will not result in a uniform distribution of the biological effect (inactivation) of tumour cells over the target volume. Suitable downward correction of the depth-dose profile

of the “physical dose” is required to achieve a uniform depth distribution of biological effect, as represented in Fig. 2. This is due to the enhanced RBE in the distal region, especially in the case of the carbon beam. The choice and application of a suitable radiobiological model is therefore the key element of any clinically applicable therapy planning system for ion radiotherapy.

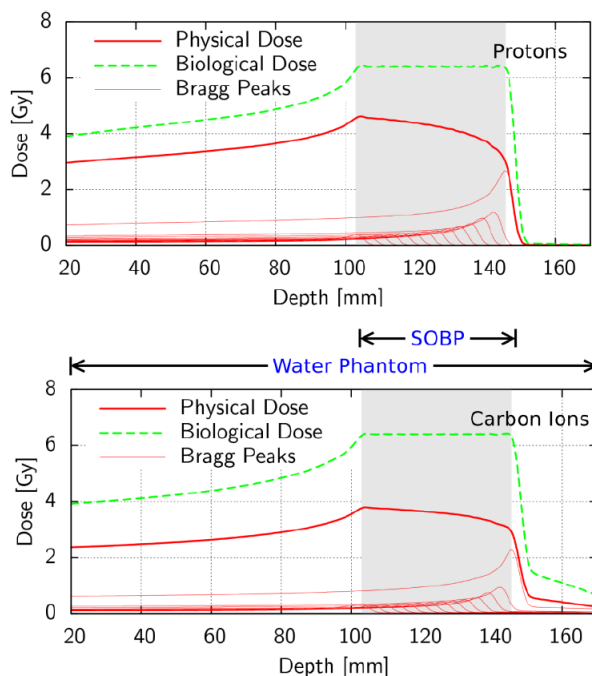


Figure 2. Illustration of depth distributions of “physical dose” (or of depth-dose) and of “biological dose” (or of depth-cellular inactivation level) in spread-out carbon and proton beams, in a water phantom. The spreading-out of the Bragg peak is achieved by a suitable superposition of ion beams of different initial energies and fluences. Reprinted from <http://totlxl.to.infn.it/>, Andrea Attili, INFN-TPS project resources.

The requirements of the treatment planning system to be applied in ion (especially carbon) beam radiotherapy are clearly much more complex than those of the TPS applied in conventional radiotherapy. The beam transport component must now also incorporate control of variation of the input beam energy, required to spread out the Bragg peak region over the tumour volume. Interactions of the beam ions with tissue lead to a complicated pattern since the energetic carbon ions produce complex energy spectra of secondary and higher generation ions and photons arising from nuclear fragmentation of lighter ions. In inelastic collisions with target nuclei, carbon ions may change into lighter fragments or may fragment nuclei of the medium, leading to production of fragments of low energies, lighter than the original ion, traveling along the direction of the original ion beam. Beam-produced fragments contribute to an undesired dose in the tail region of the dose profile. A further requirement of the beam transport component of the TPS is to calculate the locally deposited dose as a superposition of the contributions of all these fragments, usually in the form of a Monte Carlo calculation. An example of such a calculation for a mono-energetic beam is shown in Fig. 3. In this representation, the contribution to the dose due to lateral

scattering of the primary beam is not included. Nor is the additional complication to the ion beam transport calculation, due to the need to calculate the spread-out dose-depth profile of the Bragg peak from a suitable composition of ion beams of different initial energies. As a result, the suitably optimised depth-dose distribution of the physical dose is expected, as shown earlier in Fig. 2.

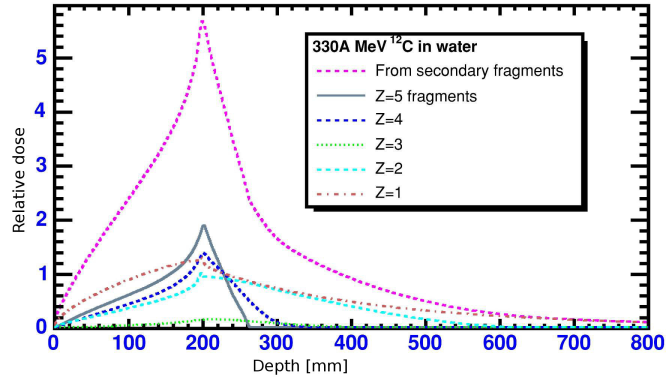


Figure 3. Monte Carlo-calculated contribution to the dose from secondary fragments of a 330 MeV/amu carbon ion in water. The nominal range of this monoenergetic carbon beam is 200 mm. Reprinted from Pshenichnov et al. [Pshenichnov et al., 2005]

Calculations of the depth-dose distributions of carbon ions can be verified by measurements with ionization chambers, solid detectors or beam profilers. However, cell survival (or inactivation), in carbon ion beams depends not only on the physical dose, but also on the yield of lighter ion fragments and on their energy spectra, which are much more difficult to determine experimentally.

The next element required in an ion beam TPS is the radiobiology component, whereby, by using an appropriate radiobiological model, a reasonably uniform distribution of the biological endpoint – survival or inactivation of cancer cells in the target volume - can be achieved by suitable modification of the physical depth-dose distribution. It is now generally accepted that in order to incorporate the complex dependence of RBE of the different ions and on low-LET radiation produced by the combination of ion beams of different initial energies, it is necessary to apply the fluence approach, i.e. to base the radiobiological calculations on the detailed knowledge of energy-fluence spectra of all ions over the complete range of this initial ion beam combination. It is essential to correctly calculate cell survival in the target region to ensure that the treatment will be successful; moreover cell survival should be estimated also outside the target region, to evaluate the survival of the neighbouring healthy tissue cells the radiosensitivity of which may be different from that of the tumour cells in the target volume. It is highly desirable to seek analytically formulated radiobiology models to enable efficient optimisation of the physical dose profile by suitable minimising computation techniques.

An analytically simple and predictive model of ion RBE has been developed by Robert Katz in the late 1960's [Butts and Katz, 1967]. The basic assumption of this track structure model is the amorphous Radial Distribution of average Dose, $D(r)$, around the path of a heavy ion. The average dose, due to delta-rays surrounding the

ion moving through the medium is assumed to be deposited in sensitive sites representing radiosensitive elements of the cell, acting in a manner similar to that after uniform irradiation of these sites by low-LET reference radiation. The difference is in the highly non-uniform dependence (typically, $1/r^2$) of average radial dose with radial distance from the ion's path. The response of the cellular system to a uniformly distributed average dose of reference radiation is given here by the "m-target" formula (see Chapter 1) which, unlike the linear-quadratic representation, gives a zero initial slope after low doses of low-LET radiation. By folding the low-LET response of the cellular system with the $D(r)$ distribution of delta-ray dose, a radial distribution of activation probability is obtained, which, when integrated over all radii, yields the activation probability cross-section per ion. While the shape of the $D(r)$ is determined by the speed and the charge of the ion, the inactivation cross section also depends on the radiosensitivity of the cell system, as described by the m-target parameters of its response after doses of reference radiation. Another important feature of the Katz model is in its application of two modes of inactivation, via "ion-kill" and "gamma-kill" components of cell inactivation probability. The model also proposes an analytical formulation of the response of a cellular system to a superposition of a mixed radiation field composed of different ions and of low-LET radiation. In its analytical (or scaled) version, based on a suitable approximation of results of numerical integrations, the model applies four parameters to describe a given cellular system and requires the knowledge of energy-fluence spectra of the ion irradiation to calculate the survival of this cellular system after any composition of ions and low-LET radiation. The Katz model has not yet been implemented in clinical treatment planning systems for ion therapy, though its applicability to ion radiotherapy has already been demonstrated [Roth and Katz, 1980]. The simplicity and proven ability to predict in-vitro cell survival after heavy ion irradiation make the Katz model a promising candidate for application in ion radiotherapy planning systems. However, additional verification studies on the consistency of the analytical approximations used in this model are required [Korcyl, 2012], as well as further development and verification of the mixed-field calculation which may then be applied with a more precise physical ion beam model. The optimization algorithms used to find a beam configuration which may deliver uniform cellular in the volume of interest, also need to be further developed.

Currently, the only radiobiological model fully incorporated into a clinical treatment planning system for carbon ion radiotherapy is the Local Effect Model (LEM) [Scholz and Kraft, 1994] developed at GSI Darmstadt, Germany. To treat their patients, the Japanese groups use an approach based on their past clinical experience with fast neutron radiotherapy, developed at NIRS, Chiba, Japan [Hawkins, 1998]. In the LEM and Japanese approaches ion fluence is applied and the general concept of the amorphous Radial Distribution of Dose originally proposed by Katz, however incorporating the linear-quadratic description of cellular survival dependences after reference (photon) radiation. LEM relates the response (cellular survival) after ion irradiation via photon dose-response, however with additional assumptions concerning the spatial distribution of dose. The distinct feature of LEM is the assumption that cell survival is related to the spatial distribution of the local lethal events resulting from the dose deposited by delta-electrons and ions. The GSI Darmstadt group led by Gerhard Kraft has developed four subsequent versions of the LEM model. A version

of the LEM is used clinically in the carbon ion beam TPS at the Heidelberg HIT ion radiotherapy centre.

In the Japanese treatment planning system, elements of LEM are also applied. The former NIRS experience from fast neutron radiotherapy is used to aid the calculation of the “biological dose”.

Although the Japanese treatment planning system has been used in the treatment of several thousand patients and the LEM-based German planning system – in a almost 1500 patients, both systems are still deficient in several areas: there is a lack of consistency with experimental data for ions lighter than carbon and quite complex computer-intensive calculations are required. Since the TPS codes of the LEM are now unavailable due to commercial limitations, it is difficult to obtain sufficient information on the German therapy planning system to analyse its performance more closely.

Aim and scope of work

The general aim of this work was to develop and test the basic algorithms of a kernel of a future therapy planning system (TPS) for carbon ion radiotherapy, using in its *radiobiology component* the cellular track structure model of Katz and applying as its *physical component* a realistic Monte Carlo-generated data base describing transport in water of carbon beams of various initial energies. Using this data set it should be possible to simulate the formation of the spread-out Bragg peak structure and to evaluate, at all beam depths, the energy-fluence spectra of the primary beam ions and of all generations of secondary ions, as required by the Katz model.

It was decided that the *libamtrack computer code library* would be used as the resource for all the computer codes that had to be developed for the purposes of this work. The libamtrack library had been co-developed earlier by the author, in collaboration with Steffen Greulich and other colleagues at the DKFZ and Aarhus research centres, as an open-source research tool, freely available to all users. Codes of the libamtrack library have already been applied in calculations of the response of alanine [Herrmann et al., 2011] and aluminium oxide [Klein et al., 2011] detector response and in radiobiological modelling of cell survival [Grzanka et al., 2011].

The *physical component* to be used in this work was a Monte Carlo (SHIELD-HIT) generated data base describing transport in water of carbon beams of various initial energies, developed by Pablo Botas and available to the author. A suitable averaging algorithm to generate the energy-fluence spectra of all ions in the beam (primary and secondary) at the required depths would need to be developed. Next, a method for modelling the depth-dose profile in the spread-out Bragg peak would also need to be devised.

The Cellular Track Structure model developed by Katz [Butts and Katz, 1967], [Katz and Sharma, 1974], [Katz and Cucinotta, 1999], [Roth and Katz, 1980] would be applied as the *radiobiological component* of the TPS kernel. Use of this model would provide the author with an alternative to the Local Effect Model (LEM) developed by Scholz and Kraft [Scholz and Kraft, 1994], [Krämer and Scholz, 2000] and used in the carbon ion therapy planning system (TPS) applied clinically at GSI Darmstadt and at the HIT facility at Heidelberg. A method of calculating a suitable adjustment of the depth-dose profile in order to obtain, at a given level of cell survival, a flat survival

vs. depth dependence over a given depth range, would need to be found. The author had earlier collaborated with Marta Korcyl [Korcyl, 2012] on developing elements of the Katz model [Grzanka et al., 2011].

Results of a radiobiology experiment where Chinese Hamster Ovary (CHO) cells were irradiated by a set of carbon beams to verify the Spread Out Bragg Peak (SOBP) calculations and the LEM-based TPS approach, are available [Mitaroff et al., 1998]. This offered the possibility of verifying the author's method of calculating the SOBP, based on the carbon beam data set and of the results of cell survival calculations using the Katz model, against results of this experiment.

Developing a Katz model-based kernel of a carbon ion TPS would offer the possibility of comparing this approach with systems based on other radiobiological models and to suggest future directions for further work in this area.

The physics and radiobiology of track structure

In this chapter the basic physical and radiobiology concepts required in track structure modelling of ion beam radiotherapy are introduced. In the physics part, stopping power, Linear Energy Transfer, dose, fluence and the Bragg peak, related to the passage of an ion through the medium (typically water), are discussed. In the radiobiology part, description of cellular survival after doses of reference radiation (γ -rays) by linear-quadratic or m-target formulae, and Relative Biological Effectiveness are introduced, followed by a brief presentation of the Local Effect Model (LEM).

1.1. Particle Track Physics

Energetic ions are able to ionise the medium through which they pass. This may occur *directly* (by charged particles, such as electrons or ions) or *indirectly* (by neutrons or photons). Neutral particles, through their interaction with orbital electrons or atomic nuclei of the medium, produce charged particles which then ionise the medium in direct processes. We will focus here mainly on ionisation and excitation processes due to the passage of energetic carbon ions through water.

As ionising particles travel through the medium they interact with atoms or higher structures of the medium (such as molecules), producing ionisations and excitations. Ions of energies ranging between a few to a few hundred MeV interact mainly by Coulomb interaction with electrons of the outer shells of atoms of the medium. For ions and media relevant to radiotherapy, direct nuclear interactions with nuclei of the atoms of the medium can be neglected, as they do not contribute much to the total dose nor do they affect the range of the primary ions. However, nuclear interactions are responsible for fragmentation of the primary beam ions. This process cannot be neglected, as secondary and higher generations of secondary fragments contribute to

the total dose deposited in the medium and to the effective range of the radiotherapy beam.

The principal concept of an *ion track* is illustrated in Figure 1.1. The illustrated passage of an α -particle of energy 4 MeV over a distance of 300 nm of water will not change much its energy over that distance. The trail (or the sequence of coordinates) of excitation and ionisation events which the ion creates along its path as it passes through the medium, is called a *track* of this ion. A *track segment* is the part of an ion track where the energy E of the ion changes only by an incremental value dE (i.e. is practically unchanged). The gradual loss of the ion's energy as it transverses the medium can then be represented by a sequence of track segments with gradually decreasing energies, by dE , as applied, e.g., in the *Continuous Slowing Down Approximation* (CSDA).

An energetic ion will knock out electrons from the atoms of the medium. The angular distribution of these electrons exhibits a maximum at about 90 degrees to the ion's path. These electrons may have sufficient energies to travel noticeable distances from the ion and also to further ionise. Such electrons are called *delta-electrons* (δ -electrons) or *delta-rays* (δ -rays). Ionisations due to δ -rays form a cloud of excitations and ionisations around the ion's path, very dense at small radii and of decreasing density at larger radial distances from the ion's path. Thus, the ion track appears to be composed of excitation and ionisation events occurring along the path of the ion and due to the passage of delta-rays.

The maximum energy, ω_{\max} , transferred to the δ -electron by an ion of speed $\beta = v/c$ in an elastic collision is given by

$$\omega_{\max} = 2m_e c^2 \beta^2 \gamma^2 \quad (1.1)$$

where m_e is rest mass of the electron and $\gamma = \frac{1}{\sqrt{1-\beta^2}}$

As the energy of the primary ion gradually decreases, so does the maximum energy of the emitted δ -rays, which limits the radial "thickness" of an ion track at the end of the ion's range. This effect is called track "thindown".

1.1.1. Stopping power and Linear Energy Transfer

The linear rate of energy loss, dE , by a charged particle to atomic electrons of the medium per unit path length of the particle, dl , $-dE/dl$, (commonly in units of MeV/cm or keV/ μm) is called the stopping power of the medium for the particle. It reflects the energy lost by the particle to the medium it transverses. According to the physical process in which energy is lost and transferred to the medium, electronic and nuclear stopping power are distinguished, as defined more precisely in ICRU Report 73 [ICRU, 2005].

The Bethe formula [Bethe, 1932], derived by applying quantum mechanics to describe the stopping power of a heavy charged particle, is as follows:

$$-\frac{dE}{dl} = \frac{4\pi}{m_e c^2} \frac{nz^2}{\beta^2} \left(\frac{e^2}{4\pi\epsilon_0} \right)^2 \left(\frac{1}{2} \ln \frac{2m_e c^2 \beta^2 \gamma^2 T_{\max}}{I^2} - \beta^2 - \frac{\delta(\beta\gamma)}{2} \right) \quad (1.2)$$

where n is the electron density of the medium, e is the elementary electric charge, ϵ_0 is the permittivity of vacuum, $\delta(\beta\gamma)$ is a density effect correction and:

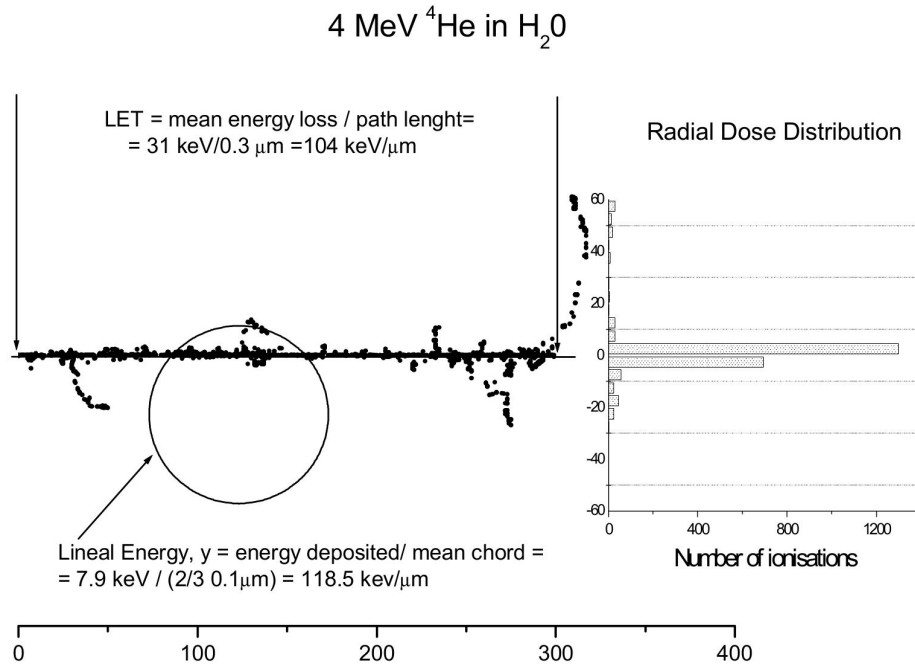


Figure 1.1. A two-dimensional representation of a 3-D track-segment of a 4-MeV α -particle in H_2O (water vapour normalised to density of 1 g/cm^3), simulated using the MOCA-14 Monte Carlo track structure code [Paretzke, 1987]. Dots denote the positions of individual ionisations. The value of Linear Energy Transfer, LET (Eq. 1.4) is calculated as the mean energy imparted to water by the 4 MeV ^4He ions (31 keV) divided by the length of the illustrated path length ($0.3 \mu\text{m}$). The insert on the right shows the radial histogram of ionisations, corresponding to the radial dose distribution, $D(r)$. Figure adapted from Goodhead [Goodhead, 1987], and reprinted from Olko [Olko, 2002].

$$T_{\max} = \frac{2m_e c^2 \beta^2 \gamma^2}{1 + 2\gamma \frac{m_e}{M} + \frac{m_e^2}{M^2}} \quad (1.3)$$

which reduces to ω_{\max} (equation 1.1) if $m_e \ll M$ (here M is the mass of the incident particle and m_e the mass of the electron). For ions of energies relevant to radiotherapy (0.1 - 500 MeV/amu), the effect of the density effect correction may be neglected. The stopping power of protons in liquid water calculated using the Bethe formula and that extracted from the PSTAR database are shown in Fig. 1.2.

The PSTAR database published by NIST [Berger et al., 2005] combines experimentally evaluated values of stopping power of protons in a several media. As can be seen from the plot of proton stopping power calculated in water using Bethe's formula and from the PSTAR database, at energies below 1 MeV results of calculations using Bethe's formula deviate from experimental values. Bethe's formula is valid down to proton relative velocity $\beta \approx 0.05$. Below this value there is no reliable theory, so one may use experimental data fits [Andersen and Ziegler, 1977] to this formula [Berger and others (Particle Data Group), 2012]. The PSTAR database contains values of proton stopping power published in the ICRU-49 report [ICRU, 1994] (at low energies,

below 0.5 MeV) combined with the Bethe-Bloch formula (at energies above 0.5 MeV). Other sources of stopping power data are the ICRU-73 report [ICRU, 2005] (stopping power of ions heavier than helium), and tables published by Janni [Janni, 1982].

The PSTAR database was chosen by the author as the source of stopping power for calculations, due to its completeness and to comply with ICRU-49 recommendations [ICRU, 1994]. Moreover, as the Bethe formula does not agree with experimental data for ions of energies below 1MeV, range estimates calculated with CSDA (Continuous Slowing Down Approximation) and the Bethe-Bloch formula will not agree with those calculated using data from the PSTAR database.

To distinguish between the energy transferred from a charged particle to the medium and the energy actually absorbed by the medium (i.e. absorbed dose), Linear Energy Transfer (LET), is defined as the average energy locally imparted to the medium by a charged particle, dE_i traversing a distance dl in the medium (to denote LET, L will be used in this work):

$$L = \frac{dE_i}{dl} \quad (1.4)$$

Not all energy lost by a particle is transferred to the medium (e.g. radiative losses, or bremsstrahlung) and some energy lost by the projectile at one location may be imparted to the medium elsewhere (e.g. carried by long range delta electrons or neutrons). To focus only on the energy deposited in the medium in the vicinity of the particle's track, the concept of *restricted linear electronic stopping power*, LET_Δ , is introduced, also referred to as restricted linear energy transfer (LET_Δ) which denotes the energy loss dE_Δ due to electronic collisions minus the kinetic energies of delta electrons of energy larger than Δ , per unit path length dl (again, here we shall use L_Δ to represent LET_Δ):

$$L_\Delta = \frac{dE_\Delta}{dl} \quad (1.5)$$

In this work we shall assume that over the energy range of carbon (and of lighter ions) relevant to radiotherapy, LET of these ions does not significantly differ from their stopping power. We will use both concepts interchangeably (i.e., if in the definition of LET_Δ all the energy deposited in the medium is accounted for, $LET = LET_\infty = dE_i/dl$). In what follows, L will denote LET_∞ , i.e. unrestricted linear energy transfer.

For ions of energies below a few MeV, partial "screening" of the ion charge (or "electron pickup") occurs, which effectively diminishes its charge. Following other authors the "effective charge", calculated using the formula of Barkas [Barkas and Evans, 1963] will be used:

$$z^* = Z \left(1 - \exp \left(-125\beta Z^{-\frac{2}{3}} \right) \right) \quad (1.6)$$

where Z the is atomic number of the ion.

One may calculate the linear energy transfer of an ion of charge Z and energy E (in MeV/amu) from that of the proton of the same energy by the following relationship involving the ratio of the effective charges of both ions, z^* :

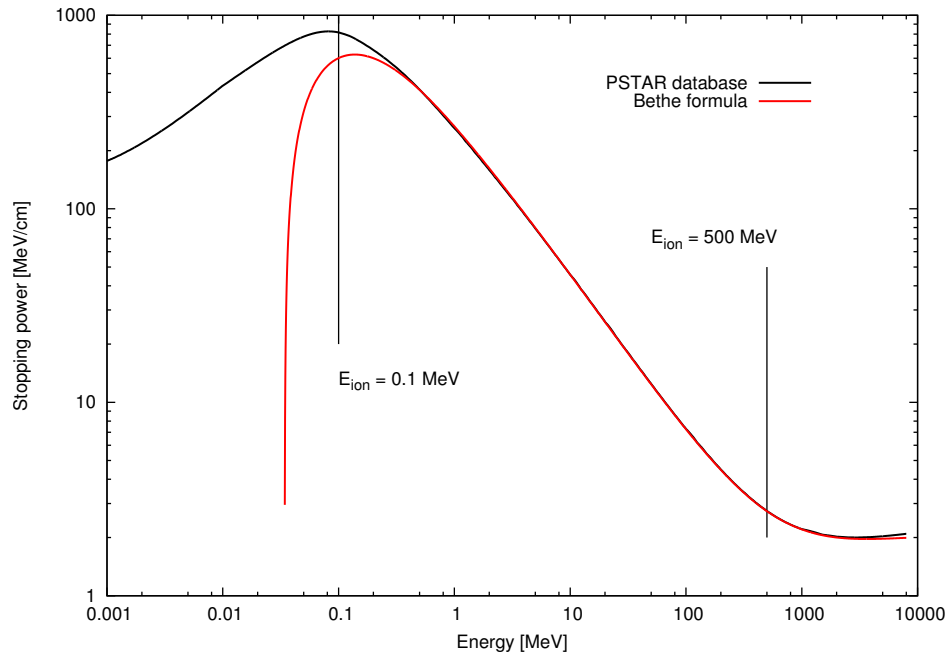


Figure 1.2. Stopping power of protons in liquid water based on PSTAR database [Berger et al., 2005] and on the Bethe formula 1.2, implemented in the libamtrack library. The range of ion energies (0.1 – 500 MeV) relevant to ion radiotherapy is shown by vertical lines

$$\frac{L_1}{L_2} = \left(\frac{z_1^*}{z_2^*} \right)^2 \quad (1.7)$$

As we shall see later in this Chapter, the biological effectiveness of energetic ions strongly depends on their LET, generally increasing as LET increases. For this reason, energetic ions are often termed “high-LET” radiation while sparsely ionising photons (X-rays or γ -rays) are termed “low-LET” radiation. However, while LET is indeed related to track structure, LET alone is not a good predictor of the biological effects of irradiation by different types of ions of different energies, if track structure considerations are not included.

1.1.2. Dose and fluence

Particle fluence and dose are basic quantities describing beam intensity and energy deposited by ions of the beam in the medium. ICRU Report 85 [ICRU, 2011] defines particle fluence F as the ratio of number dN of particles incident on a sphere with cross-sectional area dA :

$$F = \frac{dN}{dA} \quad (1.8)$$

In this work, particle fluence F will be interpreted as the number N of beam particles (all travelling in parallel along a given direction) incident on planar area A , perpendicular to the beam direction, i.e. $F = N/A$. This interpretation is close to the concept of vector fluence, defined in ICRU Report 85 [ICRU, 2011].

Absorbed dose D is defined as the mean energy dE delivered by ionizing radiation to a small but finite volume of matter of mass dm .

$$D = \frac{dE}{dm} \quad (1.9)$$

The unit of absorbed dose in the SI system is the gray (Gy) which is equal to one joule per one kilogram. Considering our interpretation of fluence, both quantities are related by the following formula:

$$D = \frac{1}{\rho} FL \quad (1.10)$$

where ρ is the density of medium. More details on fundamental quantities and definitions can be found in ICRU Report 85 [ICRU, 2011].

1.1.3. Scattering and energy straggling

The Bethe formula assumes that the primary beam is composed of monoenergetic ions, on their entrance to the medium and at all depths. In reality, the energy loss of a beam of charged particles fluctuates around a mean value. This effect, observed particularly in the passage of particles through thin absorbers, is called energy straggling. The probability distribution of energy loss is described by the Landau-Vavilov formula [Landau, 1944], [Vavilov, 1957], while for thick absorbers the mean energy loss is closer to values obtained with Bethe's formula.

In addition, the ion undergoes frequent collisions with electrons of the medium, changing its direction by relatively small angles. This results in a broader spectrum of ion energies with increasing depth. Ion scattering can be described by the scattering power T (or mass scattering power, T/ρ) defined as the mean square angle $d\theta^2$ of scattering per unit length of the medium traversed, dz . The process of multiple scattering is described by Moliere's theory [Bethe, 1953].

The processes of energy loss straggling and of multiple scattering lead to a gradual broadening of the primary ion energy spectrum with increasing depth in the absorbing medium.

1.1.4. The Bragg peak

Linear energy transfer of ions in a given medium depends on their energy, as seen in Fig 1.2. In the case of an ion beam there is much less scatter by outer-shell electrons of the medium (due to the high ratio of the ion and electron masses). Scattering of ions in the beam occurs rather via the electrostatic field of the nuclei of the medium and depends on their impact parameters. Since the dimensions of the atomic nuclei are much smaller than those of the atomic volumes occupied by their electron structures, ion-nucleus scattering does not contribute significantly to all possible processes in which ions interact with the medium. Thus, the depth-dose profile of the ion beam consists of a low and flat dose region at lower depths, and then of a distinct peak at a depth close to the end of their range - the Bragg peak. Finally a "tail" appears which consists mainly of the dose delivered by fragmentation products which, arising at some depths, will travel further than the primary ions. The characteristic depth-dose dependence of an ion beam is thus explained by the low value of LET of ions at

their initially high energy while the occurrence of the Bragg peak follows from the rapid increase of stopping power at low ion energies, as the ions slow down in the medium to below a few MeV/amu. In ion radiotherapy proton beams of initial energies between 60 MeV and 250 MeV and carbon ion beams of initial energies between 150 MeV/amu to 400 MeV/amu are applied. Heavier ions of higher initial energies and higher charges and of higher ranges and stopping powers are not considered to be suitable for radiotherapy.

For illustration, in Fig. 1.3 results are shown of the author's calculations of the depth-dose dependence, mean energy of ions in the beam vs. depth, and beam fluence vs. depth, of a pristine (non-modulated) proton beam of initial energy about 60 MeV. This represents the proton beam used for ocular radiotherapy at the Institute of Nuclear Physics of the Polish Academy of Sciences (IFJ PAN) in Krakow. As no fragmentation of protons occurs in this case, the general trends are easier to follow than in the case of a carbon radiotherapy beam, which is discussed in Chapter 4 and where the respective depth dependences are shown in Figs. 4.1 - 4.3.

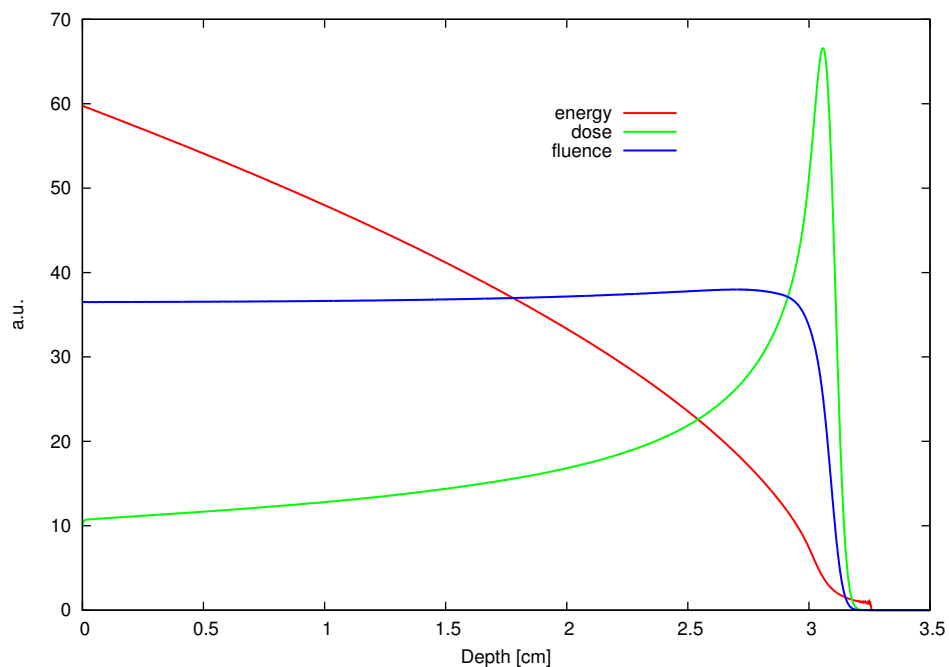


Figure 1.3. Depth-dose dependence, mean energy vs. depth, and fluence vs. depth of a pristine (non-modulated) proton beam. The entrance values (at 0 cm depth) are: energy: $E = 59.75$ MeV; dose: $D = 1.727$ Gy; and fluence: $F = 10^9$ ions/cm². Calculations made by the author, using the Geant4 package and the libamtrack library.

1.2. Radiobiology and biophysical models of cellular survival

The mechanisms of interaction of ionizing radiation with living matter which radiobiology is concerned with, have been studied for several decades, but at the level of whole organisms, such as man, they are still largely unknown. At the cellular and sub-cellular organisation levels, of interest in this work is cell survival as the biological

endpoint relevant to radiotherapy, where the objective is to inactivate, or kill (i.e., to stop proliferation of) the tumour cells by doses of ionising radiation while maintaining the normal life processes in neighbouring normal tissues. The mammalian cell is the basic autonomous component of any mammalian organism, such as man. An eukaryotic cell consists of the cell nucleus containing DNA as the basic cell replication matrix, and cytoplasm with organelles. The cytoplasm and organelles are considered to be rather insensitive to doses of ionising radiation. It is generally considered that ionising radiation affects (via production of biologically active free radicals) mainly the cell nucleus, leading to changes in the amino-acid sequence of the DNA double helix. It is possible to verify experimentally that ionising radiation may damage one of the two DNA strands the other strand remaining intact (a single strand break, SSB), or cause a double strand break (DSB) which is believed to be primarily responsible for cell death. Some of the radiation-induced changes (or deletions) in the DNA, especially DSB, may not be repaired by the many repair processes available to the cell. As a consequence, the cell may lose its capability to proliferate (i.e. will not survive) or may develop mutations, some of which may turn out to be lethal or cause cancer in later generations of daughter cells. According to these concepts, cell damage after a dose of ionising radiation may be classified as being lethal (i.e. leading directly to cell inactivation), or sub-lethal, i.e. repairable shortly after irradiation, unless additional sub-lethal damage occurs which may eventually lead to cell death or proliferation of mutated cells.

A more extensive presentation of topics related to radiobiology can be found in the textbook of Hall and Giaccia [Hall and Giaccia, 2006].

1.2.1. Cell survival and Relative Biological Effectiveness

A frequently studied biological endpoint applied in biophysical modelling is cell survival *in vitro* after irradiation with different types of ionising radiation. The experimental technique relies on culturing a known number of cells in glass or plastic vessels (Petri dishes, hence the term *in vitro* -in glass), irradiating them and counting the number of cells which have survived and are able to multiply into cell colonies on the Petri dishes, after a fixed number of cell multiplication cycles. Cells that do not proliferate following their irradiation are not able to form such colonies. Cellular survival, S , is defined as the fraction of irradiated cells that are able to proliferate (i.e. to form colonies) after irradiation (the probability of cell inactivation or cell killing is then $1 - S$). The relationship between cell survival and absorbed dose D is usually presented on a semi-logarithmic survival plot (linear scale for dose and logarithmic for survival). An example of a survival plot is shown in Fig. 1.4. Apparent is the difference between cell survival after doses of reference radiation (X-rays) and after doses of 1 MeV/amu carbon ions, where the probability of cell killing after a dose of this high-LET radiation is much higher than that after the same dose of the low-LET reference radiation.

Two types of expressions are most frequently used to represent cellular survival after doses of reference radiation: the linear-quadratic and the m -target (or, more precisely, the 1-hit m -target) formulae.

The Linear-Quadratic (LQ) [Douglas and Fowler, 1976] formula is given by the equation:

$$S(D) = \exp(-\alpha D - \beta D^2) \quad (1.11)$$

where α (in units of 1/Gy) and β (in units of 1/Gy²) are constants best-fitted to the experimental data points.

In a biological interpretation of these constants, α is believed to represent the probability, per unit dose, of creating double strand breaks (DSB) after the passage of a single track (e.g., the passage of a single ion), while β could represent the probability of DSB via two independent tracks or ionising events. From the LQ formula a characteristic parameter α/β can be derived. It is equal to the dose at which both components (linear and quadratic) are equal. In the example shown in Fig. 1.4 cellular survival after X-rays is characterised by both linear and quadratic components, while survival after carbon ions is purely exponential, interpreted as resulting from each ion track passage through the cell nucleus causing a lethal DSB.

The multi-target formula [Fowler, 1964] is given by the equation:

$$S(D) = 1 - \left(1 - e^{-\frac{D}{D_0}}\right)^m \quad (1.12)$$

where D_0 (in units of Gy) and m are constants best fitted to the experimental data points. The biological interpretation of this formula is based on the assumption that each cell nucleus contains one or more (m) “1-hit targets”. A single, or more, “hits” (i.e. energy deposition events) to each such target will inactivate it, leading to cell inactivation after all m targets in the cell nucleus have been “hit”. Simple biological systems, such as enzymes or viruses are well described by the 1-hit, 1-target model (one or more “hits” to this target will inactivate the enzyme or virus) while mammalian cells are considered to have m such 1-hit targets. Curvature of the survival curve indicates that m is larger than 1 while an exponential dependence indicates that $m = 1$ (i.e., a “1-hit, 1-target” system). In 1-hit systems, D_0 represents the characteristic dose (or radiosensitivity of the system), at which survival is equal to $\exp(-1)$, i.e. to about 0.37. Non-integer values of m can be fitted to experimental data points. This is interpreted as being an average over a large number of cells, each of which has a different (integer) number of targets. In the case of $m = 1$ (1-target, 1-hit system) formula 1.12 reduces to the purely exponential form $S(D) = \exp(-D/D_0)$ which is the same as that of the LQ model (eq. 1.11) with $\beta = 0$ and $\alpha = 1/D_0$.

Relative Biological Effectiveness (RBE) has been introduced to quantify the difference between survival curves after doses of reference radiation (usually Co-60 γ -rays or 250 kVp X-rays) and doses of the tested radiation (e.g. of high-LET radiation, such as heavy ions). At a pre-selected level of survival (or of another biological endpoint), RBE is defined as a ratio of the dose of reference radiation and the dose of the tested radiation, required to reach that level of survival (or of another biological endpoint):

$$\text{RBE}|_S = \frac{D_{\text{ref}}}{D_{\text{test}}} \quad (1.13)$$

where S is the selected level of survival (or of another biological endpoint), D_{ref} is the dose of reference radiation and D_{test} is the dose of the tested radiation. As may be

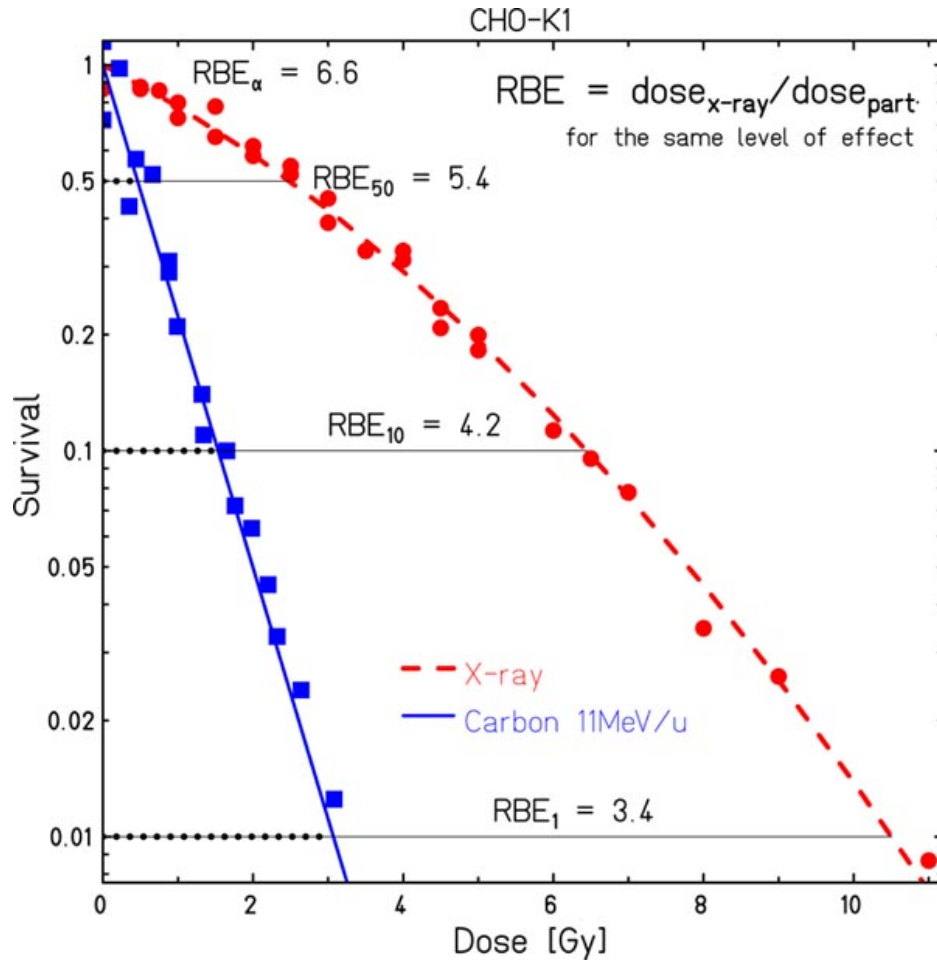


Figure 1.4. Survival of CHO cells irradiated with 1 MeV/u carbon ions or 250 kVp X-rays (reprinted from [Weyrather and Kraft, 2004]). For the carbon data, the best fitted value is $\alpha = 1.387 \text{ Gy}^{-1}$. For the X-ray data points, the best-fitted parameters of the LQ formula are: $\alpha = 0.227 \text{ Gy}^{-1}$, $\beta = 0.017 \text{ Gy}^{-2}$ (linear fit) or $\alpha = 0.224 \text{ Gy}^{-1}$ and, $\beta = 0.0185 \text{ Gy}^{-2}$ (fit to logarithms of data points). The best fitted parameters of the m-target formula to the X-ray data points are: $m=2.31$ and $D_0=1.69 \text{ Gy}$ (from a linear fit to a larger set of data, see also Fig. 3.4 and chapter 3.9).

seen in Fig. 1.4, the value of RBE depends on the level of survival chosen. In general, it depends in a complicated manner on many factors, such as level of survival, dose rate, type of ion, its energy, its LET, etc.

1.2.2. Biophysical models of cellular survival

Track Structure Theory (the Katz Model)

Track Structure Theory, developed by Katz and co-workers around 1970, is based on the concept of radial dose distribution. The model describes and predicts cellular survival after irradiation with mixed beams of ions and photons and is able to predict RBE dependences. Its principal assumption is that the energy deposition within the ion track is entirely described by the radial dose distribution due to δ -rays and that at

a given local dose, the same response is observed after photons and δ -rays surrounding the ion track. Thus, knowing the photon dose response of the cellular system and using a suitable description of track structure, it is possible to compute cell survival after ion irradiation. Several radiobiological models have since then been based on the concept of radial dose distribution first introduced by Katz. A detailed description of Katz's cellular Track Structure Theory will be given in Chapter 3.

The Local Effect Model

The Local Effect Model (LEM) was developed around 1990 by Scholz and Kraft [Scholz and Kraft, 1994] at GSI, Darmstadt as a tool for the then newly constructed experimental heavy ion radiotherapy facility. The main goal of LEM was to efficiently calculate cell survival and other biological endpoints in mixed heavy ion fields. The response (survival) of a particular cell line after photon irradiation, S_γ is parameterized by the generalized linear-quadratic equation:

$$S_\gamma(D) = \begin{cases} e^{-\alpha D - \beta D^2} & 0 \leq D < D_t \\ e^{\beta D_t^2 - (\alpha + 2\beta D_t)D} & D \geq D_t \end{cases} \quad (1.14)$$

where D_t is the dose at which a transition between the quadratic and linear parts occurs. Following the track segment approach it is assumed that the irradiated volume is thin enough to be able to perform two-dimensional calculations using x and y coordinates to describe the spatial distribution of local dose, $D(x, y)$. After a given set of energy deposition events $D(x, y)$ (due to photon or ion irradiation) the number of lethal events, $N(x, y)$ is defined as:

$$N(x, y) = -\ln(S_\gamma(D(x, y))) \quad (1.15)$$

Finally, cell survival, S_{ion} , after ion irradiation is calculated as

$$S_{\text{ion}} = e^{-N_{\text{av}}} \quad (1.16)$$

where N_{av} is the average number of lethal events in the cell nucleus within the volume V_{nucl} , defined as:

$$N_{\text{av}} = \frac{1}{V_{\text{nucl}}} \iint_{V_{\text{nucl}}} N(x, y) dx dy \quad (1.17)$$

In the LEM several free parameters are applied: the response (cellular survival endpoint) after reference radiation is described by α , β , and D_t ; a_0 is a radial dose distribution parameter and V_{nucl} characterises the volume relevant to the survival endpoint. Authors of the LEM model claim that it has only two free parameters: α and β , which are determined from the known shape of the survival curve after reference radiation. Other parameters relate to the description of track structure, i.e. radial dose distribution (a_0) and to the description of the biological endpoint (D_t and V_{nucl}). Some of these parameters are adjusted in order for the model-calculated survival curves after ion irradiation represent, as best possible, those measured experimentally. The original LEM, the basic principles of which are described above, has since gone through several further improvements, namely:

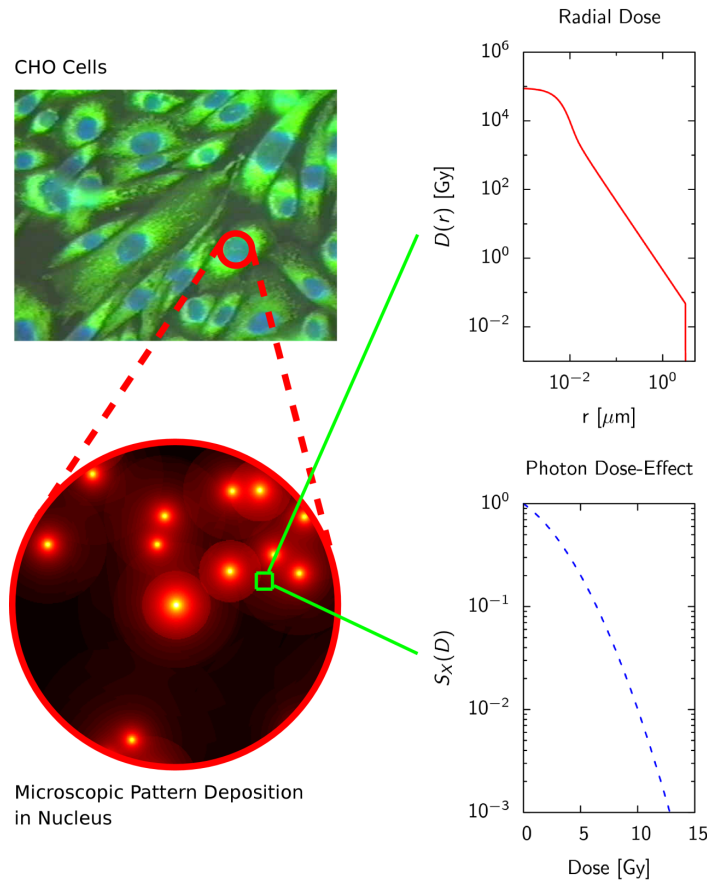


Figure 1.5. Basic assumptions of the LEM model, reproduced from Attili [Attili et al., 2008]

- LEM I - original version of the model [Scholz and Kraft, 1994], also including an approximate version in which β can be rapidly calculated from α .
- LEM II – addition of the effect of clustered damage in the DNA [Elsässer and Scholz, 2007]
- LEM III – addition of an ion energy-dependent value of a_0 to compensate for a systematic deviation in RBE predictions [Elsässer et al., 2008]
- LEM IV – addition of a relationship involving the distribution of DSB in the characteristic volume [Elsässer et al., 2010]

The Japanese approach to radiotherapy planning

The Japanese group at the National Institute of Radiological Sciences (NIRS) in Chiba has had an experience of several decades in clinical fast neutron radiotherapy. On the basis of this experience an approach was created to deliver carbon ion treatment, implemented within the HIMAC project. Instead of radiobiological modelling of cell survival distributions, the following procedure is applied: First, depth dose and LET distributions of pristine Bragg peaks are evaluated and dose-averaged LET are calculated as a function of depth. Next, a calculation of survival of the representative HSG (Human Salivary Gland) cell line is performed. Survival is estimated on the basis of the linear-quadratic formula (eq. 1.11) fitted to experimental cellular survival data.

Finally, the "biological dose" is calculated for HSG cells over the Spread Out Bragg peak, assuming the LQ formula with coefficients averaged as follows:

$$S_{\text{SOBP}}(D) = \exp(-\alpha_{\text{ave}}D - \beta_{\text{ave}}D^2) \quad (1.18)$$

Where:

$$\alpha_{\text{ave}} = \sum_i f_i \alpha_i \quad \sqrt{\beta_{\text{ave}}} = \sum_i f_i \sqrt{\beta_i} \quad (1.19)$$

And $f_i = D_i / \sum_i D_i$ is the fraction of the dose in the i -th component of the SOBP.

Knowing the "biological dose" for HSG cells, the "physical dose" profile is rescaled by a single scaling factor, termed "clinical RBE" by the authors of this approach. The value of this factor is estimated on the assumption that the therapeutic effect of a carbon ion beam of LET=80 keV/ μm is clinically equivalent to the effect of a fast neutron beam of the same average LET value. The "clinical RBE" of fast neutrons was found to be equal to 3.0, thus corresponding scaling factors can also be established for carbon ion beams of average LET values around 80 keV/ μm . Finally, the calculated individual "physical" depth-dose profile for each patient is rescaled using the established scaling factor and applied in the patient's treatment plan. This scaling factor may additionally be corrected by retrospective analysis of clinical results of treating selected tumour sites in selected groups of patients.

Evaluation of elements of track structure models

The Radial Dose Distribution, $D(r)$, is the central element of amorphous track structure models, and particularly of Katz's theory of Cellular Track Structure. Apart from Katz's derivation of $D(r)$, several other formulations have been published. The author of this thesis has implemented some of these formulations and supplementary elements in the open source libamtrack library of computer codes, as a convenient platform for model calculations. Four formulations of $D(r)$ are presented and discussed in this Chapter. The author discusses the congruence of the selected $D(r)$ formulae with experimental data and the relation between the radially integrated $D(r)$ formulae and LET of the ion. The $D(r)$ formula found to be most applicable in later track structure calculations is the formula of Zhang with ionisation potential $I = 0$, thus $\theta = 0$ in Zhang's formula shown in Table 2.2.

2.1. The libamtrack software library

The libamtrack library is a volunteer scientific project [Greilich et al., 2010] to create an open-access collection of routines, databases and functions, allowing calculations to be performed of the response of biological and physical detectors after doses of heavy charged particles. The libamtrack library was initiated by Steffen Greilich and is supported by several collaborating scientists applying amorphous track structure track calculations to radiobiology and detector physics. The present libamtrack library of codes allows calculations of several physical elements of track interactions, such as basic kinematics, stopping powers, detector response, and elements of track structure modelling. Subroutines of the library can be downloaded, edited, modified and incorporated in other software. Together with the library codes, implemented in ANSI C language, a set of wrapping methods is provided, making it possible to use these codes in other computing languages (such as Python or Java),

and in numerical simulation tools (such as R or Matlab). Some of the library functions were used to create a web interface (called libamtrack WebGUI, available under <http://webgui.libamtrack.dkfz.org/test>), where users connected to the Internet can perform basic calculations using their web browsers. The libamtrack WebGUI was based on the work of Christian Kolb, but its capabilities being extended by the author of the thesis. [Kolb, 2010]

The libamtrack library has been applied in calculations of the response of alanine [Herrmann et al., 2011] and aluminium oxide [Klein et al., 2011] detectors and in radiobiological modelling of cellular survival [Grzanka et al., 2011].

The libamtrack library consists of the following modules:

- implementation of the “scaled” and “integrated” versions of the Katz model
- grid summation method (similar to the first version of LEM)
- evaluation of compound Poissonian processes using the successive convolution algorithm [Greilich et al., 2013]
- basic radiobiological formulae (linear-quadratic, multi-target, etc.) to describe cellular survival,
- operations on energy-fluence databases stored in SPC format
- radial dose distribution formulae and their derivatives (integrated $D(r)$, averaged $D(r)$)
- stopping power data
- electron and ion energy range data
- radiation absorber data (target medium, density, electron density, etc.)
- particle (projectile) data
- operations on histograms
- numerical routines
- physical routines
- physical and radiological constants

Within this thesis project, the author developed a set of analytical functions fitted to electron energy-range data (Table 2.1) and radial dose distributions around energetic ions (Table 2.2), implementing them in C language as functions in the libamtrack library module. The libamtrack library was also applied by the author to implement different algorithms of $D(r)$ to the Katz model, and to tabularize Monte Carlo beam data (originally calculated by Pablo Botas using the SHIELD-HIT10A code) to be handled by optimization algorithms required to suitably adjust the composition of the carbon ion beams to obtain optimal depth-dose or survival vs. depth profiles.

The operating manual for the libamtrack library of computer codes is available at the <http://libamtrack.dkfz.de> webpage. Examples of calculations using radial dose distribution formulae and of energy transfer from ions to delta-electrons, are given in Appendix C.

2.2. Electron energy-range relationships

To determine extrapolated ranges of electrons simple analytical functions can be applied to fit experimental data. The first semi-empirical linear or power-law formulae describing the electron energy- range relationship were developed in the early 1960s [Butts and Katz, 1967]. These formulae could then be applied to drive the

first formulations of the radial dose distribution due to delta-rays [Butts and Katz, 1967], [Waligórski et al., 1986], [Zhang et al., 1985]. Later, to comply with improved experimental data, more complex energy-range formulae were presented in the literature. An experimental data set collected by Tabata (figure 2.1), is available for electron energies from 900 eV to about 25 MeV. These data were determined from extrapolated ranges of electrons and from transmission and projected-range straggling curves, density-scaled to water from measurements in different materials, according to Eq. 2.1. The formula of Tabata [Tabata et al., 1972] currently offers the best representation of experimental data over the broadest range of energies.

Electron energy-range formulae from the libamtrack library (see Appendix A) have been applied to calculate projected delta-electron ranges, for electron energies 50 eV - 50 MeV. Over the energy range of ions relevant for ion radiotherapy (roughly 0.1 - 500 MeV/amu, corresponding to the ejected delta-electron energy range of 220 keV - 1.4 MeV), the parameter fits of Tabata, Waligórski and Geiss all represent experimental data with sufficient accuracy.

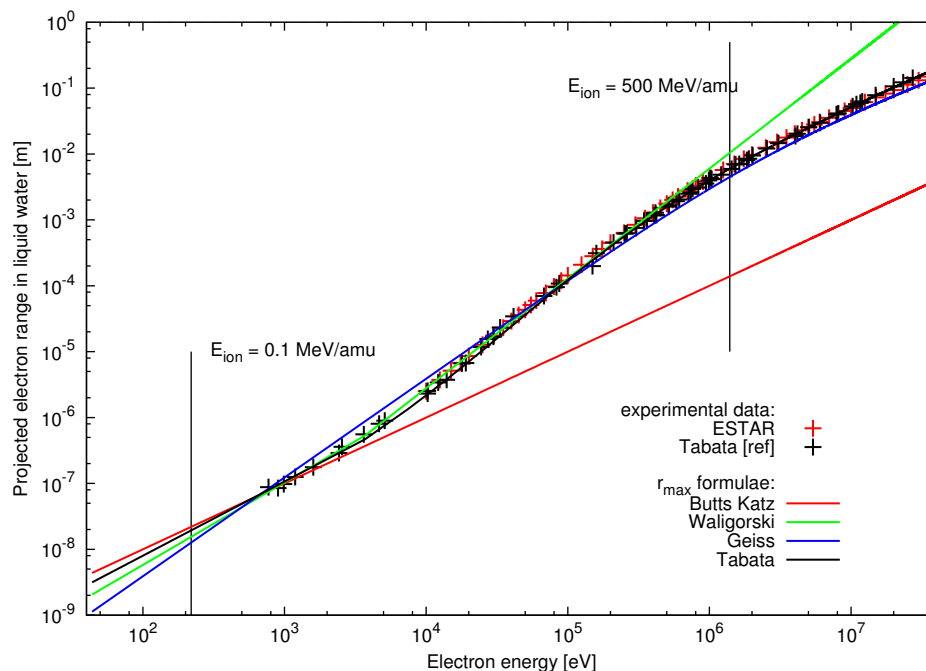


Figure 2.1. Projected electron ranges vs. initial electron energy in liquid water. Experimental data are from Tabata [Tabata et al., 1972] (measurements in different materials, density-rescaled to liquid water). The ion energy range useful in ion beam radiotherapy is indicated by vertical lines. Experimental data and the respective electron energy-range relationships have been implemented in the libamtrack library.

To apply the absorber density scaling of electron range, the simple relation is used:

$$\frac{R_{e1}}{R_{e2}} = \frac{\rho_1}{\rho_2} \quad (2.1)$$

where R_{e1} and R_{e2} are the ranges of the two particles and ρ_1 and ρ_2 are the respective densities of media they travel through.

Under the realistic assumption that delta-electrons are emitted at an angle of 90 degrees to the ion path, the maximum energy of these delta-electrons determines their maximum range and the extent of the radial dose distribution. In Table 2.1 the energy-range formulae used by different authors are listed, together with constants applied in these formulae. The units in which the electron or ion energy, denoted by ω or E , are given are keV or MeV/amu, respectively. For more details concerning these formulae, Appendix A should be consulted.

Name	Expression	Reference
Butts and Katz	$r_{\max} = 10^{-6} \text{cm} \cdot \frac{\omega}{\text{keV}}$	[Butts and Katz, 1967]
Waligórski	$r_{\max} = 6 \cdot 10^{-6} \text{cm} \cdot \left(\frac{\omega}{\text{keV}}\right)^\alpha$	[Waligórski et al., 1986]
Geiss	$r_{\max} = 4 \cdot 10^{-5} \text{cm} \cdot \left(\frac{E}{\text{MeV}}\right)^{1.5}$	[Geiss, 1997]
Scholz	$r_{\max} = 5 \cdot 10^{-6} \text{cm} \cdot \left(\frac{E}{\text{MeV}}\right)^{1.7}$	[Scholz, 2001]
Tabata	$r_{\max} = f(a_1, a_2, \dots, a_7, \omega)$	[Tabata et al., 1972]

Table 2.1. Energy-range formulae used to calculate the maximum range of delta-electrons, r_{\max} , implemented in the libamtrack library. For more details concerning the exponent α [Waligórski et al., 1986], and the function f [Tabata et al., 1972], Appendix A should be consulted. The units in which the electron or ion energy, denoted by ω or E are given, are keV or MeV, respectively.

2.3. Radial Dose Distribution formulae

Consider an energetic ion travelling through the medium along a straight line (ion scattering is neglected here). The relative speed of the ion is β , its effective charge is z^* and the electron density in the medium is N . Assume that delta-electrons, of mass m_e and maximum energy given by eq. 1.1, will then be ejected at straight angles due to ion-orbital electron Coulomb interactions, the ion gradually slowing down as it loses its initial energy (a track segment is considered here). The delta-electron energy spectrum may be given by Rutherford's formula [Beringer and others (Particle Data Group), 2012]:

$$\frac{dn}{d\omega} = \frac{2\pi N e^4 z^{*2}}{m_e c^2 \beta^2} \frac{1}{(\omega + I)^2} \quad (2.2)$$

where dn is the number of ejected delta-electrons of energies between ω and $\omega + d\omega$.

Low energy delta-electrons and the ion itself will produce most of their ionisation and excitation events close to the ion's path. Per unit mass, the average number of these events will decrease and no such events will occur beyond the maximum range

of delta-electrons. The spatial distribution of average dose deposited in the medium by such events occurring around the path of the heavy ion is called the Radial Dose Distribution, $D(r)$. Axial (cylindrical) symmetry of the $D(r)$ can be assumed.

The first distributions of radial dose derived analytically by Butts and Katz [Butts and Katz, 1967] were soon confirmed by Monte Carlo track structure calculations of Paretzke [Paretzke, 1973], which were able to numerically simulate, step-by-step, all interactions of primary and secondary particles. The present track structure calculations performed with PARTRAC ([Friedland et al., 1998]), MOCA [Paretzke et al., 1974], Fluka [Battistoni et al., 2007], or Geant4 [Agostinelli et al., 2003] codes are all consistent and in good agreement with experiment, although their precision is not satisfactory at low ion energies [Hauptner et al., 2006].

In the analytical derivation of the amorphous radial distribution of average dose around the path of an energetic ion, the following assumptions were initially made:

- the ion moves in the medium along a straight path (ion scattering is ignored)
- only ionisations due to delta-electrons contribute to the average dose
- every ionisation contributes to the dose with the same average energy, ω
- there is axial symmetry of average energy deposition around the ion's path.

Following later studies, two more postulates were added:

- the contribution of excitations to the radial dose should also be included
- on radial integration, the $D(r)$ should yield the LET of the ion in the medium

The Radial Dose Distribution, $D(r)$, may be derived from eq. 2.2 or from other assumptions by calculating the average dose in a cylindrical shell of thickness dr located at radial distances r , $r + dr$ from the ion's path. Depending on the $D(r)$ formulations developed by different authors, the maximum dose where most of the energy transfer events occur, will appear around a selected cut-off radius (usually, $5 \cdot 10^{-11}$ or 10^{-10} m), or be constant up to a selected radius. Next the radial dose rapidly decreases, approximately as r^{-2} , and reaches zero at the maximum range of the delta-rays, as calculated from the electron energy-range relationships applied by their authors. Some of the published $D(r)$ formulae implemented in the libamtrack library are listed in Table 2.2.

Name	Expression	Reference
Katz	$D(r) = C_1 \frac{z^{*2}}{\beta^2} \frac{1}{r} \left(\frac{1}{r} - \frac{1}{r_{\max}} \right)$	[Zhang et al., 1985]
Zhang	$D(r) = C_1 \frac{z^{*2}}{\beta^2} \frac{1}{\alpha} \frac{1}{r} \frac{1}{r+\theta(I)} \left(1 - \frac{r+\theta(I)}{r_{\max}+\theta(I)} \right)^{\alpha-1}$	[Zhang et al., 1985]
Geiß	$D(r) = \begin{cases} C_2 & \text{if } 0 < r < a_0, \\ \frac{C_2}{r^2} & \text{if } a_0 \leq r \leq r_{\max} \end{cases}$	[Geiss et al., 1998]
Cucinotta	$D(r) = C_1 \frac{z^{*2}}{\beta^2} f(r) \frac{1}{r^2} + C_3 \frac{\exp(-\frac{r}{2d})}{r^2}$	[Cucinotta et al., 1997]

Table 2.2. Selected formulae describing the radial dose distribution, implemented in the libamtrack library. For further details, see Appendix A.

Katz derived his first $D(r)$ formula [Butts and Katz, 1967] analytically from Ruther-

ford's formula (eq. 2.2) assuming a linear delta-electron energy range relationship (denoted as Butts and Katz in Table 2.1).

Zhang later adapted this formula by accommodating a power-law electron energy range relationship (denoted as Waligórski in Table 2.1). Zhang's formula was further improved by Waligórski [Waligórski et al., 1986] who incorporated a correction effective at small radii in order for the radial integral of $D(r)$ to yield the correct value of LET of the ion (see Fig. 2.2, right panel). For further details, see Appendix A. For a thorough review of the consecutive developments of $D(r)$ formulae by Katz and co-workers, see [Korcyl, 2012]. In further calculations presented in Chapter 5 of this thesis the formula of Zhang, modified by setting the value of ionisation potential $I = 0$ (see Table 2.2) will be used.

Geiss in his derivation of the $D(r)$ used another expression for the electron energy-range relationship (see Appendix A), postulated a $\frac{1}{r^2}$ dependence of average radial dose with distance from the ion's path at radii exceeding a_0 (a free parameter) and a constant radial dose at smaller radii, the value of which is calculated via the ion's LET, assuring that when integrated radially, $D(r)$ should yield this value of LET [Geiss et al., 1998]. For further details, see Appendix A.

Cucinotta proposed a two-component radial dose distribution formula [Cucinotta et al., 1997], the first component describing the contribution to the average dose from ionisations and the second - from excitations. In the first component, the electron energy range formula of Tabata (see Table 2.1) is used and an angular distribution of delta-rays applied which is more complex than that given by Rutherford's formula (eq. 2.2) and the assumption of delta-ray emission at 90 degrees. The contribution of the second component due to excitations is significant at small radial distances. The constant C_3 applied in this formula (see Table 2.2) is calculated by making the radially integrated sum of both components equal to the value of ion's LET. This makes this $D(r)$ formula less convenient in massive calculations, because radial integration of both its components is required to calculate the above constants each time this formula is needed. For further details, the original paper of Cucinotta et al. [Cucinotta et al., 1997], [Korcyl, 2012] and Appendix A should be consulted.

2.4. Comparison of $D(r)$ formulae with experiment

While particle tracks, due to the size of silver bromide grains, can readily be observed in nuclear emulsion [Katz et al., 1972], it is quite difficult to measure experimentally the distribution of energy (or local dose) deposited around the path of an energetic ion. The main difficulty is in the small scale of this phenomenon, where maximum ranges of delta-electrons in solid media, or water, are typically of the order of micrometres or less. However, radial dose distributions around a few ion species have been measured in air, water vapour or tissue-equivalent gas, mainly by Wingate, Baum and Varma [Katz and Varma, 1992] using ionisation chambers to evaluate the absorbed dose (or exposure) at various distances by controlling gas pressure.

In Fig. 2.2 the radial dose distribution around 377 MeV/amu neon ions, measured by Varma et al. [Varma and Baum, 1980] in tissue-equivalent gas is compared with calculations using the above-discussed $D(r)$ formulae of Katz, Zhang, Geiss and Cucinotta. This comparison is rather of a qualitative nature, as Varma's experimental

data points did not include any assessment of their uncertainty. Disagreement of the original Katz's formulation of $D(r)$ at the low-dose range stems from his over-simplified electron energy-range relationship, invalid at higher delta-ray energies (see Fig. 2.1). The remaining $D(r)$ formulations show much better agreement, except for the formulation of Geiss (over the central dose region). For ease of comparison, the same data and results of $D(r)$ calculations are also shown in a plot where the linear ordinate is in terms of $D(r)r^2$ (the r^{-2} dependence of data points and of $D(r)$ calculations is then represented as a horizontal line). The "bump" in the experimental data around radial distances about 10^{-7} m was accounted for by the $D(r)$ formulation of Waligórski et al. [Waligórski et al., 1986] (not shown in Fig. 2.2). Monte Carlo simulations are able to represent the available experimental data to within an order of magnitude [Waligórski et al., 1986]. Zhang's formulation appears to offer the best agreement with experimental data.

2.5. Radial integration of D(r) and LET

According to the above-listed assumptions and postulates, since all the energy deposited around the ion's path is to be transferred by the delta rays, integration of the radial distribution of dose over all radii should yield the stopping power (or LET) of the ion, for a given track segment. For this reason, the correction of $D(r)$ by Waligórski et al. [Waligórski et al., 1986] and the later developed $D(r)$ formulations by Geiss [Geiss et al., 1998] and by Cucinotta et al. [Cucinotta et al., 1997] were designed to comply with this postulate.

Linear Energy Transfer L , by definition, is equal to the energy dE , deposited in the medium along the length dz of a track segment, divided by dz :

$$L = \frac{dE}{dz} \quad (2.3)$$

L is related to the average dose $\frac{dE}{dm}$ in track segment by the following relationship:

$$L = \frac{dE}{dz} = \frac{dE(\pi r_{\max}^2 - \pi r_{\min}^2)\rho}{dz(\pi r_{\max}^2 - \pi r_{\min}^2)\rho} = \frac{dE}{dm}(\pi r_{\max}^2 - \pi r_{\min}^2)\rho \quad (2.4)$$

where ρ is the density of the medium, and r_{\max} and r_{\min} are the maximum range of the delta rays and cutoff radius, respectively.

The average dose $\frac{dE}{dm}$ can be also calculated by radially integrating $D(r)$:

$$\frac{dE}{dm} = \frac{1}{\pi r_{\max}^2 - \pi r_{\min}^2} \int_{r_{\min}}^{r_{\max}} 2\pi r D(r) dr \quad (2.5)$$

From eq. 2.4 and eq. 2.5 the following relation between Linear Energy Transfer L and Radial Dose Distribution $D(r)$ holds for an ion track segment:

$$L = \left(\frac{1}{\pi r_{\max}^2 - \pi r_{\min}^2} \int_{r_{\min}}^{r_{\max}} 2\pi r D(r) dr \right) (\pi r_{\max}^2 - \pi r_{\min}^2)\rho \quad (2.6)$$

Therefore:

$$L = 2\pi\rho \int_{r_{\min}}^{r_{\max}} r D(r) dr \quad (2.7)$$

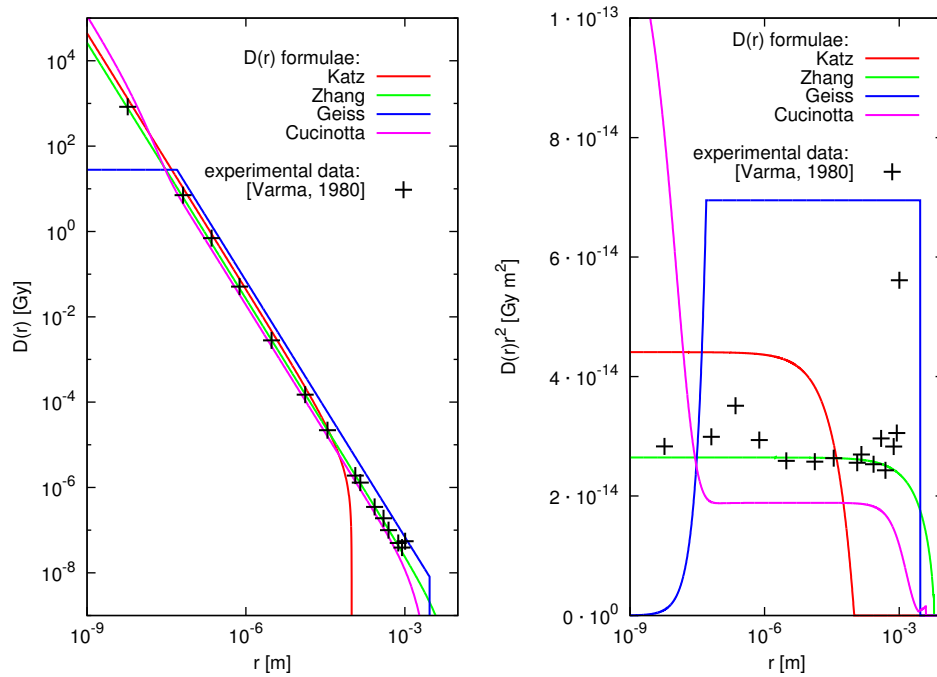


Figure 2.2. Comparison of experimentally measured radial distribution of dose around 377 MeV/amu neon ions in tissue-equivalent gas [Varma and Baum, 1980] and $D(r)$ calculated using the formulae of Katz, Zhang, Geiss and Cucinotta. Experimental uncertainties were not provided by Varma et. al. The right-hand panel shows the same data and calculations, but on a semi-logarithmic plot where data points and results of $D(r)$ calculations are multiplied by their respective r^2 values.

2.6. Conclusions

On the basis of Fig. 2.1 and its analysis, the electron energy-range formulae of Geiss, Waligórski and Tabata are found to represent the measured data well over the energy range of interest to ion radiotherapy, i.e. up to ion energy 400 MeV/amu.

Complexity of implementation and calculation time are important factors when considering the application of any $D(r)$ formulation in massive calculations required in treatment planning systems. For these reasons, the most accurate $D(r)$ formula of Cucinotta et al. which appears to best fulfil the requirements of such a $D(r)$ formula, was discarded, as evaluation of the constants in this formula requires multiple integrations every time this formula is needed in the TPS calculations or in fits to radiobiology data. Therefore, in further work the delta electron energy-range function listed here as Waligórski's was implemented in Zhang's $D(r)$ formula, however modified by neglecting the value of ionisation potential (i.e., by assuming $\theta = 0$ in that formula). Zhang's formula satisfies the postulated requirements well enough and with its simple analytical form, can be conveniently applied in the complex calculations presented in further chapters of this thesis.

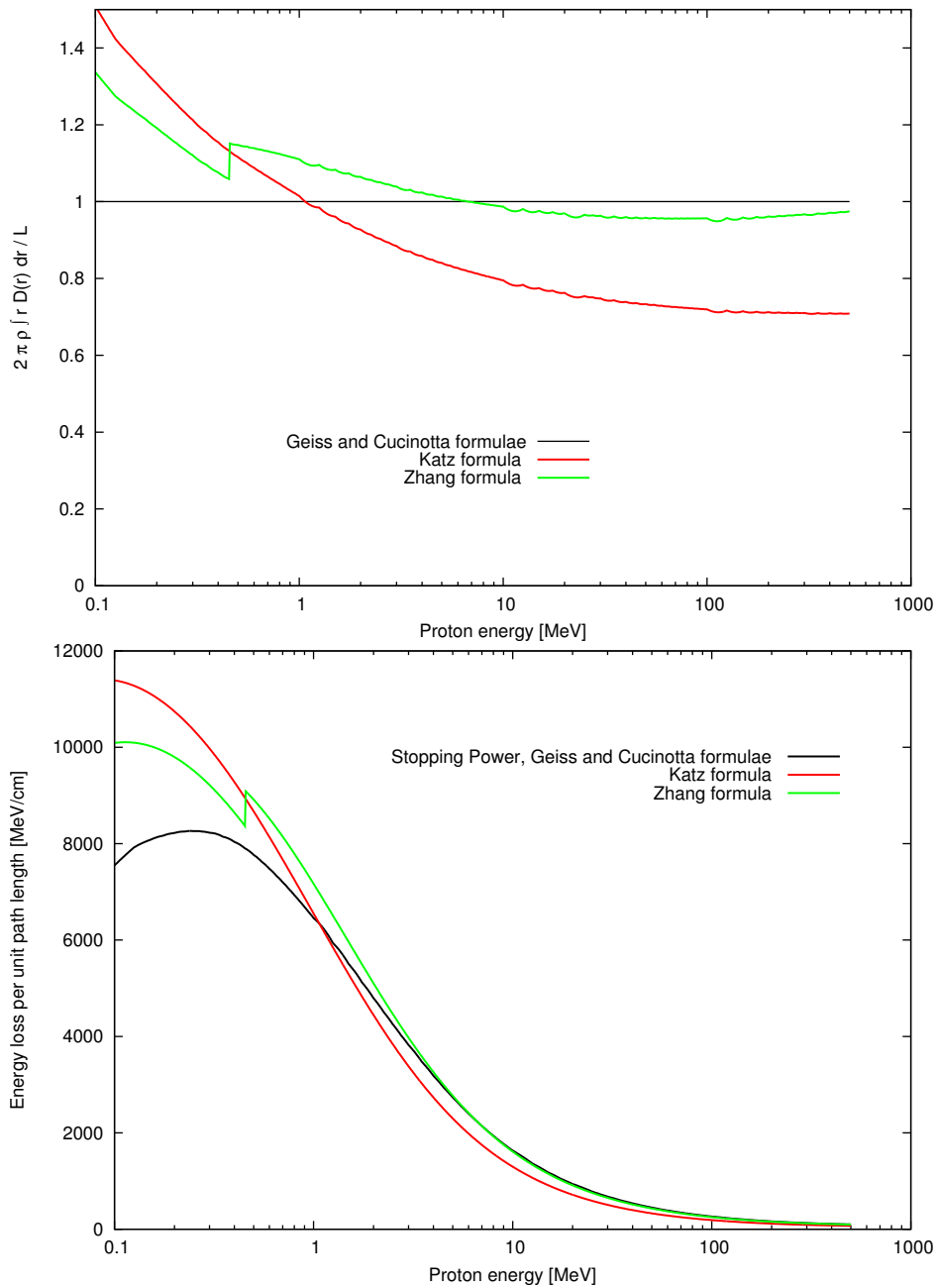


Figure 2.3. Upper plot: Ratio of the radially integrated $D(r)$ formulae of Katz and of Zhang ($\theta = 0$) and the values of LET versus proton energy. The formulae of Geiss and Cucinotta on radial integration return the values of LET by definition. Lower plot: Proton LET (i.e. the result of radial integration of the formulae of Geiss and Cucinotta) and results of radial integration of the $D(r)$ formulae of Katz and of Zhang ($I = 0$) vs. proton energy. As the LET values, the proton stopping power values from the PSTAR database [Berger et al., 2005] are used. Author's calculation based on the libamtrack library.

Chapter 3

The Katz model of cellular survival

The Cellular Track Structure model (the Katz model) is presented in detail and discussed. Following Korcyl's review of this model where model elements were recalculated and the scaling approximations originally introduced by Katz were generally confirmed, the analytically simple set of basic formulae of Katz's model will be termed here the *scaled version* of the model. The author's results of model calculations involving integration of its elements (thus termed the *integrated version* of Katz's model in what follows) suggest the possibility of further developing the Katz model. The author next justifies the use of the scaled version of the Katz model in further calculations and uses it to best fit model parameters from published data of in vitro survival of CHO (Chinese Hamster Ovary) cells after X-ray and ion irradiation. These cellular parameters and the principle of performing model calculations of cellular survival after mixed-field irradiation applied in Katz's model will be applied in later parts of this thesis.

3.1. Principles of the Katz model

Robert Katz introduced his Track Structure Theory (TST) model of RBE around 1960, basing it on the m-target formula to describe cellular survival after doses of reference radiation. In that aspect, the Katz model differs from the LEM where the linear-quadratic formula is applied. Katz's TST phenomenological analytical model is aimed at calculating the survival of biological cells and the response of physical detectors after ion irradiation. The model originates from the early works of Robert Katz and co-workers from Lincoln University, Nebraska [Katz et al., 1971]¹. The general assumption of this model is that the response of physical or biological detectors after ion irradiation can be calculated from the distribution of energy deposition (or

¹ Robert Katz and co-workers publications are freely available online on <http://digitalcommons.unl.edu/physicskatz/> by Digital Commons platform.

dose) around the ion track by scaling their response from their dose response after reference γ -rays.

Katz postulated that the probability of cellular survival after a dose D of radiation, $S(D)$, is a product of two probabilities, or modes of cell inactivation:

$$S(D) = \Pi_i(D) \cdot \Pi_\gamma(D) \quad (3.1)$$

Katz termed the first term of this product, $\Pi_i(D)$, ion-kill probability (since the cell is either “killed” or survives, the probability of “killing” a cell is $1 - S(D)$). $\Pi_i(D)$ assumes 1-hit probability of cell inactivation by direct passage of an ion:

$$\Pi_i(D) = \exp(-\sigma F) = \exp\left(-\frac{\sigma \rho}{L} D\right) \quad (3.2)$$

The inactivation cross section, σ , is calculated for a single ion. Here, F is ion fluence, related to ion dose D and ion LET, L , and density of the medium, ρ , via eq. 1.10. To evaluate σ , knowledge is required of the averaged (or extended target) radial dose distribution (see par. 3.2 below). In the second term in eq. 3.1, named gamma-kill probability (again, kill $K_\gamma(D) = 1 - S_\gamma(D)$), Katz assumes that the response of the cell system after doses of reference radiation, and also after delta-rays from overlapping ion tracks, is described by the multi-target formula:

$$\Pi_\gamma(D) = 1 - \left(1 - \exp\left(-\frac{(1-p)D}{D_0}\right)\right)^m \quad (3.3)$$

Here, D_0 is the radiosensitivity of the cell system and $(1-p)$ is the fraction of the ion dose, $D = \frac{1}{\rho} FL$, involved in gamma-kill mode. To calculate $\Pi_\gamma(D)$, values of the model parameters m and D_0 are needed, and knowledge of the value of p . The factor p , which may assume values in the range 0-1 and appears in the “ion-kill” and “gamma-kill” expressions, is the “mixing parameter” of the Katz model, which enables smooth transition between the purely exponential cell survival after ion irradiation and the m-target form if the system is irradiated only by γ -rays. In the case of irradiation by a dose D of reference γ -radiation only, $p \approx 0$ and the expression in brackets in eq. 3.3 becomes the usual m-target formula, eq. 1.12, while the “ion-kill” probability, eq. 3.2 then becomes unity. On the other hand, in the case of ion irradiation only, $p \approx 1$, hence the “gamma-kill” probability becomes unity and only the “ion-kill” term remains in eq. 3.1. The value of the model’s “mixing parameter” p may be interpreted as the degree of overlap of delta-ray “clouds” of neighbouring ions irradiating a cellular system, which strongly depends on the radial extension and ion charge-dependent dose values of the radial dose distributions of these ions. The value of p may either be evaluated by numerical calculations in the integrated version of Katz’s model (see par. 3.6) or calculated analytically from a formula in the scaled version of the model (see par. 3.7). The case of mixed radiation (i.e. cell irradiation by a mixture of ions of different charges and energies), of particular interest in this thesis, is discussed in paragraph 3.10 of this chapter.

Calculations in the Katz model are performed in two steps. First, the inactivation cross section of a single cell (target) by a single ion, σ , is calculated. Then, cellular survival is calculated by combining the inactivation cross section with ion fluences and doses resulting from the applied ion beams, where Π_i and Π_γ both contribute.

3.2. The extended target radial dose distribution

The Katz model assumes that the spatial distribution of dose delivered by X-rays or γ -rays to the entire target volume is homogenous. It also assumes that the spatial distribution of dose delivered by ions and surrounding delta-electrons is given by the radial dose distribution.

The analytical expressions of $D(r)$ discussed in Chapter 2 which describe the radial dose absorbed in an infinitesimally small volume at distance r from the path of the ion are called *point-target* distributions. By averaging the *point-target* dose distribution function D_p over a small cylindrical target of radius a_0 and length of a track segment dz (representing the cell nucleus or some volume contained within the cell, of size typically of the order of a few micrometres), another, averaged over target function, D_e , is obtained, which is called the *extended target* or *average dose* distribution:

$$D_e(r) = \frac{1}{S_r} \iint_{S_r} D_p(x, y) dx dy \quad (3.4)$$

where S_r is the target area, $S_r = \pi a_0^2$, located at a distance r from the path of the ion.

As long as the track segment assumption is valid, we can use averaging over surface, instead over volume averaging.

Assuming track-segment irradiation ($dE/dx = \text{const}$, track length dz), the integral in eq. 3.4 can be reduced to a two-dimensional intersection of the target volume. Furthermore, by changing the Cartesian coordinate system to polar coordinates, eq. 3.4 can be rewritten as follows:

$$D_e(r) = \frac{1}{\pi a_0^2} \int_{t_{\text{lower}}}^{a_0+r} D_p(t) \Phi(a_0, r, t) dt \quad (3.5)$$

where Φ is the length of an arc of radius t inside the target (a circle) of radius a_0 at the distance r from the ion track. More details on calculating extended target distributions of radial dose are given in Appendix B.

3.3. Probability of inactivation — the m-target formula

In the Katz model it is assumed that the target volume consists of several sensitive sub-targets. Each sub-target can change its state on being inactivated due to an energy deposition event from ionising radiation (in other words, by the target being hit).

The probability $P(n)$ that a single target or sub-target will be hit exactly n times is given by the Poisson distribution:

$$P(n) = f^n \frac{e^{-f}}{n!} \quad (3.6)$$

where f is the average number of hits. If D_0 is the dose after which, on average, each subtarget receives one hit, then the average number of hits, f , can be related to dose by:

$$f = \frac{D}{D_0} \quad (3.7)$$

The probability that a sub-target will receive one or more hits equals:

$$P(n \geq 1) = 1 - P(n = 0) = 1 - f^0 \frac{e^{-f}}{0!} = 1 - e^{-f} = 1 - e^{-\frac{D}{D_0}} \quad (3.8)$$

If the target contains only a single 1-hit sub-target, the probability of the target being inactivated is equal to $P(n \geq 1) = 1 - e^{-D/D_0}$. In case of an m-target configuration, where the target consists (on average) of m 1-hit sub-targets, the probability of target activation is given by the following general expression:

$$P = (1 - e^{-D/D_0})^m \quad (3.9)$$

This is the single-hit multi-target formula representing cellular survival after reference radiation, eq. 1.12, where survival is defined as the average number of targets not activated. In the Katz model it is assumed that cellular survival S after a dose D of reference radiation (X-rays or γ -rays) is described by this m-target expression:

$$S(D) = 1 - P = 1 - (1 - e^{-D/D_0})^m \quad (3.10)$$

Two parameters of the m-target expression, eq. 3.10: the radiosensitivity (or characteristic dose) D_0 and the number of 1-hit sub-targets in the target, m , can be obtained by fitting this equation to experimental data (e.g., cell survival curves after doses of reference radiation). Typically, for mammalian cells, D_0 is of the order of a few Gy and m is a number (not necessarily integer) ranging between 1 and 5.

One of the basic assumptions of amorphous track structure models is that the effect of a dose D non-homogenously distributed and deposited by delta-rays in a small target of size a_0 , is the same, per dose unit, as that of a dose D of reference radiation distributed homogenously. As already discussed, in the Katz model, survival curves after doses of reference gamma radiation are described ex definitione by the m-target formula, eq. 3.10, or eq. 1.12.

3.4. Inactivation cross-section

The probability of the target being “killed” or inactivated by an ion passing at a distance t from the target can be calculated from eq. 3.9, assuming a t -dependent distribution of extended target radial dose distribution, $D_e(t)$ where t is the radial distance between the ion path and the centre of the target:

$$P(t) = (1 - e^{-D_e(t)/D_0})^m \quad (3.11)$$

The *single-event inactivation cross section* is defined as an average probability $P(t)$ over all distances t available to the delta rays surrounding the ion, i.e. up to $r_{\max} + a_0$:

$$\sigma = \int_0^{r_{\max} + a_0} P(t) 2\pi t dt \quad (3.12)$$

In eq. 3.12 t can be interpreted as the ion's impact parameter, while r in the average radial dose distribution formula, $D_e(r)$, is the radial distance between the centre of the extended target and the ion's path. Equation 3.12 also obtains if the centre of the

extended target is considered to be displaced from the ion's path by a radial distance t , over the range of t from 0 to $r_{\max} + a_0$.

The unit of inactivation cross-section is cm^2 , i.e. that of area. Its value strongly depends on the ion's energy (which affects the extent of $D_e(t)$ via the maximum range of delta-rays, r_{\max}), and on the ion's charge (which affects the dose values in $D_e(t)$, via z^{*2}/β^2 of the ion).

In Fig. 3.1 are shown examples of systematic calculations of extended target cross sections for sensitive targets of different dimensions, in cellular systems of different radiosensitivity, versus ion LET (panel A) or z^{*2}/β^2 (panel B) for ions of different charges and different energies (as given by their relative speeds, β) [Korczyk, 2012]. In these calculations Zhang's $D(r)$ formula ($I = 0$) was used to calculate the respective extended target radial distributions of dose, $D_e(r)$. The calculated cross-section values have all been normalised to their plateau values, represented by σ_0 . Here, the scaling properties of the Katz model become evident: when plotted versus z^{*2}/β^2 (Fig. 3.1 panel B), rather than versus ion LET (Fig. 3.1, panel A), the activation cross sections for targets of widely differing sizes, calculated for ions of widely different charges and energies, appear to follow singular trends ("universal curves"), dependent on the target size and cell radiosensitivity, and only branching apart at their highest values (we note that in this example the m -target parameter remains the same, $m = 2.5$, in all calculations).

As may be observed in panel B of Fig. 3.1, the general trend of the dependence of the single-particle activation cross sections, versus z^{*2}/β^2 is as follows: with increasing z^{*2}/β^2 the cross sections first rapidly rise through several orders of magnitude, then saturate at some plateau values (represented by the σ_0 Katz model parameter) and next further increase to their maximum values and finally rapidly decrease, forming characteristic "hooks". For each family of inactivation cross-section dependences on z^{*2}/β^2 (as determined by parameters m , D_0 and a_0) one may find such a value κ on the z^{*2}/β^2 abscissa at which:

- if $z^{*2}/\beta^2 < \kappa$ - inactivation cross-sections increase,
- if $z^{*2}/\beta^2 \approx \kappa$ - inactivation cross-sections saturate at around $\sigma(z^{*2}/\beta^2) = \sigma_0$,
- if $z^{*2}/\beta^2 > \kappa$ - inactivation cross-sections increase above σ_0 and "hooks" occur.

The first region, where $z^{*2}/\beta^2 < \kappa$, is called *grain-count regime*, while the last one, $z^{*2}/\beta^2 > \kappa$ is called the *track-width regime*. These names, often used in the publications of Robert Katz, originate from his studies of ion tracks in nuclear emulsion: in tracks of ions of high energy (i.e., of low LET and low z^{*2}/β^2) ionizations appear mostly along the ion paths as sparsely distributed exposed grains. As the ion gradually slows down (i.e., as its LET and z^{*2}/β^2 increase) denser ionisations make the track continuous and then thicker and broader (hence the "track width" regime). Close to the end of the ion track (where LET and z^{*2}/β^2 are highest) the track appears to be very dense and then gradually thins down before it finally ends. Track "thin-down" effect is represented by the "hooks" in the cross-section calculations of Fig. 3.1. It is worth noting that the track thin down occurs over the region where LET is highest (i.e. over the Bragg peak region). Consequently, over the thindown region most of the dose may be "wasted", i.e. may not fully contribute to the biological effect, due to the limited range of the radial dose distribution.

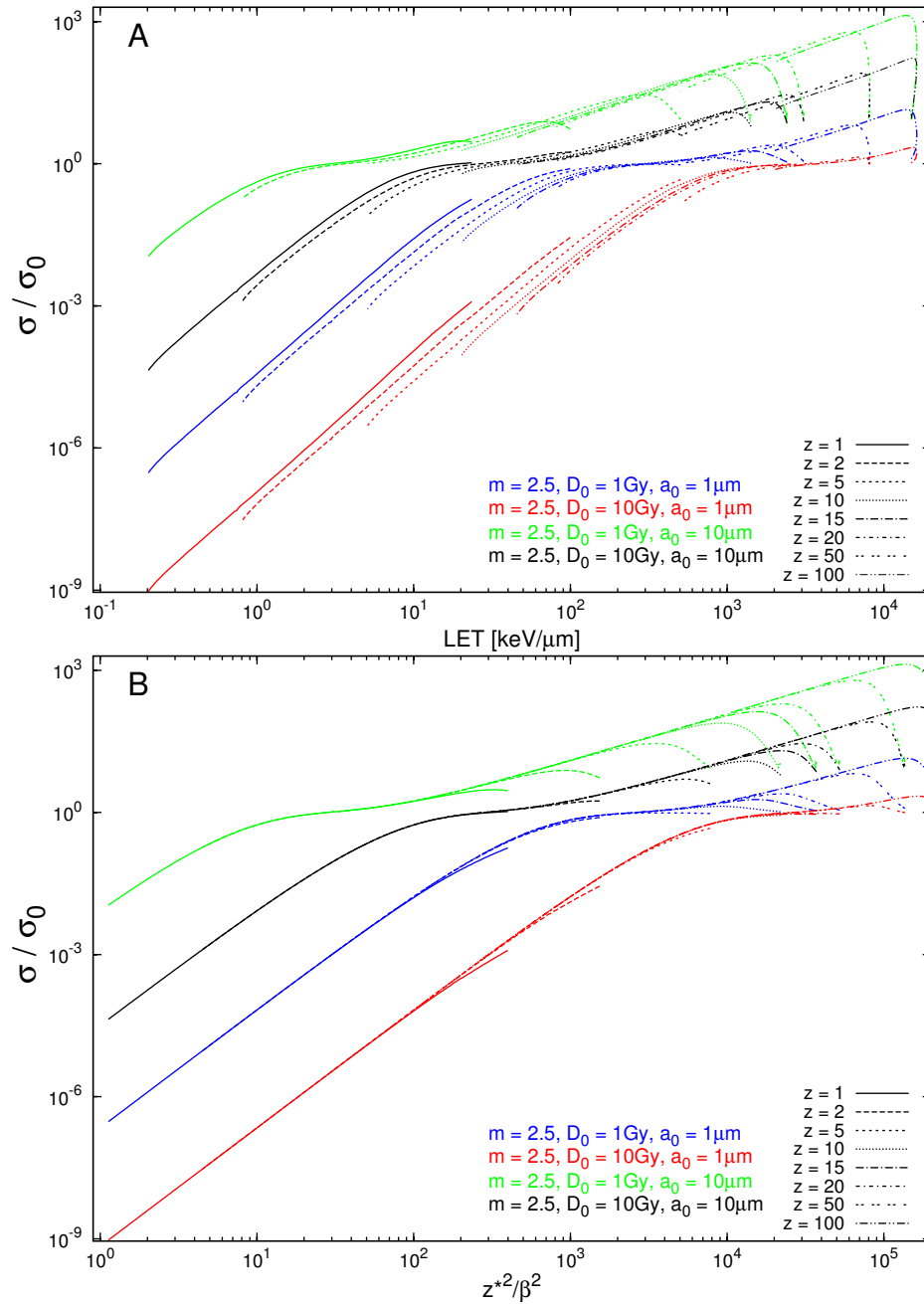


Figure 3.1. Inactivation cross-sections normalized to their plateau values (σ_0), plotted as a function of LET (panel A) or z^{*2}/β^2 (panel B) for $m=2.5$, $D_0 = 1\text{ Gy}$ or 10 Gy and $a_0 = 1\ \mu\text{m}$ or $10\ \mu\text{m}$. Each curve was plotted for ions with Z ranging from 1 to 100 and for relative ion speed β , from $\beta=0.05$ to $\beta=0.99$. The radial dose distribution function of Zhang was used in these calculations. Figure reprinted from Korcyl [Korcyl, 2012]

3.5. The ion-kill and gamma-kill modes of inactivation

As mentioned earlier in par. 3.1 ion-kill and gamma-kill modes of cell inactivation are introduced in Katz's model. The ion kill mode is related to passage of a single ion through the cell nucleus which results directly in cell death, i.e. a purely exponential survival curve. The probability of inactivation in the ion-kill mode Π_i is defined as:

$$\Pi_i = \exp(-\sigma F) \quad (3.13)$$

where F is the ion fluence and σ is the single-ion inactivation cross section.

In the case of ion irradiation, cell death in the gamma-kill mode is related to the overlap of delta rays emitted from different ions. In this case accumulation of effects from several delta-rays emitted from different ions is needed to produce a lethal effect. The gamma-kill mode of inactivation is represented by a shouldered survival curve (due to fact that typically, $m > 1$). The probability of inactivation in the gamma-kill mode is given by a formula based on the m-target model:

$$\Pi_\gamma = 1 - (1 - e^{-D_\gamma/D_0})^m \quad (3.14)$$

where D_0 and m are m-target model parameters and D_γ is a fraction P_γ of the ion dose D , delivered in gamma-kill mode:

$$D_\gamma = P_\gamma D \quad (3.15)$$

In Katz's model, the fraction P_γ of the ion dose delivered in the gamma-kill mode is assumed to be given by the following formula:

$$P_\gamma = \begin{cases} 1 - \sigma/\sigma_0 & \text{if } \sigma \leq \sigma_0 \\ 0 & \text{elsewhere} \end{cases} \quad (3.16)$$

where σ_0 is the saturation value of the inactivation cross-section σ . In the case of a monoenergetic beam of ions of one type, survival in the Katz model is defined as the product of gamma-kill and ion-kill components:

$$S = \Pi_i \Pi_\gamma \quad (3.17)$$

These two modes of inactivation are not mutually exclusive. The total ion dose D always contributes to the ion-kill mode and at the same time, a fraction of this total dose, D_γ contributes to the gamma-kill mode. Gamma kill dominates in the grain-count regime and ion-kill dominates in the track-width regime.

3.6. Algorithm of the integrated version of the Katz model

In this thesis a distinction is made between the *integrated* version of the Katz model (free parameters: m , D_0 , σ_0 and a_0) and the *scaled* version of the Katz model (free parameters: m , D_0 , σ_0 and κ). Here, the integrated version is discussed, while the scaled version is discussed in the next paragraph.

The single-particle inactivation cross-section can be calculated using formula of Section 3.4, equation 3.12. This leads to a model with four free parameters: m , D_0 ,

σ_0 and a_0 . Once the single-particle inactivation cross section is known, calculation of cell survival for different ion doses (or fluences) can be readily performed, using the ion-kill and gamma-kill mode formulae 3.13-3.17.

The calculation algorithm consists of the following steps:

Step A — calculation of inactivation cross section:

$$D_e(r) = 1/\pi a_0^2 \int_{r_{\min}}^{a_0+r_z} D(r)\Phi(a_0, r, t)tdt \quad (3.18)$$

$$P(t) = (1 - e^{-D_e(t)/D_0})^m \quad (3.19)$$

$$\sigma = \int_0^{r_{\max}+a_0} P(t)2\pi t dt \quad (3.20)$$

Step B — calculation of ion- and gamma-kill modes:

$$P_\gamma = \begin{cases} 1 - \sigma/\sigma_0 & \text{if } \sigma \leq \sigma_0 \\ 0 & \text{elsewhere} \end{cases} \quad (3.21)$$

$$D_\gamma = P_\gamma D \quad (3.22)$$

$$\Pi_\gamma = 1 - (1 - e^{-D_\gamma/D_0})^m \quad (3.23)$$

$$\Pi_i = e^{-\sigma F} \quad (3.24)$$

$$S = \Pi_\gamma \Pi_i \quad (3.25)$$

This calculation becomes more involved if cellular survival needs to be calculated after irradiation by different ions species of different energies, in which case double integration is required to calculate each single-particle inactivation cross section. This is a time consuming procedure. Evaluation of extended target dose from equation 3.5 requires calculation of the integral of function $D(t)\Phi(t)t$ which cannot be done analytically. The result of this calculation is substituted into equation 3.9 and again integrated in equation 3.12 to calculate the inactivation cross-section.

While Katz performed several such calculations to establish the scaling principles of his analytic Cellular Track Structure Theory (termed in this thesis the scaled version of his model), to apply the above approach to best-fit model parameters to survival data was impractical, as 30-40 years ago when numerical integration was a much more time-consuming task than it is today. The novel approach in this thesis is to investigate the possible introduction of an “integrated version of the Katz model” in modelling cellular survival.

One of the advantages of this integrated version of the Katz model is that it offers the possibility of applying any radial dose distribution function to describe ionisation distributions around the ion’s path. In particular, in the integrated version of the Katz model it would be possible to include Geiss’s radial dose distribution function and perhaps the linear-quadratic description of cellular survival (both are used in the LEM). It would then be interesting to investigate differences between LEM and Katz’s model approaches if the same radial dose distribution function is used in the calculations, and perhaps also if two different representations of cellular survival curves are applied.

3.7. Algorithm of the scaled version of the Katz model

The Cellular Track Structure Theory which Robert Katz [Katz et al., 1971] originally proposed, consists of a set of simple analytical formulae in which the scaling properties of his track structure approach are exploited. The possibility of applying $z^{*2}/\kappa\beta^2$ as a scaling factor in calculating inactivation cross sections is demonstrated in Fig. 3.1. A key result from Katz's numerical calculations involving multiple integrations (called here the integrated version and performed in a manner described in the preceding paragraph), was the observation that $z^{*2}/\kappa\beta^2$ could be used to scale the results of such calculations. The possibility of such scaling is closely related to choice of the point target radial dose distribution formula, $D(r)$, and to the choice of the m-target formulation in describing cellular survival after doses of reference radiation. A careful re-analysis of the scaling properties of Katz's model equations was performed by Marta Korcyl [Korcyl, 2012] and has been submitted for publication [Korcyl et al., 2013]

In Fig. 3.1 inactivation cross sections calculated for different ion species of different energies using Zhang's radial dose distribution and plotted versus $z^{*2}/\kappa\beta^2$ are seen to form families of overlapping curves. Similar behaviour is also observed if Katz's radial dose distribution function is used in such calculations, but not if Cucinotta's formula is applied [Korcyl, 2012]. If we neglect the region of "hooks" in Fig. 3.1, then for each family of curves of the same colour a "universal" dependence can be drawn, as a scaled approximate representation of inactivation cross-section for ions various values of Z and β .

Robert Katz proposed the following formula for the "universal curve" $g(m, x) = (1 - \exp(-x))^m$, which would be a valid approximation of inactivation cross-section in the grain-count regime:

$$\frac{\sigma}{\sigma_0} = g(m, z^{*2}/\kappa\beta^2) = (1 - \exp(-z^{*2}/\kappa\beta^2))^m \quad (3.26)$$

In the track-width regime there is no simple "universal" formula, but a high order polynomial $f(m, z^{*2}/\kappa\beta^2)$ can be fitted to the curves calculated using eq 3.12.

As values of $z^{*2}/\kappa\beta^2$ increase, the value of $g(m, z^{*2}/\kappa\beta^2)$ converges to unity. The g function will not reach exactly unity, thus 0.98 is taken as the value at which saturation is achieved. At this value smooth transition to approximation of the cross-section by polynomial f is possible.

The presently used formulae of the original Katz model (here termed as the scaled version of this model) are the following

For $(1 - \exp(-z^{*2}/\kappa\beta^2))^m < 0.98$:

$$\sigma = \sigma_0(1 - \exp(-z^{*2}/\kappa\beta^2))^m \quad (3.27)$$

and elsewhere:

$$\sigma = \sigma_0 f(m, z^{*2}/\kappa\beta^2) \quad (3.28)$$

where f is a polynomial approximation of the inactivation cross section.

The algorithm of the scaled Katz model calculation consists of the following steps:

Step A — calculation of inactivation cross section:

$$\sigma = \begin{cases} \sigma_0(1 - \exp(-z^{*2}/\kappa\beta^2))^m & \text{if } (1 - \exp(-z^{*2}/\kappa\beta^2))^m < 0.98 \\ \sigma_0 f(m, z^{*2}/\kappa\beta^2) & \text{elsewhere} \end{cases} \quad (3.29)$$

Step B — calculation of ion- and gamma-kill modes:

$$P_\gamma = \begin{cases} 1 - \sigma/\sigma_0 & \text{if } \sigma \leq \sigma_0 \\ 0 & \text{elsewhere} \end{cases} \quad (3.30)$$

$$D_\gamma = P_\gamma D \quad (3.31)$$

$$\Pi_\gamma = 1 - (1 - e^{-D_\gamma/D_0})^m \quad (3.32)$$

$$\Pi_i = e^{-\sigma F} \quad (3.33)$$

$$S = \Pi_\gamma \Pi_i \quad (3.34)$$

3.8. Comparison between Scaled and Integrated versions of the Katz Model

As presented above, a distinction was made in this thesis between the integrated version of the Katz model, where the free model parameters are: m , D_0 , σ_0 and a_0 , and the scaled version of the Katz model, where the free parameters are: m , D_0 , σ_0 and κ . It should be stressed that when fitting either of these versions of the Katz model to e.g., experimental data points on measured survival curves of cells in vitro, the values of best fitted parameters using either approach may differ.

Representations of the cross section in the scaled approach ignore the presence of “hooks”, or track thindown over the final parts of ion tracks. Over this region, where $z^{*2}/\kappa\beta^2 > 1$ and ions are in their Bragg peak region, values of inactivation cross sections calculated using integrated and scaled versions of the Katz model differ by up to an order of magnitude. However, satisfactory agreement between results of these two versions over the grain count regime ($z^{*2}/\kappa\beta^2 < 1$) and the fact that the “hook” regions constitute only a small fraction of the ion’s total range at ion energies of interest to radiotherapy, justifies the use of the scaled (i.e. the original) version of the Katz model. It is much simpler and faster to calculate in applications relevant to ion radiobiology and radiotherapy planning.

It appears that z^{*2}/β^2 scaling in Katz’s model may be applicable only to selected radial dose distributions [Korcyl, 2012]. This is illustrated in Fig. 3.2 where results of scaled and integrated model calculations of inactivation cross sections, obtained using the Katz $D(r)$ formula are compared. Calculations were performed over a broad range of ion energies (0.1 - 500 MeV/amu) and ion species ($Z = 1 \dots 100$).

In Fig. 3.3 a similar comparison is made, but after calculations based on Zhang’s radial dose distribution formula, demonstrating that better agreement between results of either version of the model can be obtained using Zhang’s $D(r)$ formulation.

The scaling elements of Katz’s model, such as the “universal curve”, eq. 3.26, which is apparent, e.g., in Fig. 3.3, could not be established for cross sections calculated using radial dose distribution formulae of Geiss or of Cucinotta, both of which satisfy the LET condition, eq. 2.7, by definition [Korcyl, 2012]. Thus, while they would

not appear to be suitable for use in the scaled version of Katz's model, use could be made of either of these $D(r)$ formulae in the integrated version. It would be particularly interesting to apply Geiss's $D(r)$ formula in such calculations, since it is used in LEM. The integrated version of Katz's model could be applied in radiobiology modelling but it is too computation-intensive to be used in radiotherapy planning. While, in principle, the processing times of the nested numerical integrations could be significantly reduced by special programming techniques, such as parallel code execution, application of the integrated version of the Katz model in radiotherapy planning would still be impractical.

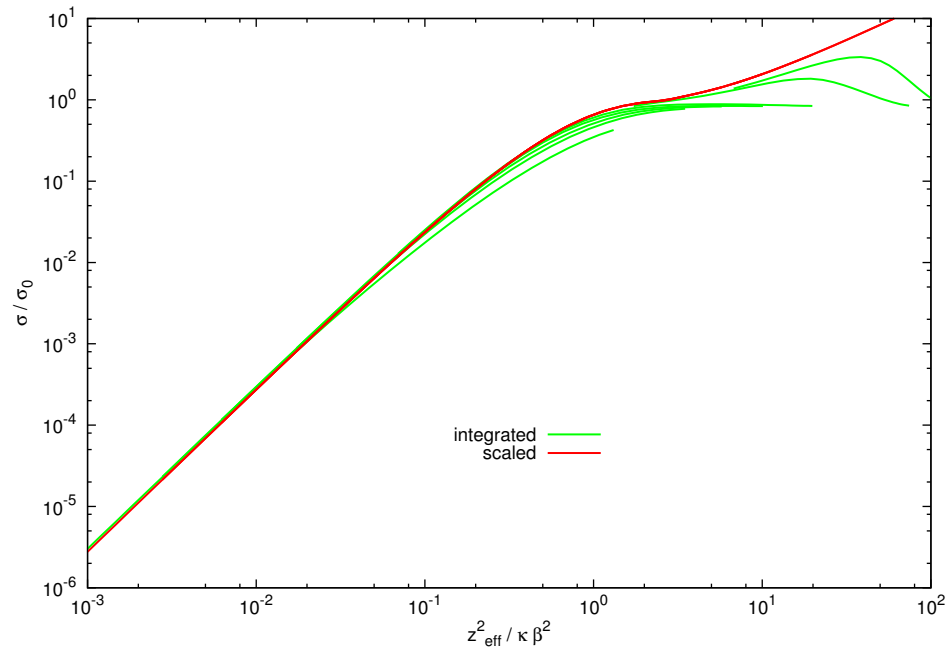


Figure 3.2. Inactivation cross-sections, normalised to σ_0 vs. $z^{*2}/\kappa\beta^2$, based on the radial dose distribution function of Katz. Calculations were performed using the integration (green lines) and scaled (red lines) versions of the Katz model, for ions of $Z=1,2,3,5,10,50$ and 100 and energies $0.1 - 500$ MeV/amu. Katz model parameters used: $m = 2$, $D_0 = 5$ Gy, $a_0 = 1\mu\text{m}$, $\kappa = 1500$, $\sigma_0 = 1.2 \pi a_0^2$

3.9. Fitting Katz model parameters from cell survival data

Values of cellular parameters of the Katz model were extracted from the published set of cellular survival curves measured after irradiation of Chinese Hamster Ovary (CHO) cells by carbon ion beams, data of Weyrather et al. [Weyrather et al., 1999]. Data points on the published survival curve plots [Weyrather et al., 1999] were digitized and formed into a data base from which values of four parameters of the Katz model (scaled version) were found, such that model-predicted values of these data points were best reproduced, as determined by the minimum value of χ^2 . Computer codes of the libamtrack library were used for this purpose.

The implementation of Katz's model in the libamtrack library was used in the following configuration:

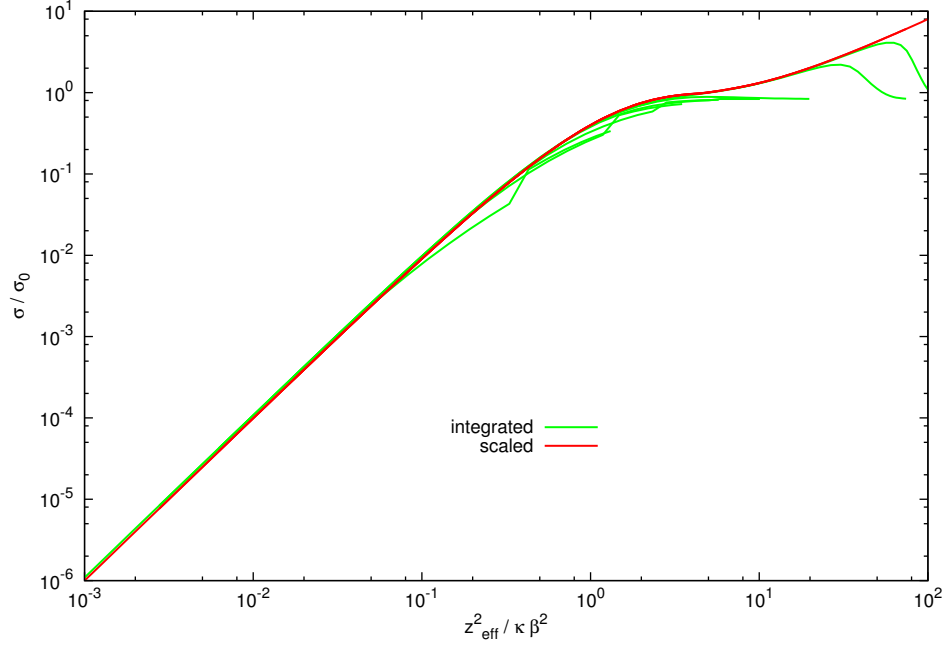


Figure 3.3. Inactivation cross-sections, normalised to σ_0 vs. $z^{*2}/\kappa\beta^2$, based on the radial dose distribution function of Zhang. Calculations were performed using the integration (green lines) and scaled (red lines) versions of the Katz model, for ions of $Z=1,2,3,5,10,50$ and 100 and energies $0.1 - 500$ MeV/amu. Katz model parameters used: $m = 2$, $D_0 = 5$ Gy, $a_0 = 1 \mu\text{m}$, $\kappa = 2500$, $\sigma_0 = 1.2 \pi a_0^2$

- Waligorski delta electron range model
- Zhang radial dose distribution function
- inactivation cross section calculated with the approximation method
- stopping power tables based on PSTAR database

Fitting of the Katz model parameters to the experimental data was performed by minimizing χ^2 defined as the sum of squared differences between model-predicted and experimental values of all data points (logarithm of survival) obtained from irradiation of CHO cells by ion beams and by reference radiation (250 kVp X-rays) :

$$\chi^2 = \chi_{\text{ion}}^2 + \chi_{\text{Xrays}}^2 \quad (3.35)$$

In the χ_{ion}^2 - ion beam component of the χ^2 sum, survival $S_{\text{Katz,ion}}$ was calculated using Katz's model (scaled version):

$$\chi_{\text{ion}}^2 = \sum_E \sum_D (\ln(S_{\text{Katz,ion}}(D, E)) - \ln(S_{\text{experiment,ion}}(D, E)))^2 \quad (3.36)$$

In the X-ray component of the χ^2 sum, survival $S_{\text{model,Xrays}}$ was calculated using the m-target formula:

$$\chi_{\text{Xrays}}^2 = \sum_D (\ln(S_{\text{model,Xrays}}(D)) - \ln(S_{\text{experiment,Xrays}}(D)))^2 \quad (3.37)$$

where:

$$S_{\text{model,Xrays}}(D) = 1 - (1 - \exp(-D/D_0))^m \quad (3.38)$$

Data published by Weyrather contain six survival curves, and in total $n = 103$ data points.

The numerical algorithm of gradient minimization L-BFGS-B (implemented in python scipy library, [Zhu et al., 1997]) was used to minimize the χ^2 function (χ^2 gradient was approximated numerically). The minimization algorithm was implemented by the author in Python programming language, cell survival calculations were implemented in the libamtrack library. As the starting point of L-BFGS-B, the following parameters were selected:

$$m = 2 \quad D_0 = 5 \text{ Gy} \quad \sigma_0 = 1.42 \cdot 10^{-12} \text{ m}^2 \quad \kappa = 1230 \quad (3.39)$$

The minimization algorithm allows limits to be set on the parameter space. In this case search for best fitted parameters was limited by following conditions:

$$\begin{aligned} 1 &< m < 5 \\ 1.1 \text{ Gy} &< D_0 < 3 \text{ Gy} \\ 10^{-13} \text{ m}^2 &< \sigma_0 < 10^{-9} \text{ m}^2 \\ 200 &< \kappa < 5000 \end{aligned} \quad (3.40)$$

As a result of the calculation, four best fitting parameters were found:

$$m = 2.31 \quad D_0 = 1.69 \text{ Gy} \quad \sigma_0 = 5.96 \cdot 10^{-11} \text{ m}^2 \quad \kappa = 1692.8 \quad (3.41)$$

Such parameter values lie well within the range of typical values of cellular parameters of the Katz model published in the literature [Katz and Sharma, 1974].

The goodness of the fit, expressed as $\chi^2/(n - n_{\text{dof}})$ is equal to 0.0061. Here n_{dof} denotes the number of degrees of freedom which here is equal to the number of parameters ($n_{\text{dof}} = 4$).

Substituting $p_1 = m$, $p_2 = D_0$, $p_3 = \sigma_0$, $p_4 = \kappa$, elements C_{jk} of the Hesse matrix of second derivatives of χ^2 may be written as:

$$C_{jk} = \frac{\partial^2 \chi^2}{\partial p_j \partial p_k} (p_1^{\text{opt}}, p_2^{\text{opt}}, p_3^{\text{opt}}, p_4^{\text{opt}}) \text{ where } j, k = [1 \dots 4] \quad (3.42)$$

and $p_1^{\text{opt}}, p_2^{\text{opt}}, p_3^{\text{opt}}, p_4^{\text{opt}}$ are the parameters for which the χ^2 function is at minimum.

Assuming Gaussian errors on the measured data, uncertainties of the fitted parameters may be read from the correlation matrix diagonal C_{jj}^{-1} , estimated from the inverse Hesse matrix:

$$\sigma_j^2 = \frac{\chi^2(p_1^{\text{opt}}, p_2^{\text{opt}}, p_3^{\text{opt}}, p_4^{\text{opt}})}{n - n_{\text{dof}}} C_{jj}^{-1} \quad (3.43)$$

The uncertainties of the best-fitted parameter values, calculated by numerical evaluation of the correlation matrix are:

$$m^{\text{err}} = 0.026 \quad D_0^{\text{err}} = 0.016 \text{ Gy} \quad \sigma_0^{\text{err}} = 9.45 \cdot 10^{-13} \text{ m}^2 \quad \kappa^{\text{err}} = 9.7 \quad (3.44)$$

In Fig. 3.4 comparison is shown between the Katz model-predicted survival curves (based on best-fitted parameters) and experimentally measured data points, over the dose range 0-10 Gy of carbon ion beams (of energies 4.2, 11, 18, 76.9 and 266.4 MeV/amu) and 250 kVp X-rays. Although model calculations reproduce the experimental data quite well, for two survival curves (11 MeV and 18 MeV carbon ions) cell survival is overestimated by these calculations.

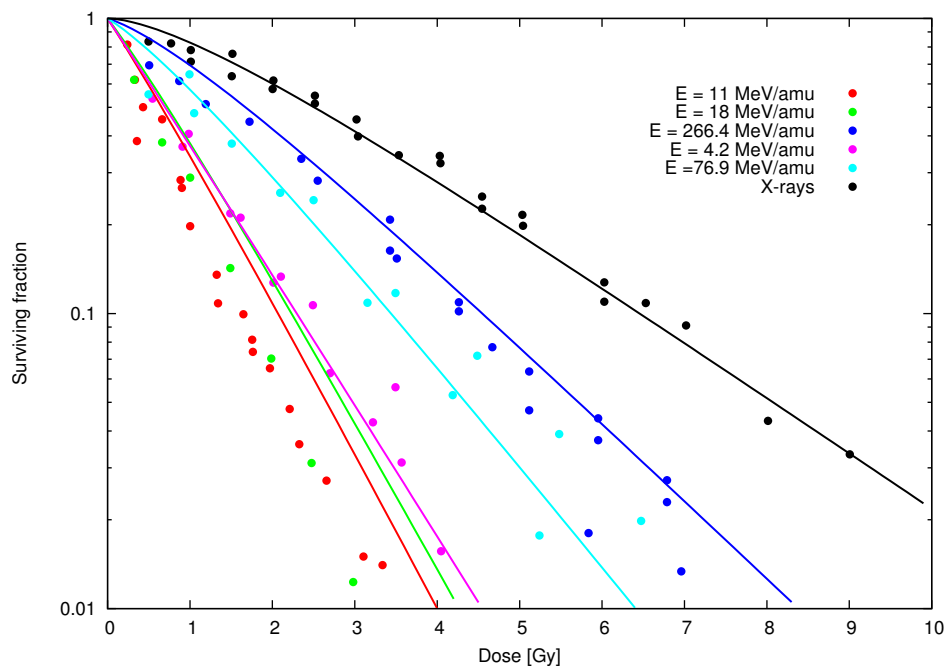


Figure 3.4. Katz model-predicted CHO cell survival curves (based on best-fitted parameters) and experimentally measured data points for carbon beams (of energies 4.2, 11, 18, 76.9 and 266.4 MeV/amu) and for 250 kVp X-rays. The experimental data is from [Weyrather et al., 1999]. The Katz model parameters are: $m = 2.31$, $D_0 = 1.69 \text{ Gy}$, $\sigma_0 = 5.96 \cdot 10^{-11} m^2$, $\kappa = 1692.8$ Calculations based on the libamtrack library.

3.10. Mixed-field calculations

Katz model parameters were derived in the previous section under the assumption that all irradiations were performed using monoenergetic carbon ions. In mixed radiation fields, irradiation by a set of carbon ions of different energies and by different ion species, due to carbon fragmentation, needs to be accounted for. Track segment irradiation is assumed, i.e. that the energy and fluence of each ion species are specified. According to the principles of the Katz model, gamma kill and ion kill need to be calculated for each component and combined together to yield the final cell survival. The following procedure of a mixed-field calculation has been proposed by Katz [Katz et al., 1971]:

Let us assume that the total dose D is delivered as a sum of N dose components

$D_i (i = 1 \dots N)$ due to N ions, each of charge $Z_i (i = 1 \dots N)$, energy $E_i (i = 1 \dots N)$. Let the respective fluence of each component be denoted as F_i .

Let P_i be fraction of the dose D_i delivered in gamma-kill mode by the i -th field component, defined as:

$$P_i = \begin{cases} \sigma_i/\sigma_0 & \text{if } \sigma_i \leq \sigma_0 \\ 1 & \text{elsewhere} \end{cases} \quad (3.45)$$

where σ_i is the inactivation cross section for the i -th component.

The combined ion-kill mode survival is then equal to:

$$\Pi_i = \exp\left(-\sigma_0 \sum_{i=1}^N P_i F_i\right) = \prod_{i=1}^N \exp(-\sigma_0 P_i F_i) \quad (3.46)$$

The combined gamma-kill mode survival is equal to:

$$\Pi_\gamma = \left(1 - \left(1 - \exp\left(-\frac{1}{D_0} \sum_{i=1}^N (1 - P_i) D_i\right)\right)^m\right) \quad (3.47)$$

Finally, the combined surviving fraction SF can be written as the product of both modes

$$S = \Pi_i \Pi_\gamma \quad (3.48)$$

In the ion kill mode the total surviving fraction is a product of ion kill survivals of the components, according to equation 3.46. In the gamma kill mode the total surviving fraction is neither a product nor a sum of surviving fractions of the components. The overall result is calculated by estimating the contribution of each component to the ‘‘ion dose’’ and then mixed using the non-linear m-target formula, as shown in equation 3.47.

3.11. Conclusions

The Katz model (here termed as its scaled version) is a fast and reliable method to describe and predict biological cell survival in carbon ion beams. The model has been continuously developed over the last 50 years [Katz and Cucinotta, 1999], [Korcyl, 2012]. One of the aims of this thesis was to demonstrate the features of the model (here - its integrated version) if integration is applied explicitly, as compared to its usual analytical form (scaled version). In the scaled version, track thindown, as represented by ‘‘hooks’’ in the cross-section dependences at the highest ion LET values, is neglected. This may lead to discrepancies for slow, stopping ions. For ions of energies relevant in radiotherapy, the predictive capability of the Katz model (its scaled version) is quite satisfactory. Due to its analytic simplicity, it is extremely time-efficient in computation. The model offers a well-specified procedure for calculating cellular survival in mixed ion fields, provided that energy-fluence spectra are available for all the ion field components.

The author of this thesis has implemented in the freely available open-source libam-

track library both versions of the Katz model: Katz's original formulation (scaled version) and the integrated version.

The scaled version of Katz's model, applying Zhang's radial dose distribution formula, was used by the author to find best-fitted values of model parameters describing cell survival of CHO cells irradiated with carbon ions. Although the overall agreement between model predictions and experiment is quite satisfactory, model calculations overestimate the measured survival of these cells after low energy (11 MeV/amu and 18 MeV/amu) carbon ions. This variant of the Katz model will be applied in later calculations in Chapter 5 of this thesis.

The best fitted values of the Katz model parameters will be applied in the mixed-field calculations of survival of CHO cells in a realistic carbon beam model. This beam model includes ion fragmentation and spread-out Bragg peak (SOBP) configuration, as discussed in Chapter 4 of this thesis.

Modelling the Transport of Carbon Beams

A therapeutic carbon ion beam travelling through the patient's tissues undergoes a complicated pattern of interactions, including slowing down, scattering and ion fragmentation. In order to apply the Katz model to calculate survival of cells of those tissues after their exposure to this carbon beam, prior knowledge of fluence and energy spectra of primary and secondary particles is required at all beam depths. The region of the spread out Bragg peak, which is adjusted to match the tumour volume, is one where establishing such energy-fluence spectra may be particularly difficult.

In this chapter an approach is developed and presented which allows energy-fluence spectra of carbon ions and all fragments to be calculated at different depths in water. The results of Monte-Carlo transport calculations of the carbon beam in water performed by Pablo Botas using the SHIELD-HIT10A code (Aarhus branch of the original development line) [Gudowska et al., 2004], [Hansen et al., 2012] were organized in the form of a look-up database attached to the libamtrack library. The author of this thesis developed an interpolation algorithm to calculate fluence and energy values at intermediate energies, and also a tool to calculate a linear combination of pristine Bragg peaks which gives the desired depth-dose profile (i.e. a flat depth-dose distribution over the Spread-Out Bragg Peak region). The developed codes are now included in the libamtrack library.

4.1. Monte-Carlo simulations and energy-fluence spectra.

4.1.1. Monte-Carlo simulations of carbon ion beams.

The SHIELD hadron transport code performs Monte Carlo simulation of the interaction of hadrons and atomic nuclei with complex extended targets. Its medical version, SHIELD-HIT (Heavy Ion Therapy), is designed to simulate interactions of therapeutic beams of protons and heavier ions with human tissues over the energy range relevant for radiotherapy. Models of nuclear reactions which describe various stages

of the inelastic hadron-nucleus and nucleus-nucleus interactions, developed mainly by Demenyev and Sobolevsky at JINR (Dubna) and INR RAS (Moscow), are applied. The models are grouped together in the MSDM-generator (Multi Stage Dynamical Model) which allows simulation of a whole chain of nuclear reactions. Ionization losses of charged hadrons and nuclear fragments in SHIELD-HIT10A are calculated according to the Bethe-Bloch equation but include various models and data for computation of mean ionization loss, fluctuations of the ionization loss and of multiple Coulomb scattering.

Transport of 50-500 MeV/amu carbon ion beams in water was simulated using SHIELD-HIT10A by Pablo Botas (DKFZ). Results of Monte-Carlo (MC) simulations concerned primary beam attenuation, beam broadening with increasing depth and production of secondary fragments. Fluences of the primary beam and its fragments were scored over planes perpendicular to the ion paths and averaged. Thus, a one-dimensional set of energy-fluence spectra versus depth was obtained for a large number of carbon beams over a large range of initial energies. It is in principle possible to extend the existing MC simulation to obtain results in three-dimensional sets by increasing significantly the number of simulated particles and using a three-dimensional scoring grid (or to assume rotational symmetry and use only two-dimensions with cylindrical scoring volumes). SHIELD-HIT10A results were applied in this work as they reproduced the experimental data well [Gudowska et al., 2004] and because the code was suitable for producing spectral data in binary form. Other Monte Carlo codes, such as Geant4, FLUKA and PHITS were considered for this purpose, but their application would require more effort in adapting their output to the existing libamtrack environment.

4.1.2. The energy-fluence spectra database in the libamtrack library — SPC files

A module for reading and writing energy-fluence spectra in binary format was implemented in the libamtrack library. Binary SPC file format is used in the TRiP98 treatment planning system and also in the Siemens “Syngo PT Planning” carbon therapy planning system at HIT, Heidelberg. The author of this thesis participated in implementing the SPC module in the libamtrack library. In the libamtrack code library a sample set of SPC files is provided. Each file contains spectra of carbon ions in water at various depths for a number of initial beam energies. Files included in the libamtrack library cover the range of initial carbon beam energies between 50 MeV/amu and 400 MeV/amu. A typical SPC file¹ contains energy fluence spectra at 50 depths, densely covering the region of the Bragg peak and less densely over the entrance channel. At each depth, spectra of up to 6 different ion species (from protons to carbon ions) are provided. At each depth and for each ion species, the energy histogram is divided into bins of the same width, containing fluences of particles of corresponding energy.

¹ <http://bio.gsi.de/DOCS/TRiP98/DOCS/trip98fmtspc.html>

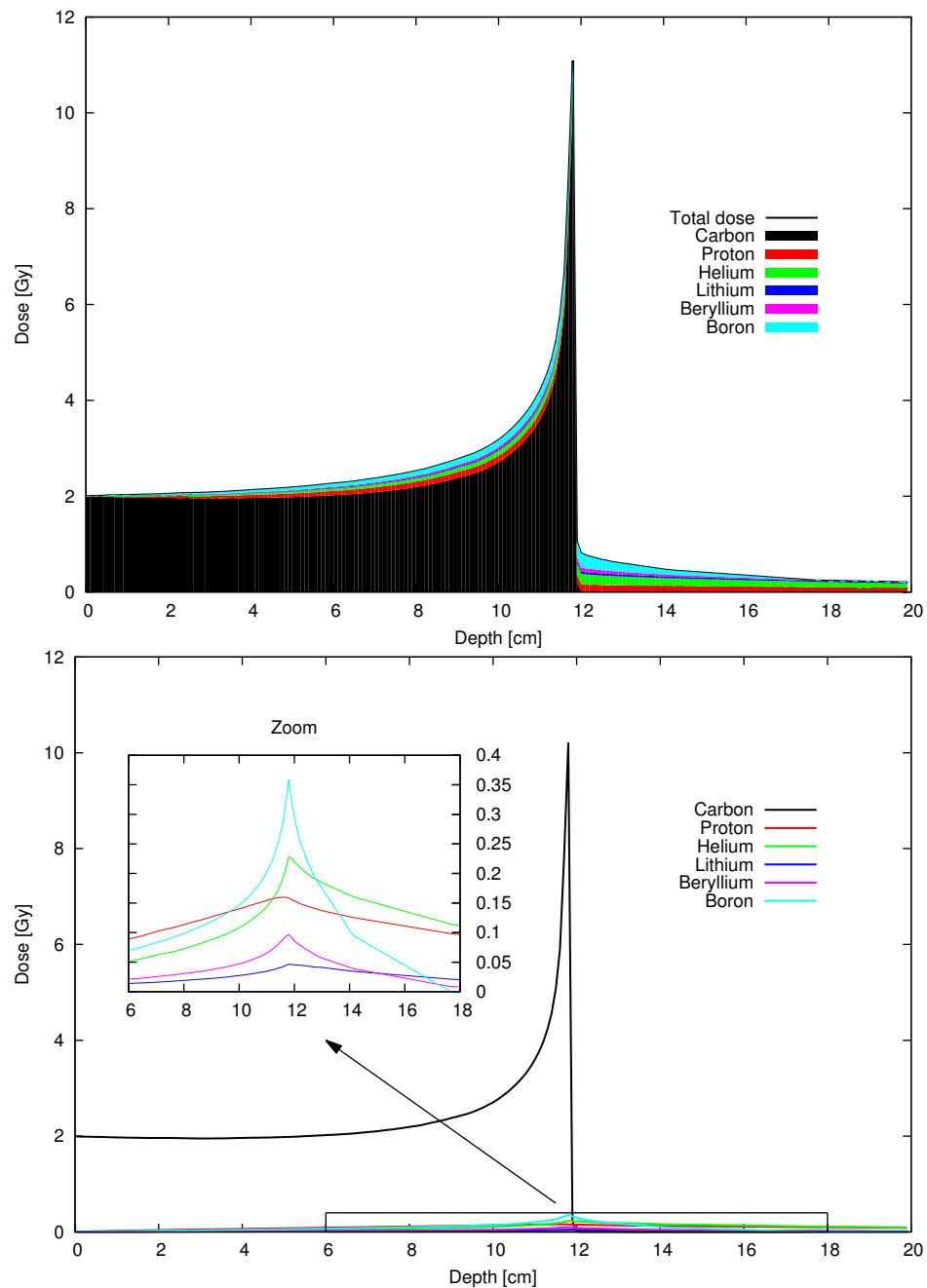


Figure 4.1. Dose vs depth of a carbon beam of initial energy 270 MeV/amu in liquid water and of beam fragments. Data extracted from data sets available in the libam-track library, were generated using the SHIELD-HIT10A code [Gudowska et al., 2004]. The entrance channel dose is 2 Gy. Upper panel: cumulative representation. Lower panel: individual depth-dose distributions of the primary beam and of secondary ion species. In the lower panel the 6-18 cm depth region is magnified to better visualise the individual dose contributions of secondary particles. Data beyond the depth of 20 cm have not been plotted.

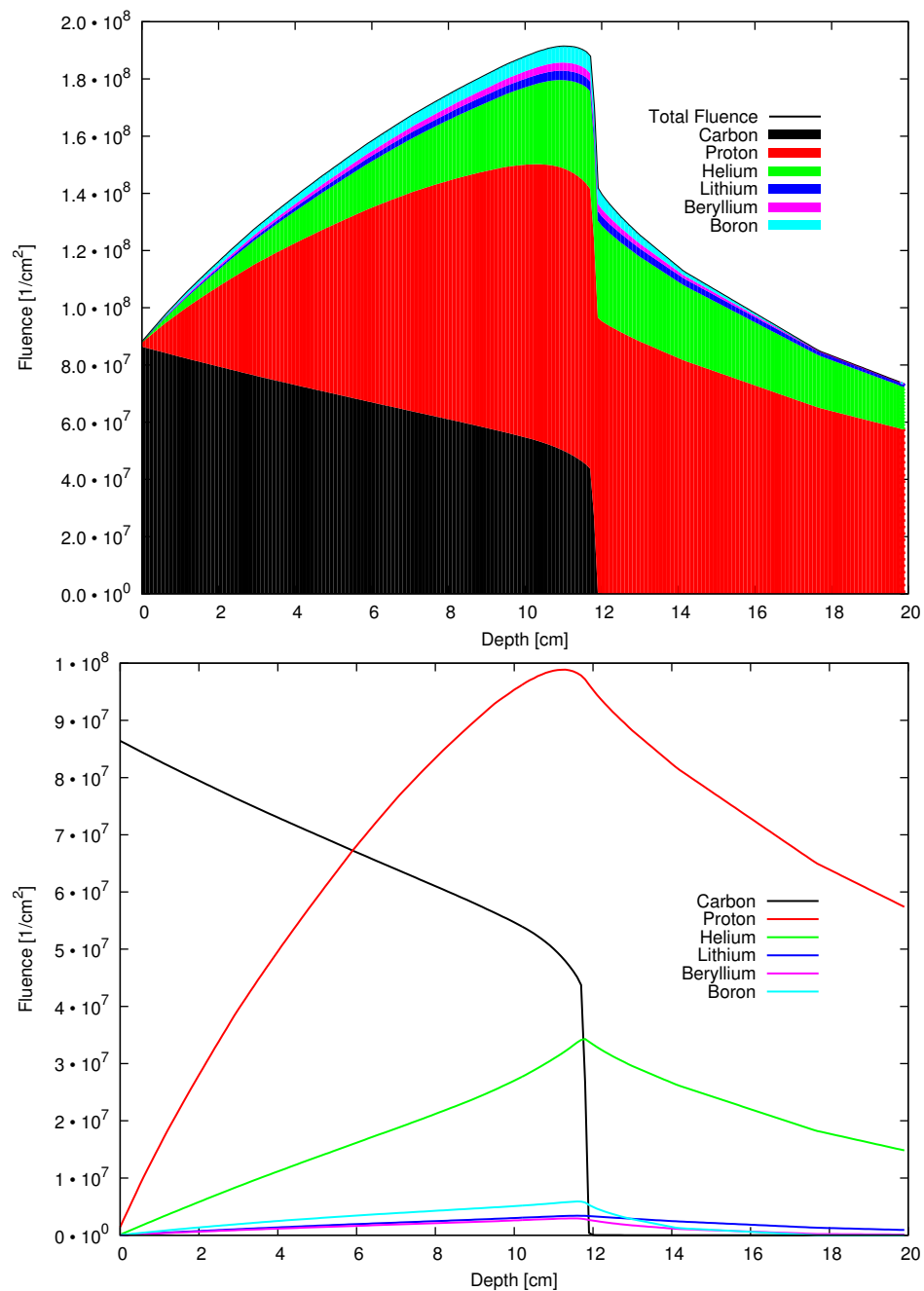


Figure 4.2. Fluence vs depth of a carbon beam of initial energy 270 MeV/amu in liquid water and of beam fragments. Data extracted from data sets available in the libamtrack library, were generated using the SHIELD-HIT10A code [Gudowska et al., 2004]. The primary beam fluence in the entrance channel was adjusted to represent the beam entrance dose of 2 Gy, to conform with Fig. 4.1. Upper panel: cumulative representation. Lower panel: individual depth-fluence distributions of the primary beam and of secondary ion species. Data beyond the depth of 20 cm have not been plotted.

4.1.3. Algorithm for interpolation of the energy-spectrum data files.

Energy-fluence spectra at an arbitrary depth in water d for a carbon beam of initial energy E can be interpolated from the discrete SPC files using the following algorithm. Interpolation is performed in the following steps:

1. Over the initial beam energy,
2. Over penetration depth
3. Over energy in the energy-fluence spectrum.

Let us calculate the fluence F of particles (fragments) of charge Z , and energy E , at depth d in a beam of initial energy E_{in} : $F(Z, E, d, E_{\text{in}})$. Two SPC files are taken, with initial beam energies $E_{\text{in,min}}$ and $E_{\text{in,max}}$ closest to E_{in} . The initial energy interpolation is performed as follows:

$$F(Z, E, d, E_{\text{in}}) = (1 - \alpha)F(Z, E, d, E_{\text{in,min}}) + \alpha F(Z, E, d, E_{\text{in,max}}) \quad (4.1)$$

where $\alpha = (E_{\text{in}} - E_{\text{in,min}})/(E_{\text{in,max}} - E_{\text{in,min}})$. The next step is to interpolate between depths: two depths d_{min} and d_{max} , closest to d are needed (assuming they are at the same depth binning as those for $E_{\text{in,min}}$ and $E_{\text{in,max}}$):

$$\begin{aligned} F(Z, E, d, E_{\text{in,min}}) &= (1 - \beta)F(Z, E, d_{\text{min}}, E_{\text{in,min}}) + \beta F(Z, E, d_{\text{max}}, E_{\text{in,min}}) \\ F(Z, E, d, E_{\text{in,max}}) &= (1 - \beta)F(Z, E, d_{\text{min}}, E_{\text{in,max}}) + \beta F(Z, E, d_{\text{max}}, E_{\text{in,max}}) \end{aligned}$$

where $\beta = (d - d_{\text{min}})(d_{\text{max}} - d_{\text{min}})$.

The next step is to interpolate between energies in energy-fluence spectra (histograms): two energies E_{min} and E_{max} , closest to E are needed (assuming there is the same energy binning for d_{min} and d_{max}):

$$\begin{aligned} F(Z, E, d_{\text{max}}, E_{\text{in,min}}) &= (1 - \gamma)F(Z, E_{\text{min}}, d_{\text{max}}, E_{\text{in,min}}) + \gamma F(Z, E_{\text{max}}, d_{\text{max}}, E_{\text{in,min}}) \\ F(Z, E, d_{\text{max}}, E_{\text{in,max}}) &= (1 - \gamma)F(Z, E_{\text{min}}, d_{\text{max}}, E_{\text{in,max}}) + \gamma F(Z, E_{\text{max}}, d_{\text{max}}, E_{\text{in,max}}) \\ F(Z, E, d_{\text{min}}, E_{\text{in,min}}) &= (1 - \gamma)F(Z, E_{\text{min}}, d_{\text{min}}, E_{\text{in,min}}) + \gamma F(Z, E_{\text{max}}, d_{\text{min}}, E_{\text{in,min}}) \\ F(Z, E, d_{\text{min}}, E_{\text{in,max}}) &= (1 - \gamma)F(Z, E_{\text{min}}, d_{\text{min}}, E_{\text{in,max}}) + \gamma F(Z, E_{\text{max}}, d_{\text{min}}, E_{\text{in,max}}) \end{aligned}$$

where $\gamma = (E - E_{\text{min}})/(E_{\text{max}} - E_{\text{min}})$.

Energy-fluence spectra stored in SPC data files are normalized to entrance fluence of 1 cm^{-2} , thus a method was provided to normalize spectra to the fluence corresponding to a given entrance dose (i.e. 2 Gy). Methods to access SPC data are provided in the AT_SPC module in the libamtrack library.

4.1.4. A sample calculation of energy-fluence spectra

In Fig. 4.2 fluences of the ion species generated by a 270 MeV/amu carbon beam in water are shown as a function of depth and of ion energy. The range in water of this carbon beam is about 12 cm. The fluence of carbon ions decreases from its initial value ($8.8 \cdot 10^7 \text{ cm}^{-2}$, corresponding to 2 Gy) to zero at depths beyond 12 cm. Buildup of secondary fragments is observed at all depths. The contribution to the total fluence of protons and helium ions is the highest. The total particle fluence, understood as

the fluence of carbon ions plus the fluence of all fragments, at some depths exceeds the fluence of carbon ions in the entrance channel (see Fig. 4.2). This is because in nuclear reactions a single ion may produce several secondary fragments - ions of lower charges.

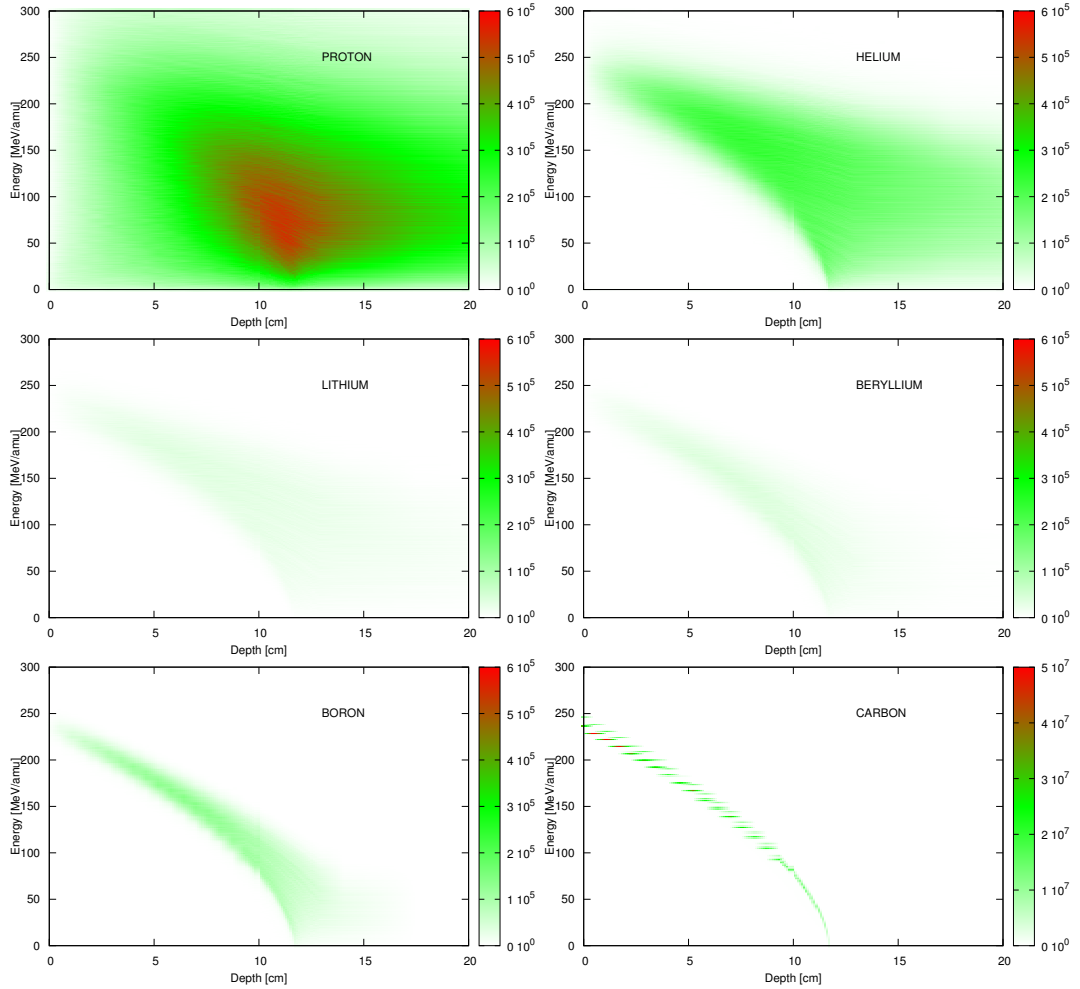


Figure 4.3. Fluences of primary and secondary ions primary carbon beam of initial energy 270 MeV/amu in liquid water, shown as a function of depth (along the x-axis) and energy (along the y-axis). The entrance carbon beam dose is 2 Gy. On each panel energy-fluence spectra are shown for each ion species (protons thru carbon). The fluence values for the different ions are represented by different colours: red is the highest (range: $5 \cdot 10^7 \text{cm}^{-2}$ to $6 \cdot 10^5 \text{cm}^{-2}$), green - intermediate values, white background - no ions (fluence=0).

4.2. Optimization of dose vs. depth distributions

4.2.1. The depth-dose profile optimization algorithm

The Spread-Out Bragg Peak (SOBP) is a depth dose distribution curve composed of several pristine Bragg peaks to form a uniform dose distribution in the region of interest

(in proton radiotherapy) or a predefined shape of depth dose distribution, designed to obtain uniform biological response over that region (in carbon radiotherapy).

The SOBP is created as a sum of pristine Bragg peaks, produced by beams with different initial energies and different intensities (fluences). The position (depth) of the pristine Bragg peak maximum increases with initial energy and the peak amplitude is proportional to the initial dose (or fluence). One of the methods of passive beam shaping is application of a rotating energy modulator, where the ion beam traverses absorber sectors, each of different thicknesses placed on the modulator ring. The thickness of the absorber determines the position of the pristine Bragg peak and the fraction of time the beam passes through the given sector - the relative amplitude of the pristine beam component in the SOBP.

Adjustment of the positions $\{p\}_i$ and heights $\{h\}_i$ of pristine Bragg peaks in order to obtain a “flat” or constant dose over a given depth range can be formulated as an optimization problem. Let us consider a continuous function $f(x)$, representing dose (or survival) depth profile which is required to be flat and equal to a value C over a range of depths x between a and b . A measure of flatness M_{ftn} of such a curve can be defined as:

$$M_{\text{ftn}}(p_1, \dots, p_m, h_1, \dots, h_m) = \sum_{j=1}^n (f(x_j, p_1, \dots, p_m, h_1, \dots, h_m) - C)^2 \quad (4.2)$$

where $\{x\}_j$ forms a regular grid of n points over the interval $[a, b]$. If M_{ftn} equals 0, function f does not show any significant oscillations. If the $\{x\}_i$ grid is dense enough, function $f(x)$ is flat and almost equal to C over the interval $[a, b]$.

To simplify calculations it can be assumed that positions of pristine Bragg peaks p_i also form a regular grid inside the interval $[a, b]$. We seek such heights h_i of the Bragg peaks for which the measure M_{ftn} of flatness is as close to zero as possible.

The function f describes a sum of pristine Bragg peaks with maxima at p_i and heights h_i :

$$f(x_j, p_1, \dots, p_m, h_1, \dots, h_m) = \sum_{i=1}^m h_i f(x_j, p_i) \quad (4.3)$$

where $f(x, p)$ is dose at a depth x in a pristine Bragg peak with a maximum at p and height equal to 1.

Numerical problem of finding minimum of function M_{ftn} is well-defined as the minimized function is a quadratic form with partial derivatives which can be calculated analytically:

$$\frac{\partial M_{\text{ftn}}}{\partial h_i} = \frac{\partial}{\partial h_i} \sum_{j=1}^n \left(\sum_{i=1}^m h_i f(x_j, p_i) - C \right)^2 = \sum_{j=1}^n 2 \left(\sum_{i=1}^m h_i f(x_j, p_i) - C \right) f(x_j, p_i) \quad (4.4)$$

Thus the gradient minimization method can be used to find the coefficients $\{p\}_i$. The above method was implemented by the author in python language and added to the libamtrack library. Dose in carbon ion pristine Bragg peaks was interpolated from SPC data sets.

The procedure of generating SOBPs can be extended to find such coefficients of pristine Bragg peaks that their linear combination gives any arbitrary depth-dose profile $g(x)$ over the interval $[a, b]$. Here instead of a measure of flatness we define another parameter M_{prf} , which tells us how close is the linear combination of pristine Bragg peaks to the desired profile $g(x)$:

$$M_{\text{prf}} = \sum_{j=1}^n (f(x_j, p_1, \dots, p_m, h_1, \dots, h_m) - g(x_j))^2 \quad (4.5)$$

where $\{x\}_j$ form a regular grid of n points over the interval $[a, b]$. As in the previous case, such a numerical problem can be solved by gradient minimization methods. This method was also implemented by the author in python language and added to the libamtrack library. The author also implemented a version of this algorithm optimized for parallel execution on machines with multiple processor cores. Optimization is based on dividing the grid $\{x\}_j$ into as many parts as the number of cores in the computer, and calculating parts of the sum in M_{prf} in parallel. Calculations were performed by the author using the Cracow Cloud infrastructure at IFJ PAN in Krakow [Chwastowski et al., 2012] and at the Academic Computer Centre ACK Cyfronet AGH in Krakow.

4.2.2. A sample calculation of a flat dose vs. depth profile

In a sample calculation the algorithm described in the preceding paragraph was used to calculate a combination of Bragg peaks of carbon ion beams of different initial energies and fluences to produce a flat depth dose profile over the range between 8 and 12 cm in liquid water.

In the calculations pristine Bragg peaks were used, which show narrow shapes of their Bragg peak (compared i.e. to pristine proton beams). The typical full width of a carbon Bragg peak at half maximum is about 3 mm. In the sample calculation 49 Bragg peaks were used to obtain a flat dose profile over a 40 mm region spanning between 8 and 12 cm in depth. Maximum deviations from the desired dose level of 1 Gy are below 1 (see Figure 4.4, upper panel) which is acceptable within standards applied in clinical radiotherapy. Using more Bragg peaks would lead to lower deviations. The experimentally observed “smearing out” of the initial energy of a pristine Bragg peak by inserting PMMA elements of variable thickness into the beam also results in broader shapes of the Bragg peaks and in decreasing any deviations from flatness of the dose profile. A depth profile of cell survival was also calculated for this flat dose profile, using the Katz model with parameters previously fitted in chapter 3 of this work (cf. Fig. 3.4). The resulting profile is also shown in Figure 4.4 (lower panel). As could be expected, while the dose over the region between 8 and 12 cm is constant, cell survival varies between 50% and 75%. This is due to changes with depth of energy spectra in the SOBP of the carbon ions and of their fragments, resulting in their biological effectiveness increasing with depth. To obtain a flat dose distribution over depths between 8 and 12 cm, carbon beams of initial energies ranging between 191.5 MeV/amu and 242.5 MeV/amu have to be applied with carefully adjusted fluence contributions, related to the dose required over the flat part of the depth-dose distribution. The required initial energy-fluence spectrum of these beams is shown in Figure 4.5.

The right-most peak of the highest fluence, corresponding to the component with the highest energy represents the pristine carbon beam of the highest energy and range in water of about 12 cm. The remaining components of lower fluence and lower initial energies contribute to the dose distribution over lower depths.

To demonstrate the efficiency of the optimization algorithm used to achieve the flat depth-dose distribution shown in Fig. 4.4, the degree of convergence vs. number of iteration steps is shown in Figure 4.6. Flatness of the dose distribution was evaluated on a grid consisting of 200 points equally spaced between 8 and 12 cm. The algorithm stopped after 68 steps at a minimum value of $\chi^2 = 0.000512$. The maximum and minimum dose values found over the flat region were 1.007351 and 0.990312, respectively, against the target value of 1 Gy, i.e. deviating by less than 1%. As may be seen in Fig. 4.6, reasonable convergence was obtained after about 35 iteration steps.

4.3. Conclusions

As the result of SHIELD-HIT10A Monte-Carlo simulations of the transport in water of pristine carbon beams with initial energies ranging between 50 and 500 MeV/amu, a set of look-up files in SPC format containing energy-fluence spectra of primary carbon ions and their fragments at various depths was available to the author. In these simulations, the Bragg peak region was covered by a denser grid to obtain better accuracy in the section where high dose gradients and larger fluences of secondary ions arise. The author developed and implemented an interpolation algorithm to estimate energy-fluence spectra at the desired beam ranges for all contributing ion species. Using this algorithm, data could be efficiently extracted from the look-up tables (as shown in Fig. 4.3) and applied in further calculations.

The energy-fluence interpolation procedure was necessary for enabling the pristine carbon beams to be combined into a spread-out Bragg peak configuration in order to obtain a flat depth-dose distribution over a given depth range. An optimisation algorithm was developed for this purpose by the author, whereby the fluences and initial energies of a given number of pristine carbon beams could be found which, when combined together, gave the required depth-dose profile with satisfactory precision. The required dose profile can be made flat over a pre-defined depth range, or assume any other shape. The developed optimisation algorithm showed good convergence and computing efficiency. The accuracy of the optimized solution, of better than 1%, would fulfil the requirements of clinical radiotherapy.

By suitably adding at pre-designed beam depths all ion contributions of the ion beam combination configured to yield the desired depth-dose profile, it was possible to implement the mixed-field calculation of cellular survival according to the principles of the scaled version of the Katz model, developed in the preceding parts of this thesis (Chapter 3). The best-fitted values of the four parameters of Katz's model, representing CHO (Chinese Hamster Ovary) cells were applied in this mixed-field calculations for the carbon beam combination, showing that applying a uniform (flat) dose profile to irradiate these cells would result in a highly non-uniform depth distribution of cellular survival. The results obtained in this chapter will be further developed to find combinations of pristine carbon beams of different energies and fluences to yield the desired flat depth-survival distributions.

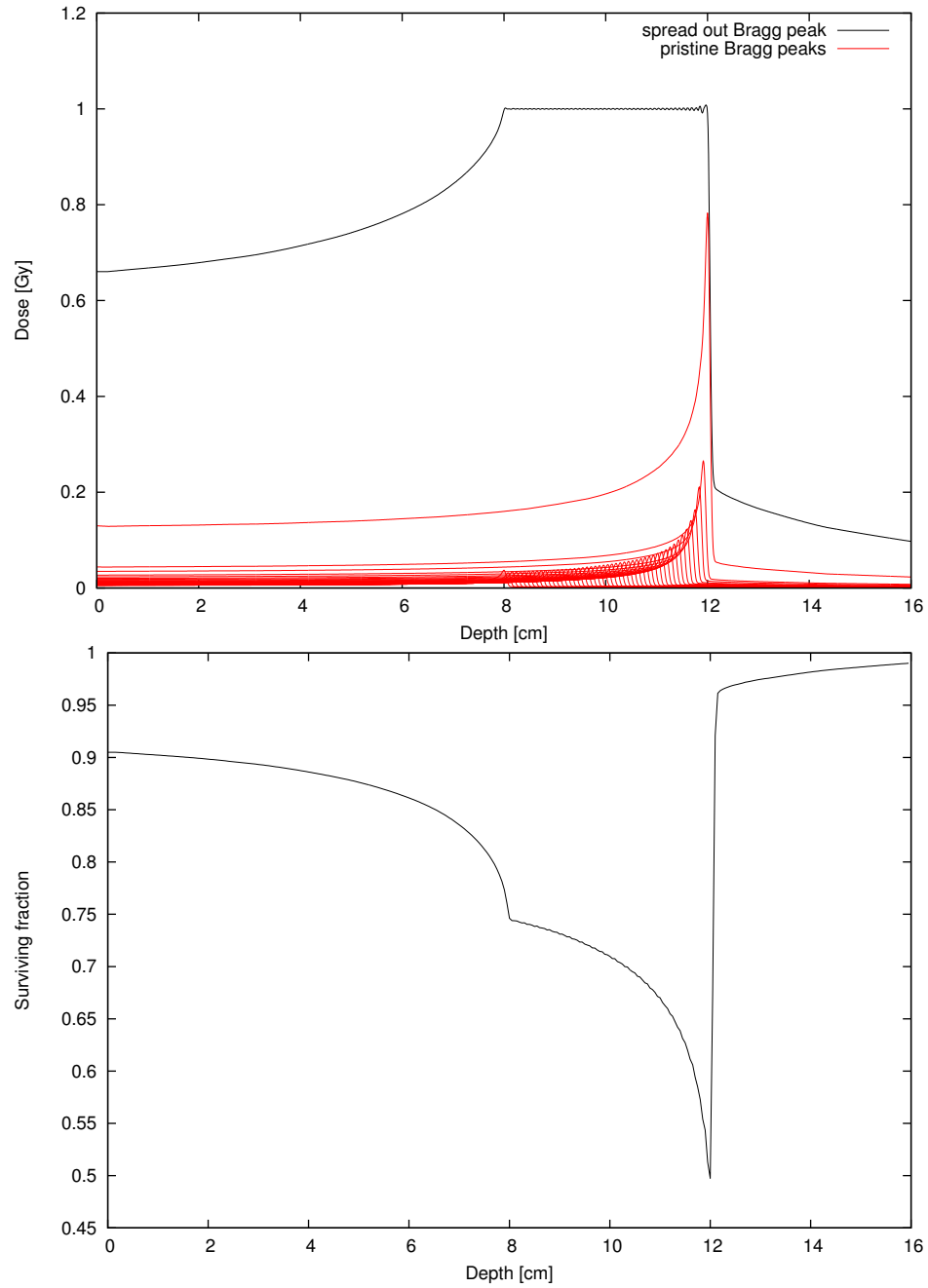


Figure 4.4. Upper panel: A flat depth-dose distribution of 1 Gy over the depth range 8-12 cm, obtained by summing the contributions of Bragg peaks of 49 pristine carbon beams of different initial energies and fluences (see Fig. 4.5). Lower panel: Survival vs. depth of CHO cells irradiated by the carbon beam with flat dose distribution shown in the upper panel. Calculations of CHO cell survival vs. depth were performed using the scaled Katz model, where CHO cells were represented by model parameters $m = 2.31$, $D_0 = 1.69$ Gy, $\sigma_0 = 5.966 \cdot 10^{-11}$ m², and $\kappa = 1692.8$ (see par. 3.9). All calculations were performed for liquid water, using the libamtrack library.

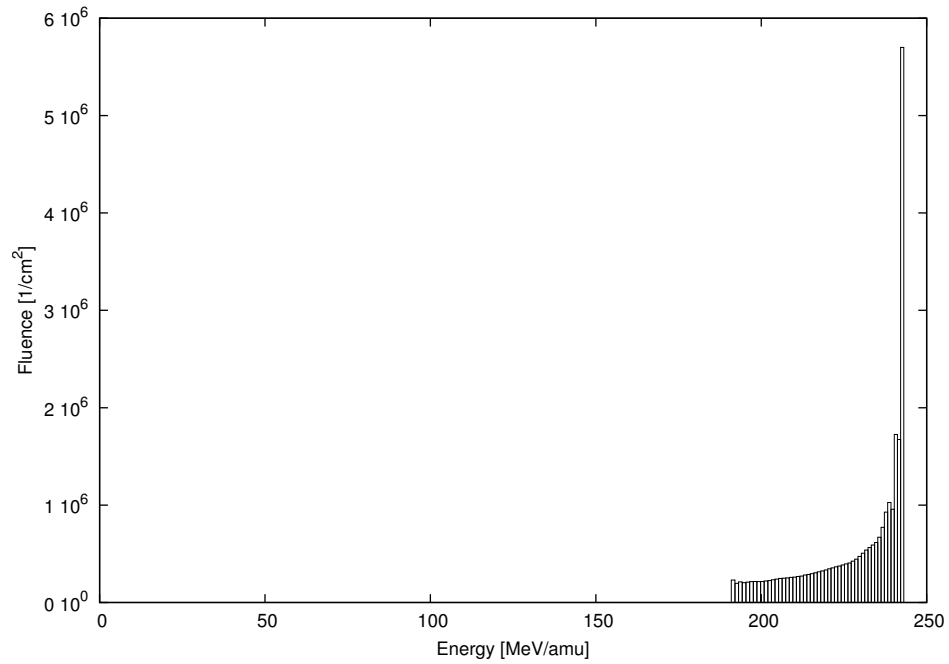


Figure 4.5. Initial energies and fluences of the 49 carbon ion beams required to achieve the flat dose profile presented in the upper panel of Fig. 4.4. Each bar corresponds to a single pristine Bragg peak of initial energy given on the abscissa. Calculations performed using the libamtrack library.

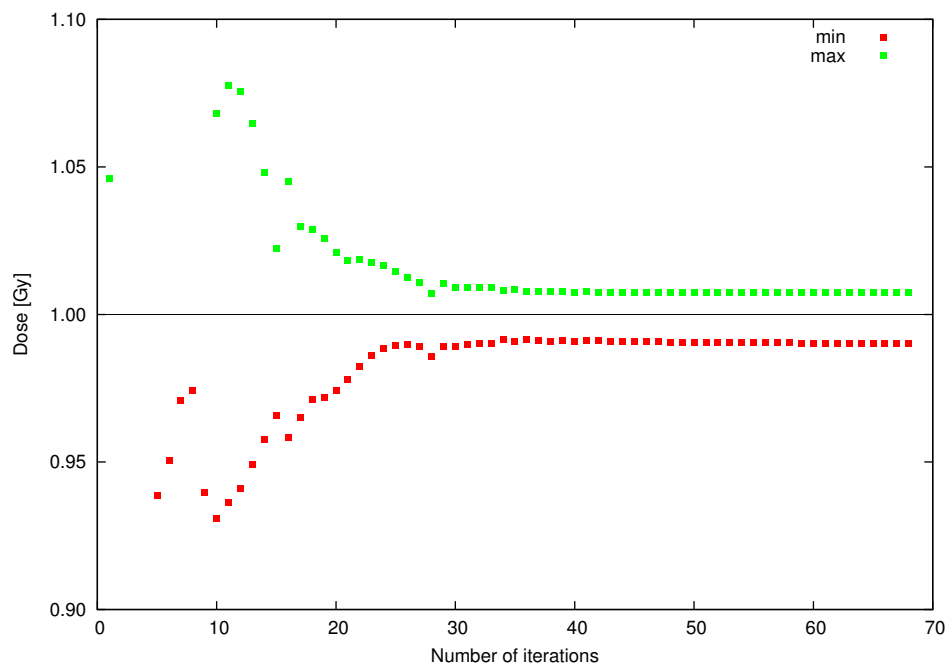


Figure 4.6. Convergence of the dose profile optimization algorithm. Points show the minimum and maximum dose values over the depth of the flat region (8-12 cm) after each iteration step. Calculations performed using the libamtrack library

Modelling the Depth Distribution of Cellular Survival

In conventional radiotherapy with external beams of X-rays, γ -rays or electrons, optimisation in therapy planning implies achieving a uniform dose distribution in the treated volume, as uniform distribution of dose implies uniform distribution of biological effect, i.e. cell survival or cell inactivation (killing). It is evident, as illustrated, e.g. in Fig. 4.4, that optimisation in ion radiotherapy implies achievement of uniform distribution of the biological endpoint (cell survival or killing) over the treated volume, rather than uniform distribution of dose. Considering the strong and quite complex dependence of cellular inactivation cross sections on ion characteristics, such as LET or z^2/β^2 (as demonstrated, e.g., in Fig. 3.1) and the complex arrangement of pristine ion beams required to achieve uniform depth-dose distribution (e.g., as shown in Fig. 4.4), a method needs to be developed of finding a combination of pristine carbon beams, each of suitable initial energy and fluence, which will result in obtaining a constant level of cell survival over a given range of depths.

It is shown in this chapter how to develop such a method of optimising the combination of pristine carbon beams in order to achieve a flat depth profile of CHO (Chinese Hamster Ovary) cell survival over a given range of depths. The scaled version of the Katz model (par. 3.7) will be used and the CHO cells will be characterised by the best-fitted values of model parameters representing this cell line (par. 3.9). The developed approach to modelling survival-depth distributions will then be verified against published results of an experiment in which CHO cells were irradiated at different depths by a combination of pristine carbon beams, to achieve 20% survival over a depth of 4 cm in water [Mitaroff et al., 1998]. The effect of varying the input dose on SOBP flatness will next be studied. By applying in these calculations the best-fitted values of model parameters representing aerated (representing normal cells) and hypoxic (representing cancer cells) V79 cells, the effect of cell oxygenation status on the resulting depth-survival profiles will also be studied.

5.1. Calculation of cellular survival in a mixed ion field

The linear combination of pristine Bragg peaks forming the SOBP or adjusted to an arbitrary dose profile is well defined by a set of two parameters:

- height h_i of the pristine Bragg peak maximum, which is related to its initial dose, D_{start}
- position p_i (depth) of the pristine Bragg peak maximum, which is related to its initial energy E_{start}

The fluence F_i at given depth d in a pristine Bragg peak of height equal to unity ($h_i = 1$) can be decomposed into the sum of fluences of the carbon ions and of secondary fragments or, more generally, into a sum of fluences of ions of Z ranging from 1 to 6 (for the six ion species involved, $Z = 1 \dots 6$) :

$$F_i(d) = \sum_{Z=1}^6 F_i(d, Z) \quad (5.1)$$

The fluence of ions of charge Z at depth d is a sum of the ion energy-fluence spectra:

$$F_i(d, Z) = \sum_{j=1}^{n_Z} F_i(d, Z, E_j) \quad (5.2)$$

where n_Z is the number of components of the energy-fluence spectra of ion of charge Z .

Assuming that the linear energy transfer of an ion of charge Z and energy E is equal to $L(Z, E)$ one may calculate the dose of ion Z at depth d , as:

$$D_i(d, Z) = \sum_{j=1}^{n_Z} \frac{1}{\rho} L(Z, E_j) F_i(d, Z, E_j) \quad (5.3)$$

The dose $D_i(d)$ in a pristine Bragg peak at depth d is then given by the following equation:

$$D_i(d) = \sum_{Z=1}^6 D_i(d, Z) = \sum_{Z=1}^6 \sum_{j=1}^{n_Z} \frac{1}{\rho} L(Z, E_j) F_i(d, Z, E_j) \quad (5.4)$$

In a linear combination of N Bragg peaks, fluence and dose at depth d are calculated as follows:

$$F(d) = \sum_{i=1}^N h_i F_i(d) \quad D(d) = \sum_{i=1}^N h_i D_i(d) \quad (5.5)$$

This may be expanded into:

$$F(d) = \sum_{i=1}^N h_i \sum_{Z=1}^6 \sum_{j=1}^{n_Z} F_i(d, Z, E_j) \quad (5.6)$$

$$D(d) = \frac{1}{\rho} \sum_{i=1}^N h_i \sum_{Z=1}^6 \sum_{j=1}^{n_Z} L(Z, E_j) F_i(d, Z, E_j) \quad (5.7)$$

Or by changing the order of summation:

$$F(d) = \sum_{Z=1}^6 \sum_{j=1}^{n_Z} \sum_{i=1}^N h_i F_i(d, Z, E_j) \quad (5.8)$$

$$D(d) = \frac{1}{\rho} \sum_{Z=1}^6 \sum_{j=1}^{n_Z} L(Z, E_j) \sum_{i=1}^N h_i F_i(d, Z, E_j) \quad (5.9)$$

At a depth d we may thus split the beam into n components (where $n = n_1 + \dots + n_6$), each related to ion of type Z ($Z = 1 \dots 6$), each of energy E_j ($E_j = 1 \dots n_Z$), fluence $F_k(d)$, and dose $D_k(d)$ ($k = 1 \dots n$), given by the following equation:

$$F_k(d) = \sum_{i=1}^N h_i F_i(d, Z, E_j) \quad (5.10)$$

$$D_k(d) = \frac{1}{\rho} L(Z, E_j) \sum_{i=1}^N h_i F_i(d, Z, E_j) \quad (5.11)$$

Now, using the equations of the Katz scaled model with parameters: m , D_0 , σ_0 , and κ , introduced in chapter 3, a method is provided to calculate the fraction of surviving cells, $S(d)$, at depth d :

$$S(d) = \Pi_i(d) \Pi_\gamma(d) \quad (5.12)$$

where:

$$P_k = \begin{cases} 1 - \sigma_k(Z, E_j)/\sigma_0 & \text{if } \sigma_k(Z, E_j) \leq \sigma_0 \\ 0 & \text{elsewhere} \end{cases} \quad (5.13)$$

and

$$\Pi_i(d) = \exp(-\sigma_0 \sum_{k=1}^n P_k F_k(d)) \quad (5.14)$$

$$\Pi_\gamma(d) = 1 - \left(1 - \exp\left(-\frac{1}{D_0} \sum_{k=1}^n (1 - P_k) D_k(d)\right) \right)^m \quad (5.15)$$

The above-described method was also used to calculate the survival vs. depth profile shown in the lower panel of Fig. 4.4 (Chapter 4).

5.2. Calculation of survival vs. depth profile

5.2.1. The optimization algorithm

The method of finding a linear combination of pristine Bragg peaks to form a flat SOBP dose vs. depth profile, described in par. 4.2.1 of Chapter 4, can be extended

in order for the resulting survival profile to be constant (or flat) at a given level of survival, S , over a given range of depths. The measure, Spf, of survival profile flatness is then defined as follows:

$$\text{Spf} = \sum_{j=1}^n (S(x_j, p_1, \dots, p_m, h_1, \dots, h_m) - C)^2 \quad (5.16)$$

where $\{x\}_j$ forms a regular grid over the interval $[a, b]$ and $S(x_j, \dots)$ is the survival level at depth x_j , calculated using eq. 5.12

$S(x_j, p_1, \dots, p_m, h_1, \dots, h_m)$ is a non-linear function of h_1, \dots, h_m , so the gradient minimization algorithm is more time consuming than that of the dose profile optimization problem as in this case the derivative of S needs to be evaluated numerically.

Such an optimization algorithm was implemented by the author in python language, along with the dose profile optimization algorithm (of par. 4.2.1), as an extension of the libamtrack library

5.2.2. A sample calculation of a flat survival vs. depth profile

In a sample calculation the survival optimization algorithm was used to find a combination of carbon Bragg peaks of different initial energies and fluences which would give a flat depth survival profile at survival level 0.2 over the range between 8 and 12 cm in liquid water. As the irradiated biological system, Chinese Hamster Ovary (CHO) cells were selected, represented by four parameters of Katz's scaled model (see Chapter 3): $m = 2.31$, $D_0 = 1.69$ Gy, $\sigma_0 = 5.96 \cdot 10^{-11} \text{m}^2$, and $\kappa = 1692.8$.

In this calculation pristine Bragg peaks were used, in a configuration similar to that of par. 4.2.2, consisting of 49 Bragg peaks placed on a regular grid over a region spanning between depths of 8 and 12 cm.

The algorithm converged to a solution which gave a dose profile which decreased with depth, as shown in the upper panel of Fig. 5.1. At the depth of 8 cm a dose of 3.25 Gy was needed for survival to decrease to the level of 0.2, while at the end of the SOBP, at 12cm, only a dose of 2.16 Gy was required to obtain the same survival level. The optimized survival vs. depth dependence is shown in the lower panel of Fig. 5.1. Maximum deviations from desired survival level of 0.2 were below 0.005 (see Fig. 5.1) and were observed at the distal part of the SOBP, while in central region deviations were of the order of 0.001. A similar argument to that concerning dose profile optimization can be raised: the use of a larger number of ion beams (Bragg peaks) and beam smearing will lead to further smoothing of the depth-survival profile.

The initial energy-fluence spectrum of the ion beams is presented in Figure 5.2. The single peak at the energy of 242.5 MeV/amu corresponds to the pristine carbon beam of the highest energy and range, contributing about 2 Gy to the dose of at the end of SOBP. A high fluence of beams of energies between 191.5 MeV/amu and about 210 MeV is required to deliver the dose of about 3 Gy in the proximal part of the SOBP.

Flatness of the survival profile was evaluated on a grid consisting of 1333 points equally spaced between 8 and 12 cm. The algorithm stopped after 68 iteration steps at a minimum value of $\chi^2 = 0.000493$. Maximum and minimum survival levels found in the target region were 0.203155 and 0.195413 respectively, the relative deviation not

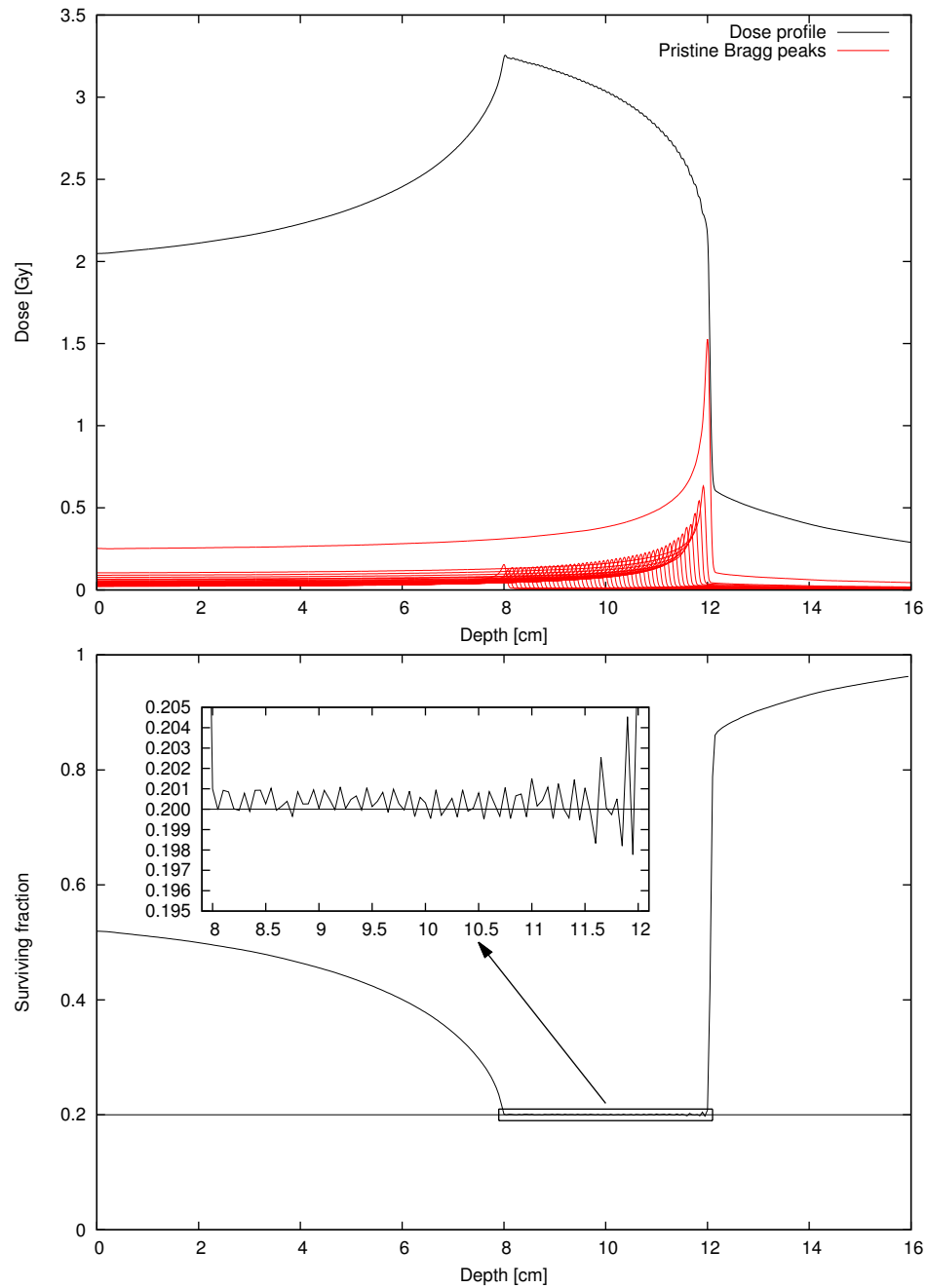


Figure 5.1. Upper panel: Depth-dose profile of a sum of 49 pristine Bragg peaks with different initial energies and fluences yielding a flat profile of survival of CHO cells vs. depth at the survival level of 0.2 over depths between 8 and 12 cm, shown in the lower panel. CHO cells survival was calculated using Katz's scaled model. The model parameters representing CHO cell survival are: $m = 2.31$, $D_0 = 1.69$ Gy, $\sigma_0 = 5.96 \cdot 10^{-11} \text{m}^2$, and $\kappa = 1692.8$. A magnified inset of the flat survival region demonstrates small oscillations in the survival level, due to the sharpness of pristine Bragg peaks. Calculations performed in liquid water, using the libamtrack library.

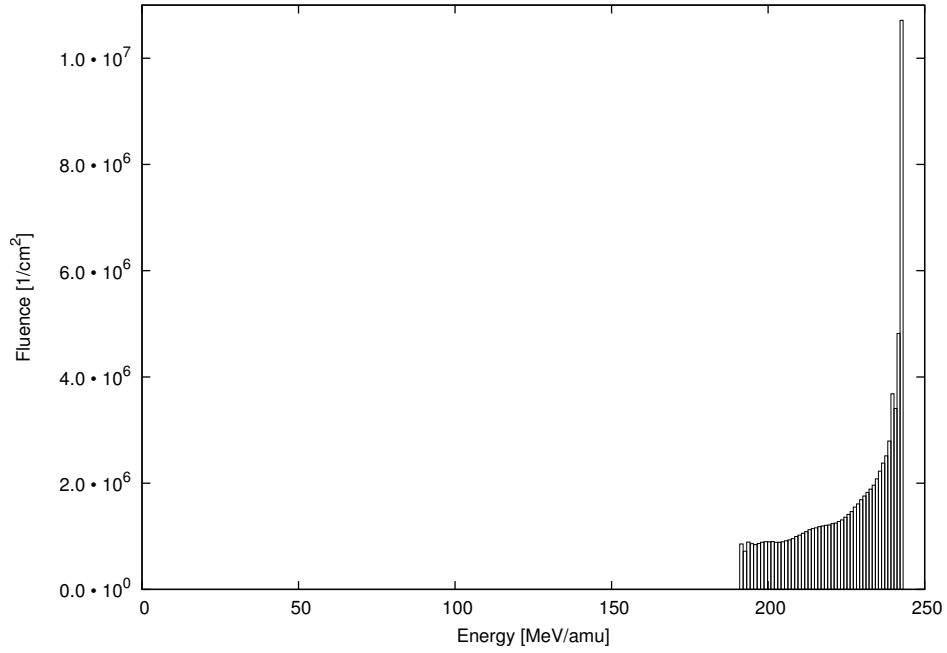


Figure 5.2. Initial energies and fluences of the 49 carbon ion beams required to achieve the flat survival profile presented in the upper panel of Fig. 5.1. Each bar corresponds to a single pristine Bragg peak of initial energy given on the abscissa. Calculations performed in liquid water, using the libamtrack library.

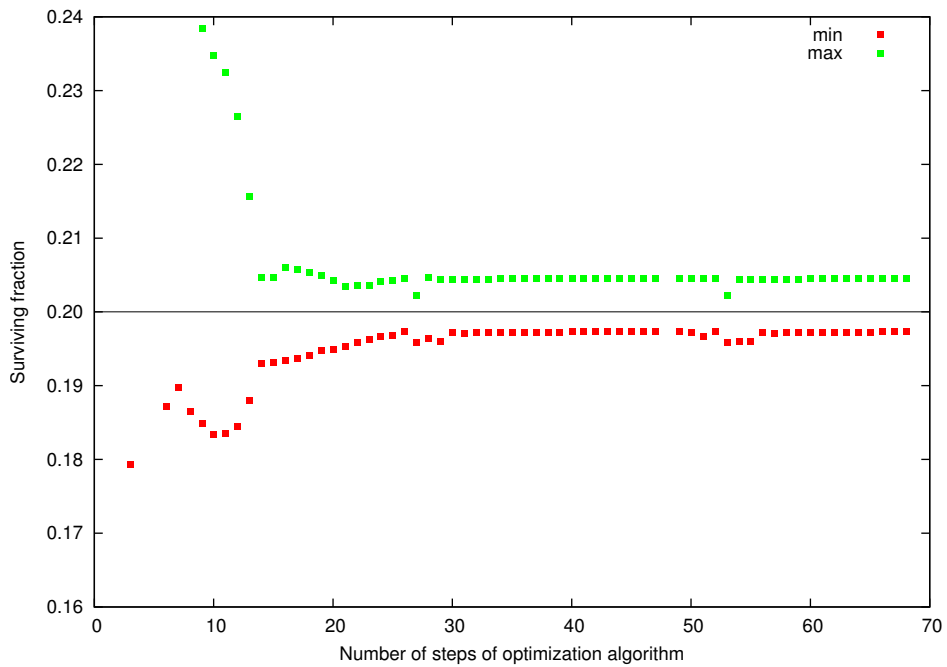


Figure 5.3. Convergence of the dose profile optimization algorithm. Points show the minimum and maximum dose values over the depth of the flat region (8-12 cm) after each iteration step. Calculations performed using the libamtrack library

exceeding 2.5%. As may be seen in Fig. 5.3, reasonable convergence is obtained after about 30 iteration steps,

5.3. Comparison with a cell survival vs. depth experiment

Mitaroff et al [Mitaroff et al., 1998] published results of a radiobiological experiment designed to test the radiobiological models to be implemented in the TRiP98 TPS system at GSI, Darmstadt. CHO K1 cell cultures in vitro were exposed at a range of depths to carbon beams of initial energies ranging between 196 and 244 MeV/amu. An early version of LEM (LEM I) was used to find such irradiation conditions (entrance energy-fluence spectra) at which survival in the target region, between 8 and 12 cm in depth, would be constant and equal to 0.2. Flasks with cells were positioned in a water phantom at depths ranging between 1 and 19 cm, separated by 0.5 or 1 cm. The measured values of survival of CHO cells in the flasks were then compared with the planned survival level of 0.2 in the target region.

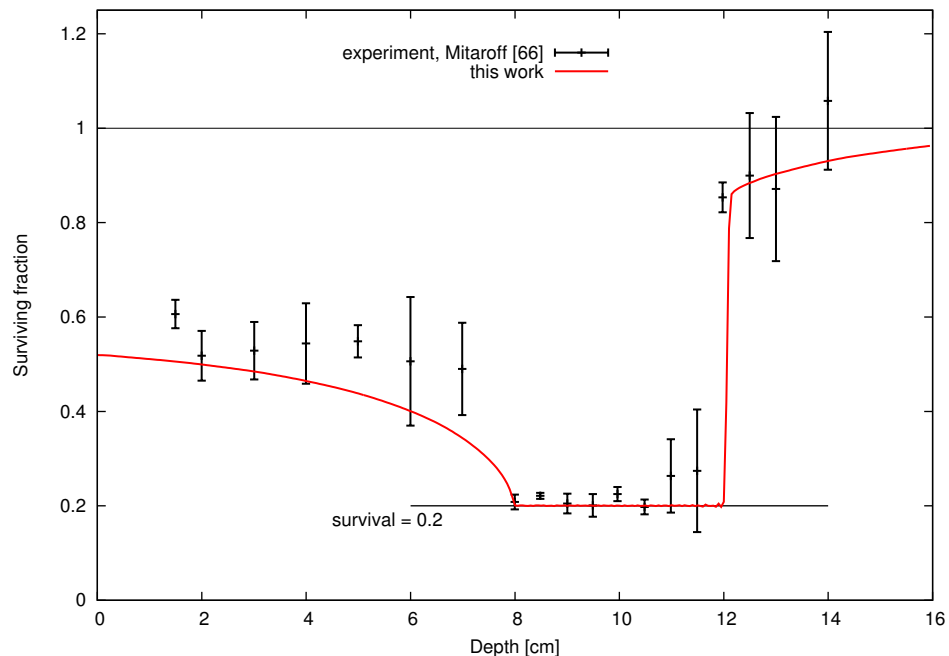


Figure 5.4. Survival of CHO cells vs depth: results of calculations using the survival optimization algorithm and the scaled Katz model, where CHO cells are represented by the model parameters: $m = 2.31$, $D_0 = 1.69$ Gy, $\sigma_0 = 5.96 \cdot 10^{-11} \text{ m}^2$, and $\kappa = 1692.8$ (cf. Fig. 5.1, lower panel), calculations performed using the libamtrack library, compared with experimental data published by Mitaroff et al. [Mitaroff et al., 1998].

The scaled Katz model implemented in the libamtrack library was used to calculate cell survival. The values of the best fitted parameters, found earlier in par. 3.9: chapter 3: $m = 2.31$, $D_0 = 1.69$ Gy, $\sigma_0 = 5.96 \cdot 10^{-11} \text{ m}^2$, and $\kappa = 1692.8$, were used in these calculations. In Figure 5.4 the optimized survival vs. depth profile of Fig. 5.1 (lower panel) is compared with the experimental results of Mitaroff et al. [Mitaroff et al., 1998]. There appears to be satisfactory agreement between the results based on the Katz model and experimental data of Mitaroff et al., at least over the target region.

5.4. Comparison with LEM-based survival vs. depth calculations

In order to compare results of calculations of depth-survival profiles based on Katz's scaled model shown in Fig. 1 with results of calculations using LEM published by Kramer and Scholz [Krämer and Scholz, 2000], the depth-dose profile obtained in this work (cf. Fig. 5.1, upper panel) and that published by Kramer and Scholz are compared in Fig. 5.5. To apply the depth-dose profile of Kramer and Scholz in calculating the depth-survival dependence according to the present calculations, a fourth-order polynomial, $D(z)$, was fitted to the dose profile of Kramer and Scholz over the depths between 8 and 12 cm:

$$D(z) = a_3z^3 + a_2z^2 + a_1z + a_0 \quad (5.17)$$

where $a_0 = 20.7499$; $a_1 = -5.61387$; $a_2 = 0.607124$ and $a_3 = -0.0222678$.

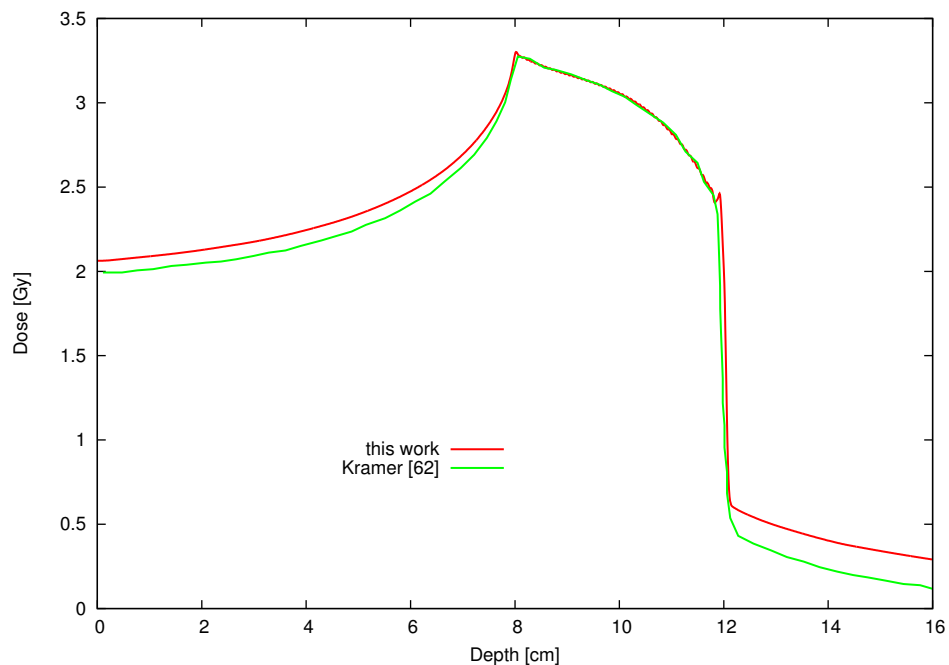


Figure 5.5. The depth-dose profile used in calculation of Kramer and Scholz [Krämer and Scholz, 2000] (green line) compared with depth dose profile calculated with the aid of the libamtrack library (red line). Profile marked with red line was adjusted to agree with Kramer's profile in depths range between 8 and 12 cm. Calculations performed using the libamtrack library.

Next, by using the optimization procedure described in chapter 4, implemented in libamtrack library, a linear combination of pristine Bragg peaks was found, such that the dose profile described by $D(z)$ was maintained. The resulting depth-dose profile is presented in figure 5.5 (red line). It agrees, as assumed, with the dose profile used in LEM model over the depth range between 8 and 12 cm, but is generally lower elsewhere. This discrepancy could be connected to different beam model used in LEM model. Comparison between the depth-survival dependences: calculated in this work

(cf. Fig. 5.1 and Fig. 5.4) and that published by Kramer and Scholz is shown in Fig. 5.6.

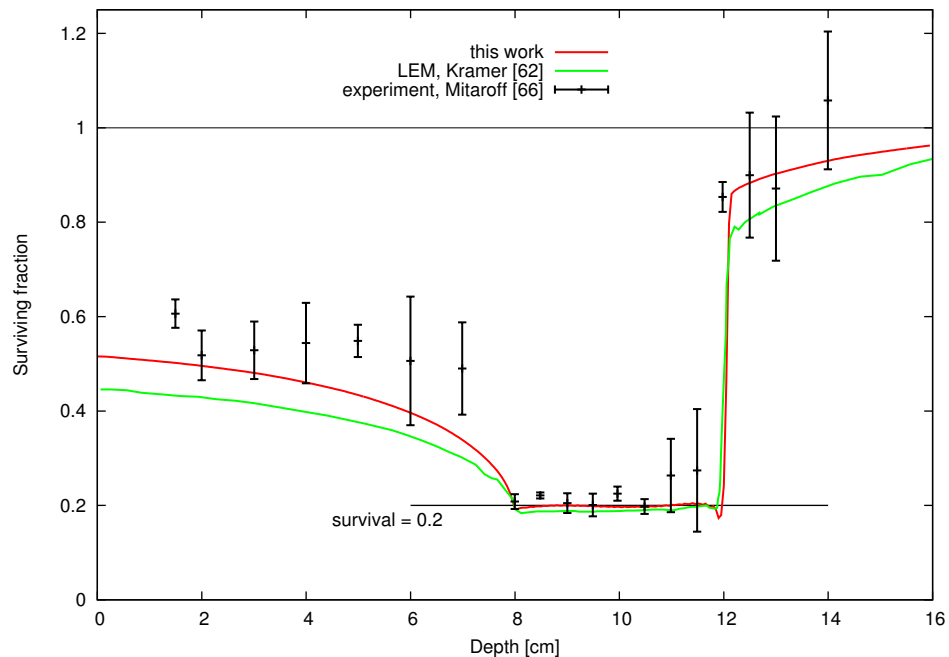


Figure 5.6. Survival of CHO cells vs depth: results of calculations using the dose optimization algorithm (dose profile presented on figure 5.5) and the scaled Katz model, where CHO cells are represented by the model parameters: $m = 2.31$, $D_0 = 1.69$ Gy, $\sigma_0 = 5.96 \cdot 10^{-11}$ m², and $\kappa = 1692.8$, calculations performed using the libamtrack library, compared with results of LEM calculations (reproduced from Kramer et al. [Krämer and Scholz, 2000]).

The depth-survival dependences calculated using Katz’s model and LEM show good agreement with experimentally measured CHO cell survival over the depth range between 8 and 12 cm. Over the entrance channel and behind, both calculations tend to predict lower survival rates than those measured experimentally: by some 5-15% in the case of calculations made in this work, and by some 5-30% for LEM-based calculations. Interestingly, the Katz model-based calculations show a higher entrance dose to achieve the required 0.2 survival level in the target area than do the LEM-based calculations. Yet, outside the target region, the Katz model-predicted cell survival appears to be higher than that resulting from LEM-based calculations – and perhaps better representing the actually measured CHO cell survival. A more detailed comparison, at 1.5 cm depth, is given in Table 5.1. This difference may be related both to the different assumptions concerning beam transport and to the differences in the radiobiological models used.

5.5. Dependence of survival vs. depth on beam entrance dose

An interesting question in carbon ion beam radiotherapy is to what extent is scaling with dose valid? Assuming over the target region a flat depth-survival profile at a given

	Dose [Gy]	Cell survival
LEM	2.03	0.432
Katz	2.11	0.502

Table 5.1. Cell survival corresponding to dose calculated at 1.5cm depth, using the Katz model and LEM.

survival level, how will the survival level over that region vary on varying the beam entrance dose? And how flat will this changed depth- survival profile remain on varying the beam entrance dose?

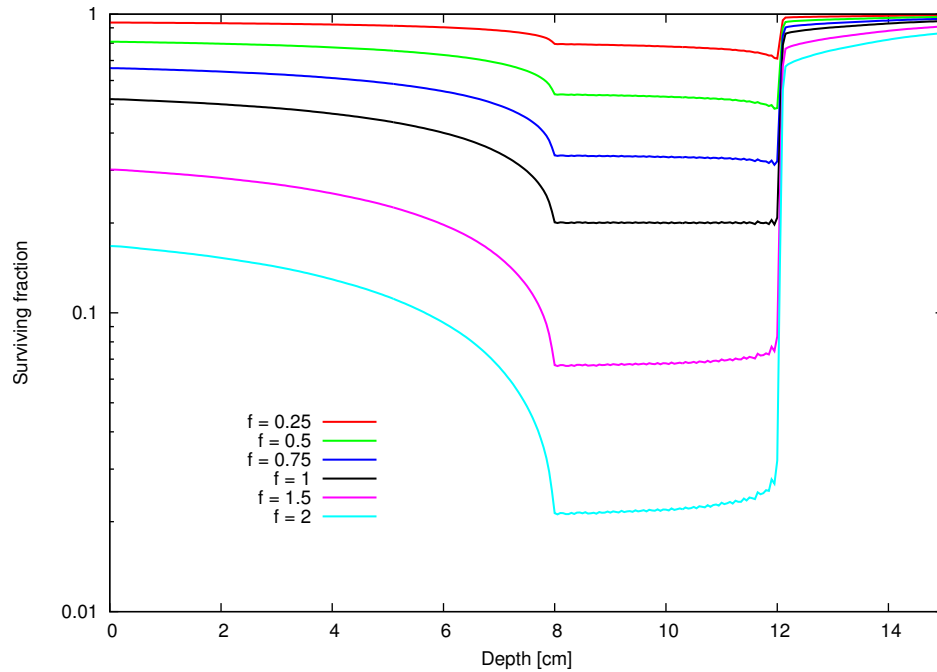


Figure 5.7. Variation of depth-survival profiles with beam entrance dose. A CHO survival vs. depth profile was designed to give a flat survival level of 0.5 between 8 and 12 cm depths (scaling factor, $f=1$, black full line). Next, the input energy-fluence spectrum of the beam was re-scaled by factors: 0.25, 0.5, 1.5 and 2, and the respective depth-survival profiles were re-calculated (coloured full lines). For the Katz model parameters representing CHO cells, used in these calculations, see Fig. 5.1. Calculations performed using the libamtrack library. .

To investigate this matter, a survival vs. depth profile was designed to yield a flat survival level of 50% (0.5) over the depth region between 8 and 12 cm, as plotted in Fig. 5.7. ($f=1$). Next, the initial energy-fluence spectrum (not shown) was multiplied by factors: 0.25, 0.5, 1.5 and 2.0 and entered into the survival profile calculations. The resulting depth-survival dependences are plotted in Fig. 5.7 with values of their respective scaling factors. On increasing the beam entrance dose by a factor of two ($f=2$) the survival level over the target region decreased from 0.5 (50%) to about 0.022 (2.2%) and the survival level over the target region did not remain constant. A

systematic change of the “slope” of the of the depth-survival profile over the target region may be observed with decreasing beam entrance dose.

5.6. Dependence of survival vs. depth on cell oxygenation status

Another interesting question is the dependence of the depth-survival profile on the oxygenation status of the cell. One may assume that tumour cells may remain in hypoxic conditions due to the insufficient supply of oxygen to the rapidly growing tumour. Typically, hypoxic cells are more radioresistant. It is therefore interesting to investigate the effect of the cell oxygenation status on the design of the depth-survival profile.

A systematic study of the radiobiological parameters of Chinese hamster V79 cells in aerobic and hypoxic conditions was performed by a Japanese group at NIRS and published by Furusawa et al. [Furusawa et al., 2000]. Systematic measurements of survival of V79 cells under aerobic or hypoxic conditions after their irradiation by the following ion beams: helium (energies between 1.17 and 9.74 MeV/amu), carbon (energies between 1.9 and 123 MeV/amu) and neon (energies between 7.7 and 124 MeV/amu). From these two data sets, Katz model parameters representing V79 cells in aerobic and hypoxic conditions, fitted by Korcyl [Korcyl, 2012] are shown in Table 5.2

	m	D_0 [Gy]	σ_0 [m ²]	κ
Aerobic	2.91	2.0504	$5.06 \cdot 10^{-11}$	689
Hypoxic	3.22	5.26	$5.529 \cdot 10^{-11}$	1002.2

Table 5.2. Best-fitted parameters of the Katz model, representing aerobic and hypoxic V79 cells [Korcyl, 2012]

Applying the approach described in par. 5.2, two carbon ion beam configurations were prepared aimed at achieving a constant cell survival of the level of 0.5 over 8 and 12 cm depth, for V79 cells in aerobic or hypoxic conditions, respectively. The respective calculated cell depth-survival profiles are shown in figure 5.8. The same Katz model parameters were used to calculate survival at all depths, including the target region.

The depth-dose profiles required to achieve the depth-survival profiles of Fig. 5.8, are shown in Fig. 5.9. As the V79 cells irradiated in hypoxic conditions are more radioresistant than cells well-oxygenated (aerobic), one may observe in Fig. 5.8 that to achieve the same survival of 50% over the target region, about twice as high entrance dose is required for the hypoxic cells than for aerated cells. The difference between these two dose profiles can be attributed to the LET-spectrum of the carbon beam varying with depth.

The initial energy-fluence spectra of the two beams are shown in figure 5.10. The beams are composed of 49 pristine Bragg peaks each, with initial energies ranging between 191.5 MeV/amu and 242.5 MeV/amu.

Beam configurations, planned for iso-survival of hypoxic and aerobic cells respectively, were used to calculate the predicted depth-survival profiles in the case where

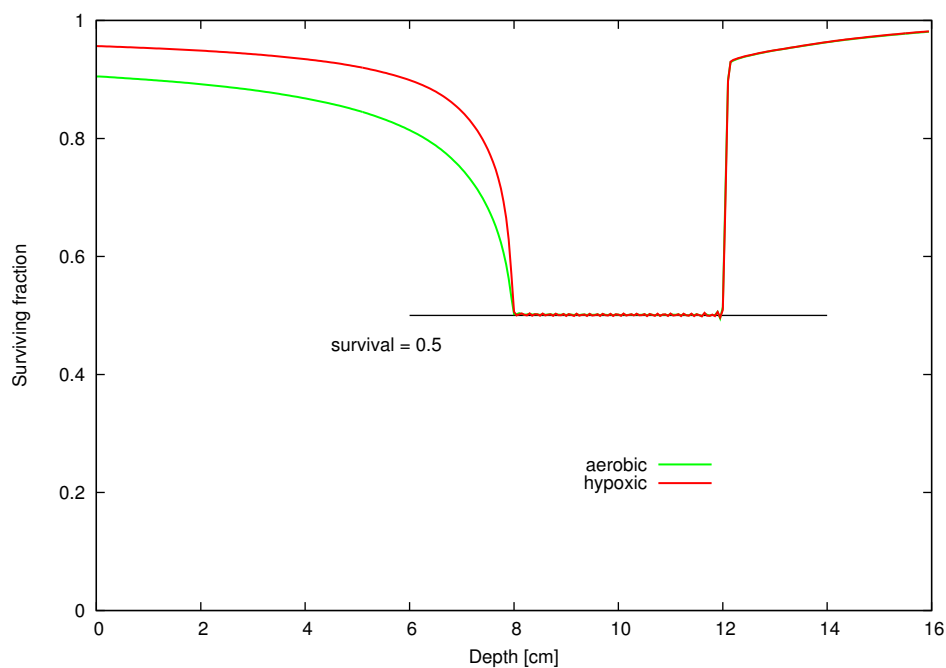


Figure 5.8. Cell survival depth-profiles calculated for aerobic and hypoxic V79 cells using Katz model (parameters listed in Table 5.2). For each case: aerobic and hypoxic two different beam configurations were used, each prepared in such way that the designed survival was equal to 0.5 over the interval between 8 and 12 cm. Calculations performed using the libamtrack library.

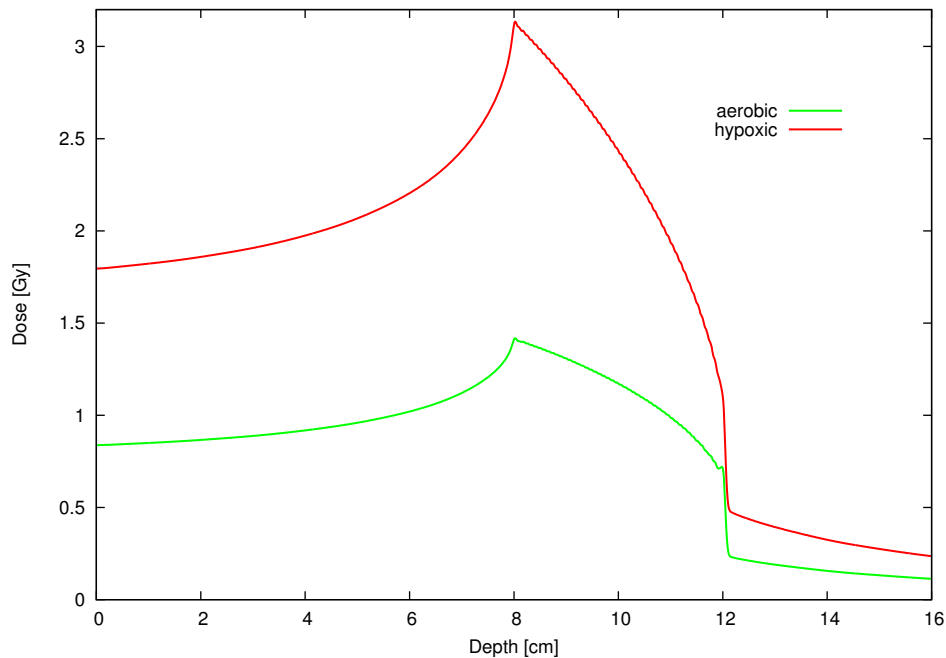


Figure 5.9. Dose depth-profiles related to cell survival profiles presented on figure 5.8. Calculations performed using the libamtrack library.

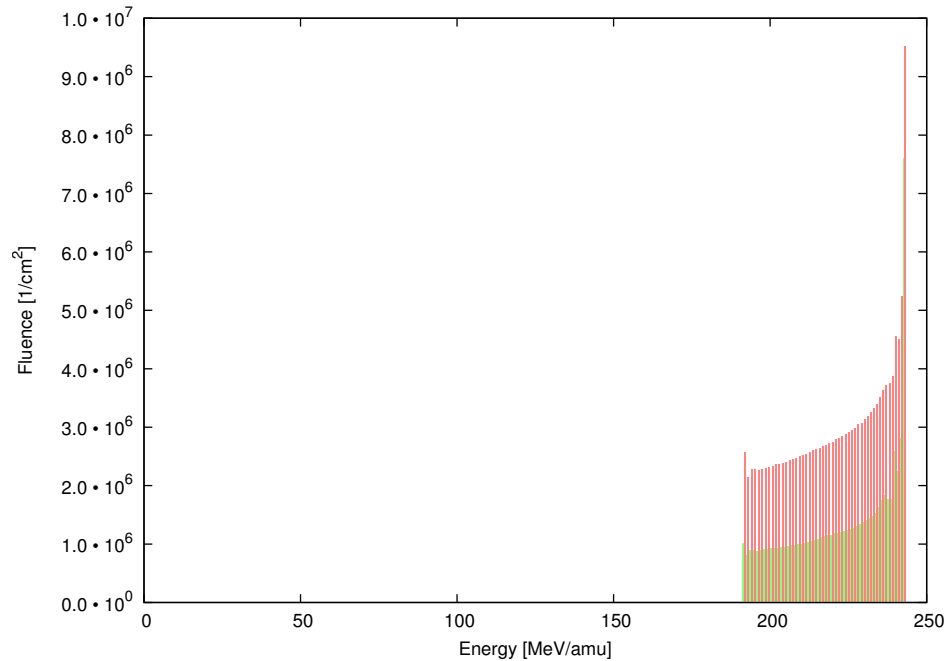


Figure 5.10. Initial energy-fluence spectra related to cell survival presented in figure 5.8. Calculations performed using the libamtrack library.

the same beam combination was used to obtain a flat 50% survival of aerobic cells or flat 50% survival of hypoxic cells (Fig. 5.11). In the first case, “cancer” (i.e. hypoxic) cells would not be sufficiently treated; in the second, the “normal tissue” (aerobic) cells would show over-exposure (or “complications”). This example illustrates the predictive capacity of the model calculation in optimising likely therapy situations, provided that suitable representative model parameters to represent cells in different oxygenation conditions, are available.

5.7. Conclusion

In this Chapter, all the elements discussed in earlier parts of this thesis have been brought together and applied in a radiobiology-based approach to developing a treatment planning system for carbon radiotherapy, albeit in one dimension (depth) only. While the major part of this work has been performed by the author, his collaboration with Steffen Greulich, Marta Korcyl and Pablo Botas is gratefully acknowledged. All codes used in this work which he developed have now been implemented in the libamtrack library.

The radiobiological model of Katz in its scaled version (Chapter 3), based on the radial dose distribution (Chapter 2) has been applied to a model of a carbon beam propagating through liquid water, as represented by 1-dimensional energy-fluence spectra of the carbon beam and its secondary ions, obtained at several depths, basing on Monte Carlo simulations (Chapter 4). Crucial to the possibility of handling the approach presented in this chapter was the libamtrack code library (Chapter 2) which contains all codes necessary for performing the calculations. Application of interpolation techniques to calculate the energy-fluence spectra over a regular grid (Chapter

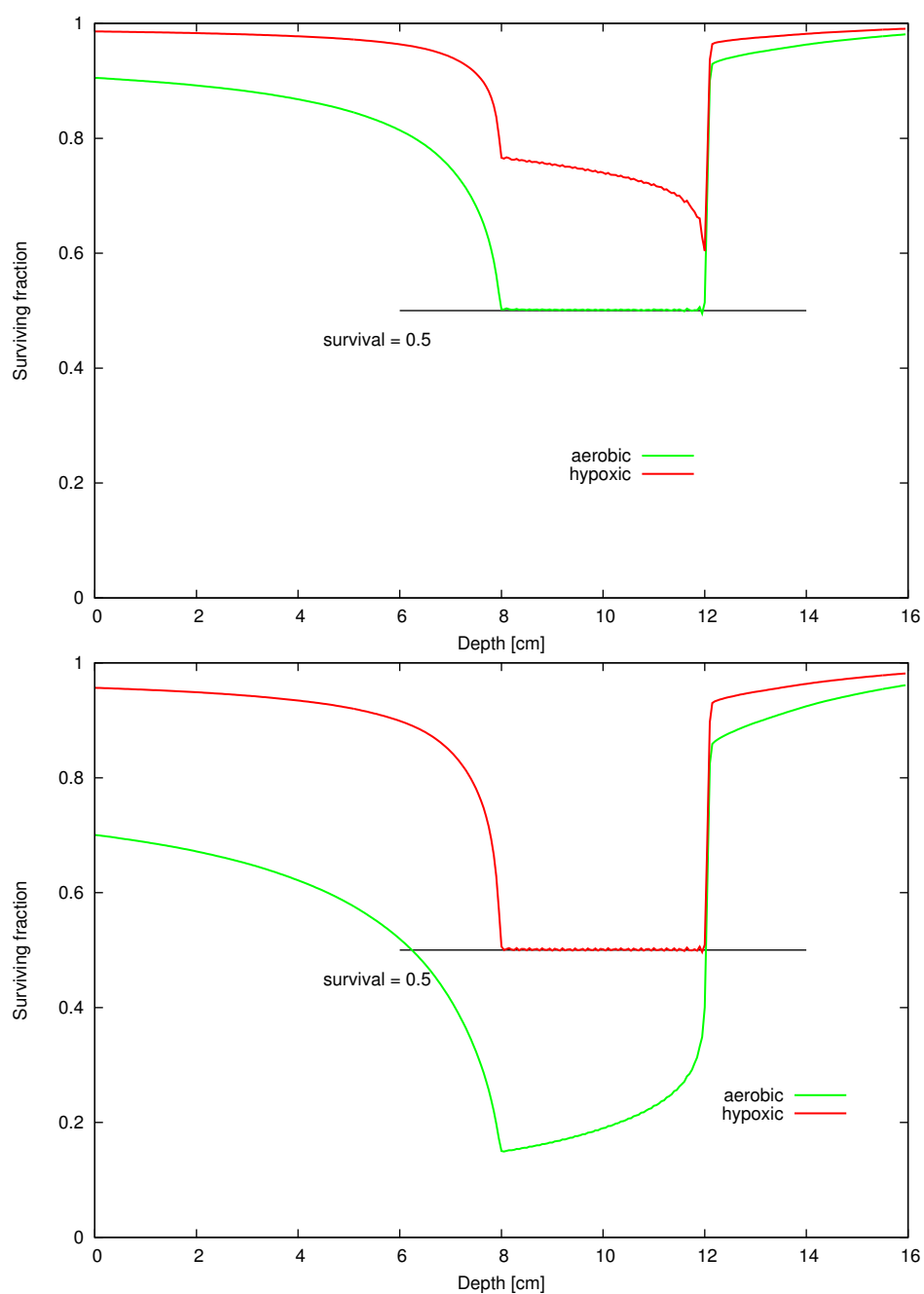


Figure 5.11. Cell survival depth-profiles calculated for aerobic and hypoxic V79 cells in two identical carbon ion beams. Initial beam configuration was prepared for the survival of hypoxic cells to be 50% (0.5) over the target region between 8 and 12 cm.

4) and development of numerical methods to optimize the distributions of depth-dose (Chapter 4) and survival-depth (Chapter 5) dependences, was necessary. It is very satisfying that the results of model calculations were able to closely predict the results of a radiobiological experiment using CHO cells (par. 5.3) and that the optimised beam configuration in calculations representing this experiment were found to closely agree with those evaluated independently by other authors. This agreement suggested that predictions could be made of the effects of varying the input dose (par. 5.5) and of the cell oxygenation status (par. 5.6) on the depth-survival profiles.

Thus, a quantitative model of a treatment planning kernel has been developed and presented in this chapter, based on a highly efficient and predictive radiobiological model, which enables quantitative predictions to be made of the expected survival-depth dependences in a manner amenable for future development into a carbon ion therapy planning system.

A more extensive discussion of the results obtained in this thesis is presented in Chapter 6.

Discussion and conclusions

This final chapter contains a more detailed discussion of results obtained in Chapters 2-5, a summary of this work, where key issues that have been resolved by the author are listed, followed by brief conclusions and proposed future work suggested by this thesis.

6.1. Discussion

Carbon ion radiotherapy is a new and fairly rare treatment modality. Only six centres in the world are currently in operation, three in Japan (Chiba-NIRS, Hyogo and Gunma) and single centres in Germany (HIT-Heidelberg), Italy (CNAO-Pavia) and China (Lanzhou). As of March 2013, some 10 thousand patients have been treated by carbon ions, most of them in Japan and some 1500 at the HIT and GSI facility¹. Pioneering work in the development of carbon radiotherapy began around 1997 at GSI Darmstadt in Germany where about 600 patients were treated. The Local Effect Model (LEM) was developed at that time at GSI [Scholz and Kraft, 1994] as the radiobiological basis for the carbon ion treatment planning system, now in use at HIT. Elements of LEM are also applied in the Japanese treatment planning systems. The cellular Track Structure Theory (or the Katz model) was developed earlier [Butts and Katz, 1967], but was believed to be less amenable to clinical radiotherapy due to its reliance on the m-target rather than linear-quadratic formalism. The rationale for this thesis was to investigate the possibility of applying Katz's radiobiological model in a carbon ion therapy planning system. Attractive were the simplicity of the analytical formulation of the Katz model and its well-known predictive power in describing RBE and cell survival in vitro [Katz et al., 1994].

Development of a TPS for clinical application is a major project, however the basic features of such a system could be studied by developing its one-dimensional

¹ http://ptcog.web.psi.ch/patient_statistics.html

kernel in which the scaled Katz model would be implemented as its radiobiology component while the physical component would be supplied by a data base of Monte Carlo-calculated beam transport calculations of carbon beams and secondary ions in water, available to the author of this thesis. The open-source libamtrack code library which has been co-developed by the author would serve as the repository for the codes that were to be developed in the course of this project, enabling free access to all these codes and results of this research. Since the Katz model differs in many aspects from LEM [Krämer and Scholz, 2000], [Scholz and Kraft, 2004], [Beuve, 2009], [Elsässer and Scholz, 2010], new insights to carbon therapy planning were expected, especially since the LEM-based TPS in clinical use, e.g. at HIT in Heidelberg is now a commercial product with no access to its code, nor is it available for research purposes outside HIT.

The cellular Track Structure Theory (or the Katz model) uses many elements shared by other amorphous track structure model approaches, such as the radial distribution of average dose, $D(r)$, around the path of a heavy ion (par. 2.3) which, combined with the response after uniform irradiation by a reference radiation, given by the m-target formula (eq. 3.9), yields the inactivation cross-section (eq. 3.12). The possibility of applying scaling factors in this model appears to be closely related to the selection of scalable average $D(r)$ formula (e.g., the averaged equation of Zhang, see Table 2.2 and Appendices A and B), and to the use of m-target formalism. Marta Korcyl in her Ph. D. thesis [Korcyl, 2012] proposed an efficient method of calculating the inactivation cross section based on Zhang’s formula (see Chapter 2 and Appendix C). It was then possible to find best-fitted values of model parameters from sets of published survival curves for normal human skin fibroblasts [Korcyl and Waligórski, 2009]. Following a careful analysis of the scaling properties of Katz’s model [Korcyl et al., 2013], the validity of the set of simple analytic formulae (eq. 3.29-3.34), originally proposed by Katz, was confirmed, the “track-width” approximations were re-calculated and the scaled version of the Katz model was implemented by the author in the libamtrack code library. This scaled version of the Katz model, including Zhang’s radial dose distribution formula, was first used by M. Korcyl to model relative effectiveness of alanine and effect of heavy ion bombardment on E.Coli spores [Korcyl et al., 2013].

This version of the scaled Katz model is also used in this thesis in all calculations presented in Chapter 3 and Chapter 5. The author further developed and implemented the parameter-fitting routine into the libamtrack library and applied it to find best-fitting values of m , D_0 , σ_0 and κ representing survival of Chinese Hamster Ovary (CHO) cells (eq. 3.41) and their uncertainties (eq. 3.44), from a set of data published by Weyrather et al. [Weyrather et al., 1999] (par. 3.9), to be used in calculations presented in Chapter 5.

One may argue that no less than four parameters are required to describe the variation of cellular survival curves after a fluence of ions of specified charge Z and energy: two (m and D_0) to describe the “curvature” of the response (via the m-target expression) after doses of reference radiation, one (σ_0) to give the purely exponential response (such as that shown in Fig. 1.4) and one (κ) as a “mixing parameter” to generate intermediate “curvatures” of the survival curves after ions of various charges or energies. Taking this view, the linear-quadratic parameters (α and β in eq. 1.11) are too few to provide the full description of cell survival after ion doses (or fluences),

without additional assumptions. Indeed, several such assumptions are made in LEM, and a microdosimetry approach [Beuve, 2009] is used rather than that of average dose assumed in Katz’s model. A comparison was made by Paganetti and Goitein between the Katz model and an early version of LEM (LEM I) with respect to V79 cell line survival. Some discrepancies were found between calculations and experimental data for irradiation by proton beams [Paganetti and Goitein, 2001].

The Katz model has been applied in many areas, and recently in modelling the risk from space radiation [Cucinotta et al., 1997, Cucinotta et al., 1999]. Since galactic cosmic rays are composed mostly of energetic protons ($>200\text{MeV}$), amorphous track models are suitable for such studies.

The set of equations, eq. 3.29-3.34, was termed the “scaled Katz model” by the author of this thesis and is used in all further calculations, due to their simplicity and computational efficiency. The version of the model where integration of the averaged $D(r)$ and of the cross section are performed explicitly was termed the integrated version of this model (par. 3.6). Here, “non-scalable” $D(r)$ formulae may be applied. In the integrated version, the author proposes to replace κ by the radius of the sensitive site, a_0 , as the fourth model parameter. The integrated version of the model can also be used to best fit model parameters, however best-fitted parameter values may in that case be different from those fitted by the scaled version of the model. Application of the integrated version of the Katz model may lead to interesting results, as other $D(r)$ formulae, e.g. that of Geiss [Geiss, 1997], also used in, e.g., LEM or other models [Geiss et al., 1998] may then be applied for comparative studies. However, the integrated version of Katz’s model is too computing-intensive to be used in practical TPS development.

To evaluate the combined effect of a mixed-field (i.e. a field composed of track segments of several ions of different charges, velocities and fluences) the Katz model offers a well-defined analytical prescription (eq. 3.45-3.47), while in LEM an “ansatz” for calculating the effective value of β from a combination of α values representing cell survival curves after irradiation by the component ions, multiplied by their respective dose contributions [Krämer and Scholz, 2006] is proposed. While a difference between the results of mixed-field calculations of either model may then be expected, this was not verified.

The feature shared by the Katz model and by other amorphous models, such as LEM, is the need to base model calculations on energy-fluence spectra of the ions in the beam. In all calculations in this work, such energy-fluence spectra were based on results of Monte Carlo simulations, as these spectra cannot be reliably measured. Results of Monte Carlo simulations should closely match results of available measurements, e.g. of depth-dose distributions. The precision of Monte-Carlo generated beam profiles is good enough, such that dose deviations in the plateau of numerically generated spread-out Bragg peaks is typically less than 1% which is a level satisfying clinical conditions for ion beam radiotherapy.

Nuclear interaction models, implemented in SHIELD-HIT10A were recently updated (compared to the previous version, the SHIELD-HIT08) and benchmarked against experimental data, as reported by Armin et al [Lühr et al., 2012]. Most of these updates are relevant for carbon ion interactions with nuclei in the target, and in that case agreement within two sigma with data is achieved [Hansen et al., 2012].

SHIELD-HIT10A, when compared with other Monte-Carlo codes, such as Geant4 [Agostinelli et al., 2003] or Fluka [Battistoni et al., 2007] is able to adequately reproduce fragment yields of ions lighter than lithium. For boron and beryllium Fluka and Geant4 show better agreement with data. It has to be stated that none of these codes alone could be recommended to best cover all ion types and ion energy ranges considered in carbon ion radiotherapy. SHIELD-HIT 10A Monte Carlo transport calculations of 50-500 MeV/amu carbon beams in water performed by Pablo Botas at DFKZ (Heidelberg) served as the initial input to beam transport modelling in this work. A suitable energy-fluence spectra data base, in the format of SPC files, was implemented by the author in the libamtrack library (par. 4.1.2). An algorithm was developed by the author in order to estimate fluence-energy spectra at desired intermediate depths of carbon ion beams of different initial energies (par. 4.1.3). The algorithm used for this purpose is similar to the bilinear interpolation of energy-fluence spectra used by Kramer and Scholz in LEM I [Krämer and Scholz, 2000]. In 2006 a description of an improved version of LEM was published [Krämer and Scholz, 2006] which included a more efficient derivation of tabularized data and an improved data access algorithm, based on a lookup-table containing pre-calculated values of alpha and beta parameters of the linear-quadratic model at different depths.

As an illustration of the complex interactions of carbon beams in water, it is interesting to note the difference between the contribution of the primary and secondary ions in a pristine 270 MeV/amu carbon beam to the depth-dose (Fig. 4.1) and to depth-fluence (Fig. 4.2) distributions, as presented in cumulative and differential forms (upper and lower panels in these figures). While the fluence of secondary protons from nuclear reaction clearly dominates that of the primary carbon ions, the major contribution to the dose is still from the primary carbon component of the beam. Also, interesting is the decrease of the fluence of the primary carbon beam with depth (Fig. 4.2, lower panel), caused by nuclear reactions and scattering.

The author's development of the interpolation algorithm (par. 4.1.3) was essential to achieve linear superposition of energy-fluence spectra within regular steps in depth, as shown in Fig. 4.3, in preparation for spread-out Bragg peak calculations where such a linear superposition of pristine carbon beams of given initial energies and fluences was to yield the required flat depth-dose distribution over a given depth region. The optimizing routine implemented for this purpose is also able to find the optimum solution for desired depth-survival dependences of shapes other than flat. By applying an inverse optimization algorithm developed by the author (par. 4.2.1), in the example shown, a flat dose of 1 Gy over the depth region 8-12 cm (Fig. 4.4, upper panel) was achieved by a linear superposition of pristine carbon beams of initial energies and fluences shown in Fig. 4.5, where the beam of the highest energy clearly dominates. Good convergence of the developed optimization algorithm (within about 30 steps, as illustrated in Fig. 4.6) attests to its computation efficiency. Application of a mixed-field calculation of the Katz (scaled) model using cellular parameters representing CHO cells to this dose-depth profile results in a highly non-uniform distribution of cellular survival (Fig. 4.4, lower panel).

This example clearly illustrates the basic problem of carbon ion beam radiotherapy: achieving a uniform dose distribution over a given target region will not result in a uniform distribution of cellular survival over that region. This is due to the complex

variation with depth of biological effectiveness (RBE) of the carbon beam and its secondaries.

The presented dose profile optimization algorithm does not take into account many aspects relevant for treatment planning system: plan robustness, multiple beams, complex treatment volume shape, and presence of organs at risks. Its main goal was to show the possibility of modifying the entrance energy-fluence spectra of carbon ion beams in order to obtain the desired depth-dose profile. Linearity of χ^2 minimization in that case is exploited in the gradient algorithm, which is an approach similar to that used in the TRiP98 planning system, where a conjugate gradient algorithm is used [Krämer et al., 2000].

The simple analytic calculation of mixed-field irradiation in the Katz model (par. 3.10) was applied to the set of interpolated energy-fluence spectra, resulting in the algorithm given in par. 5.1, to which another optimisation algorithm (par. 5.2.1) was developed by the author. Results of sample calculation: a flat depth-survival over a selected depth region, the corresponding non-uniform depth-dose distribution (Fig. 5.1) and the initial energy-fluence spectrum (Fig. 5.2), have been achieved efficiently, within about 30 iteration steps of the optimizing routine (Fig. 5.3). This example of a calculation of a flat survival-depth profile (20% survival over depths 8-12 cm) with Katz model parameters representing CHO cells was chosen deliberately to verify the model prediction against published results of a radiobiological experiment [Mitaroff et al., 1998]. The comparison is shown in Fig. 5.4, where agreement between the levels of survival measured outside the flat region and those predicted by the calculation are very satisfactory, considering the experimental uncertainties and the difficulty of the experiment itself. The calculated depth-dose profile to achieve the flat depth-survival dependence of Fig. 5.3 is shown together with a similar profile published by Kramer and Scholz [Krämer and Scholz, 2000], used to verify LEM calculations against the experiment of Mitaroff et al. For additional verification, the author fitted a polynomial to the appropriate part of the profile published by Kramer and Scholz (Fig. 5.5) and re-calculated the depth-survival dependence. Results of this calculation and the published results of LEM calculations [Kramer and Scholz, 2000] are compared with the experimental data in Fig. 5.6. Interestingly, while in the author's calculation using the Katz model, a higher entrance dose is required than that in the LEM calculation, the Katz model-predicts survival levels which are systematically higher outside the flat region than those calculated by LEM (see Fig. 5.6 and Table 5.1). Since in either model the beam transport calculation is intimately and non-linearly tied up with the radiobiology calculation, it is not possible to decide whether the source of this difference lies in differences between the beam or the radiobiology components of these two model calculations. One should add that this intercomparison is very limited in scope, as only one cell line was studied and a very simple target location was investigated. Broader studies could shed more light on the quality of predictions of LEM and the Katz models.

Encouraged by this result, the dependence of the survival-depth curve on the input dose (or fluence) was studied, also applying CHO cell parameters (Fig. 5.7), to demonstrate that not only does the survival level over the flat region depend non-linearly on beam entrance dose, but so do the slope and flatness of the survival vs. depth curve. In another example, where cellular parameters representing aerated or hypoxic V79 cells

fitted by Korcyl [Korcyl, 2012] were applied (par.5.6), it was found that quite different depth profiles (Fig. 5.9) and initial energy-fluence spectra (Fig. 5.10) are required to achieve the same 50% survival vs. depth profiles over their flat regions (Fig. 5.8). It was observed, as expected that less radiosensitive hypoxic V79 cells require higher input fluence than aerobic cells, but also that the input fluence does not scale equally with depth. As can be seen from Fig. 5.10, hypoxic cells require about 2.5 times higher fluence of lowest energy carbon ions and about 1.25 times higher fluence of carbon ions of the highest energy than aerobic V79 cells.

The impact of rescaled input fluence on predicted cell survival level was investigated in chapter 5.3. As was expected, the predicted survival did not scale uniformly with input fluence. The survival profile did not remain constant as the initial fluence was rescaled by factors ranging from 0.25 to 2. Largest deviations are observed in the distal region of the SOBP. This observation suggests that in carbon ion beam treatment one cannot introduce a universal physical depth-dose profile to be applied in preparing plans with different dose in the target region.

The possibility of adjusting carbon ion beam treatment plans according to oxygenation distribution in the tumour volume could lead to increased tumour control. As was shown in Chapter 5 (Fig. 5.11) this cannot be realized by simply increasing the dose by a constant factor, but has to be handled on the basis of the survival optimization algorithm. Another attempt to solve that problem is the so called LET-painting: a method to reshape the LET distribution in the carbon beam, while maintain a given dose profile, described in [Bassler et al., 2010].

The above comment not only illustrates the general feature of the developed calculation - that the shape of the resulting survival vs. depth profile is strongly affected by the values of cellular parameters applied, but it also demonstrates the likely difficulty in finding optimum conditions in carbon therapy to correctly treat tumour cells (here represented by anoxic V79 cell parameters) and healthy tissue cells (aerated V79 cells) – as shown in Fig. 5.11.

The inverse planning procedure, recognized usually as inverse planning is a crucial component of any Treatment Planning System in hadron therapy. All present treatment planning systems incorporate inverse planning procedures [Krämer and Scholz, 2000]. As most of the radiobiological models exploit the linear-quadratic dose response model, biological dose optimization algorithms also follow this approach by incorporating alpha-beta formalism within the optimization procedure. The optimization procedure presented in this thesis is based on a different, multi-target dose-response model. The differences between m-target and alpha-beta models were widely discussed in the literature [Katz, 2003], [Scholz and Kraft, 2004]. The linear-quadratic approach has wider acceptance in clinical practice, but there is yet no solid proof of the superiority of one approach over another.

In the core of developed cell survival optimization algorithm lays the non-linear minimization problem. In this work it can however be easily tackled as Katz's scaled model is fully analytical. As may be seen in Fig. 5.3, the survival optimization algorithm converged in about 30 steps and relative deviations of cell survival over the target region did not exceed 2.5 %, an acceptable level, with room for further improvement.

The calculation tool developed in Chapter 5 can then be accepted as the one-di-

mensional kernel of a therapy planning system based on Katz's cellular track structure theory, to be further compared against systems based on other biophysical models, such as LEM.

The cell survival optimization algorithm presented in this thesis is a step towards implementing the Katz model in a Treatment Planning System. Availability of the open-source code within the libamtrack library may facilitate the implementation of the developed kernel in a realistic TPS.

The clinical situations in many aspects are far more complex than the presented model calculation of a one-dimensional passively shaped beams in a homogenous environment. TPS algorithms are required to handle many aspects which remain outside the scope of this thesis: multiple field optimization, complex patient geometry or plan robustness.

The presented approach is limited to one dimension (along the beam depth). It would be possible to extend it to a full 3-D beam model by repeating the Monte Carlo simulations of carbon ion beams with increased statistics and to save such data in a look-up table indexed not by depth z only, but by position (x,y) at depth z . In such an approach various configurations could be studied: pristine Bragg peaks emitted from a point-source, mono-energetic pencil beams, clinical pencil beams and also broad beams of carbon ions. However, Kramer and Scholz [Krämer and Scholz, 2006] reported a much simpler approach, incorporated in the TRiP98 treatment planning system, namely that carbon ion pencil beam energy-fluence spectra are tabulated along the Z-axis and an analytical Gaussian function is used to describe the beam profile in X and Y-axes. Such a beam model was applied in the GSI raster scan system and is presumably used in the clinical TPS at HIT. Analytical beam models used to describe pencil beams appear to describe well the total dose deposited by the beam, but their consistency in representing beam fragmentation has not yet been proven.

Full three-dimensional beam models are used at the Heidelberg Ion Therapy Center (HIT) where a FLUKA Monte-Carlo code coupled with LEM [Mairani et al., 2010] has been integrated within their treatment planning system. Using the FLUKA code, energy-fluence spectra calculated at HIT are saved into plain files in SPC format and used in the treatment planning system. The choice of SPC file as energy-fluence spectra file format in libamtrack library was made to facilitate possible integration of this library with existing treatment planning system (TRiP98, Syngo PT planning) and Monte Carlo codes (SHIELD-HIT, FLUKA). Such integration would allow direct comparison of treatment plans prepared using different radiobiological models.

6.2. Summary and conclusions

The general aim of this work was to develop and test the basic algorithms of a kernel of a future therapy planning system for carbon ion radiotherapy, using in its radiobiology component the cellular track structure model of Katz and applying as its physical component a realistic Monte Carlo-generated data base describing transport in water of carbon beams of various initial energies, available to the author. Using this data set it was possible to simulate the formation of the spread-out Bragg peak structure and to evaluate the energy-fluence spectra of all generations of secondary

ions up to the energy of the primary carbon ions, at all beam depths. It was desirable to gather all necessary codes and data in an open-source research code library

For this purpose, the author, in collaboration with Steffen Greulich and other colleagues at the DKFZ and Aarhus research centres, developed a computer library of codes - the libamtrack library. This open-source library is generally available to all users. Subroutines of the library can be downloaded, edited or modified and incorporated in other software. Together with the library, implemented in ANSI C language, a set of wrapping methods is provided, making it possible to use it in various computing languages or in numerical simulation tools. Some of the library functions have now been incorporated into a web interface, the libamtrack WebGUI ², where users connected to the Internet can perform some basic calculations using their web browsers. The libamtrack library is presented in Appendix C.

The author verified several aspects of the Katz model, notably the relationship between the “integrated” version of the model which requires sequences of numerical integrations to calculate its output, and its much faster analytical or “scaled” version which exploits the scaling properties of this model with respect to some of its parameters. In some parts of work in this area, the author collaborated with Marta Korcyl [Korcyl, 2012]. The author also performed a detailed analysis of the parameter-fitting procedures in the “integrated” and analytical representation of the Katz model, developing his algorithm of a fitting procedure and implementing it as a tool in the libamtrack library.

Next, the author verified the consistency of the physical carbon ion beam model to ensure that it reflected the major physical processes of interactions of energetic carbon ions with water. SHIELD-HIT Monte Carlo transport calculations of carbon ions in water were originally performed by Pablo Botas in collaboration with DKFZ, Heidelberg. The author adapted the result data sets to be handled by the libamtrack library routines and co-developed the algorithms of data extraction from these data sets, to be used as input for Katz’s cellular track structure model calculations and for handling and presenting results of these calculations.

As a benchmark of the carbon TPS elements under development, an algorithm to optimise beam properties in order to obtain constant levels of survival over the required depth was developed and implemented by the author. Here, the radiobiological model and beam model had both to be optimized to work correctly in the minimization algorithm. As a result of these studies, the author developed and implemented a general tool for adjusting the parameters of a one-dimensional carbon beam in such a manner that a pre-selected constant survival level could be achieved over a given range of beam depths.

The consistency of the physical and radiobiological components of the developed TPS elements was next verified by the author against published results of a radiobiological experiment involving measurement of the survival levels of Chinese Hamster Ovary (CHO) cells placed at different beam depths and irradiated by a pre-designed set of carbon beams of energies ranging between 196 and 244 MeV/amu [Mitaroff et al., 1998]. The planned level of survival was 20% over 8-12 cm depths, and the experiment was designed to verify an earlier version of the LEM. By fitting the Katz model cellular

² <http://webgui.libamtrack.dkfz.org/test>

parameters to this cell line and applying the benchmark optimisation calculations, the author was able to consistently represent the results of this experiment to within 15% relative difference, well in agreement with the results of LEM calculations.

Finally, using the tools developed by the author, the effect of varying the input beam fluence and varying the cellular parameters in the Katz model to represent aerated (healthy tissues) or hypoxic (tumour cells), in a study of the respective survival-depth dependences, the author showed in a predictive manner the difficulties which may arise in achieving correct optimisation of such dependences.

The following overall conclusions can be drawn:

- The general objective of this work - to develop and test the basic algorithms of a kernel of a future therapy planning system for carbon ion radiotherapy, using in its radiobiology component the cellular track structure model of Katz and applying as its physical component a Monte Carlo-generated data base describing transport in water of carbon beams of various initial energies, available to the author - was successfully accomplished.
- In the course of this work, the author proposed improvements to the Katz model, derived algorithms required to model the survival of cells in vitro by a realistic carbon beam propagating through water and derived optimisation routines required to achieve a pre-designed depth survival profile by the inverse planning approach. Efficient optimization algorithms for achieving desired depth-dose and survival-depth distributions were developed.
- All codes developed by author in the course of this work have been implemented in the freely accessible libamtrack code library.
- The basic kernel algorithm was successfully verified against published experimental data. Results of the author's calculations were found to somewhat differ from published results of LEM-based calculations. These differences may reflect differences in modelling within the radiobiology or the physical components of the Katz- and LEM-based approaches.
- While the developed kernel of the carbon ion therapy planning system is one-dimensional only, it can be useful as a tool for predicting the likely outcome of various beam configurations and of irradiating various cell types, as represented by their sets of radiosensitivity parameters of the Katz model.
- The one-dimensional TPS kernel developed in this thesis could be further extended to a 3-D calculation for use in realistic 3-D therapy planning systems in carbon ion radiotherapy.

6.3. Future Work

Many avenues could be followed in continuing this thesis: A comprehensive database of the radiobiological data was published [Sørensen et al., 2011], presented in the form of the alpha and beta coefficients, fitted using linear-quadratic model. Such data could serve as an initial stage for studies of the Katz model predictions for other cells or endpoints than CHO or V79 cells of different oxygenation status, studied in this work.

A very interesting and promising area is in inter-comparison studies of various radiobiological models: Katz, LEM and other models. Only a limited number of paper has been published dealing with this issue and no reasonable conclusions have yet been drawn.

The approach presented in this work was limited only to carbon ions. It would be interesting to follow the idea of Cucinotta to calculate cell survival in proton beams using the Katz model approach (scaled or integrated) and the latest versions of LEM. Such comparisons could provide better understanding of the applicability of constant RBE equal to 1.1 in proton radiotherapy. Exploiting the predictive power of the Katz model, predictions of ion radiotherapy using ions lighter than carbon (He, Li, Be, B or N) could also be studied.

The scaled version of the Katz model can be based only on radial dose distribution formulae which have particular “scaling properties”. In the integrated version of the Katz model any radial dose distribution formula may be applied, such as e.g., Geiss’s $D(r)$ formula, also used in LEM. At this stage there are at least three features of the Katz model in which it differs from LEM: radial dose distribution, description of the reference radiation survival profile (m -target model) and the concept of inactivation cross-section. By using Geiss’s $D(r)$ formula in the integrated version of Katz’s model, the number of distinctive features could be reduced to two, making inter-comparisons easier. One could also go one step further and make more sophisticated changes to the Katz model, e.g., replacing the m -target approach by the linear-quadratic formulation. In this case, a scaled and fast version of the model might be difficult to construct, but expressing the prediction in linear quadratic formalism could make it more appealing for physicians. The Katz model is thought to incorrectly predict cell survival and detector response for lighter ions, such as protons or alpha particles, a fault also shared by LEM. This discrepancy might be related to the radial dose distribution model incorporated in these models. Further improvement in this area is still possible, but requires more detailed studies. It is also important because among fragmentation products produced by carbon ion beam protons have the highest fluence.

Finally, some technical work could be performed to further improve the efficiency of the present algorithms contained in the libamtrack library, to bring them up to industry standards.

Appendix A (Radial Dose distribution and Electron range models)

Delta electron range formulae

Delta electron range r_{\max} models implemented in the libamtrack library are summarized in table 2.1. Here a detailed listing of formulae is presented. The maximum delta electron range r_{\max} can be expressed as a function of the ion energy E , or as a function of maximum delta electron energy ω .

Formulae of Geiss and Scholz

Two models, described as Geiss and Scholz encompass ion energy E , but yield different coefficients for Geiss:

$$r_{\max} = 4 \cdot 10^{-5} \left(\frac{E}{\text{MeV}} \right)^{1.5} \text{ cm}$$

than for Scholz:

$$r_{\max} = 5 \cdot 10^{-6} \left(\frac{E}{\text{MeV}} \right)^{1.7} \text{ cm}$$

Formula of Butts and Katz

The model of Buttz and Katz shows a linear dependence on the delta electron energy ω :

$$r_{\max} = 10^{-6} \frac{\omega}{\text{keV}} \text{ cm}$$

Formula of Waligórski

Model of Waligórski shows a power dependence on the delta electron energy ω , with exponent α which is taken to be 1.079 for $\omega < 1\text{keV}$ and 1.667 elsewhere:

$$r_{\max} = 6 \cdot 10^{-6} \left(\frac{\omega}{\text{keV}} \right)^{\alpha} \text{ cm}$$

Formula of Tabata

Tabata's formula incorporates a more complicated dependence of r_{\max} on ω :

$$r_{\max} = a_1 \left(1/a_2 \ln(1 + a_2\omega/mc^2) - \frac{a_3\omega/mc^2}{1 + a_4(\omega/mc^2)^{a_5}} \right)$$

where:

$$a_1 = b_1 A/Z^{b_2}$$

$$a_2 = b_3 Z$$

$$a_3 = b_4 - b_5 Z$$

$$a_4 = b_6 - b_7 Z$$

$$a_5 = b_8/Z^{b_9}$$

and b_i are constants dependent on the material in which range is calculated. If the material is a mixture of chemical elements, then Z and A need to be exchanged by average values. Values of the b_i coefficients are as follow:

$$b_1 = 0.2335 \left[\frac{\text{g}}{\text{cm}^2} \right]$$

$$b_2 = 1.209$$

$$b_3 = 1.78 \cdot 10^{-4}$$

$$b_4 = 0.9891$$

$$b_5 = 3.01 \cdot 10^{-4}$$

$$b_6 = 1.468$$

$$b_7 = 1.18 \cdot 10^{-2}$$

$$b_8 = 1.232$$

$$b_9 = 0.109$$

Radial dose distribution formulae

Radial dose distribution formulae implemented in the libamtrack library are summarized in table 1.2. Here a detailed listing of these formulae is presented.

Formula of Zhang

$$D(r) = C_1 \frac{z^{*2}}{\beta^2} \frac{1}{\alpha} \frac{1}{r} \frac{1}{r + \theta(I)} \left(1 - \frac{r + \theta(I)}{r_{\max} + \theta(I)} \right)^{\alpha-1}$$

Where $C_1 = Ne^4/mc^2(4\pi\epsilon_0)^2$ (N - electron density of the material, e - electron charge, m - electron mass, c - speed of light, ϵ_0 - electrical permittivity of vacuum). $\theta(I)$ is the range of delta electrons of energy equal to ionization potential I .

Formula of Katz

Applying in Zhang's formula $\alpha = 1$ and $I = 0$, one obtains Katz's formula:

$$D(r) = C_1 \frac{z^{*2}}{\beta^2} \frac{1}{r} \left(\frac{1}{r} - \frac{1}{r_{\max}} \right)$$

Formula of Geiss

$$D(r) = \begin{cases} C_2 & \text{if } 0 < r < a_0, \\ \frac{C_2}{r^2} & \text{if } a_0 \leq r \leq r_{\max} \\ 0 & \text{elsewhere} \end{cases}$$

In the formula of Geiss, the C_2 constant is taken to such value that average total dose deposited around single track yields stopping power value:

$$C_2 = \frac{L}{\pi \rho (a_0^2 + 2 \ln(r_{\max} a_0))}$$

Formula of Cucinotta

$$D(r) = \begin{cases} C_1 \frac{z^{*2}}{\beta^2} f_S(r) f_L(r) \frac{1}{r^2} + C_3 \frac{\exp(-r/2d)}{r^2} & \text{if } 0 \leq r \leq r_{\max} \\ 0 & \text{elsewhere} \end{cases}$$

where:

$$f_S(r) = \left(\frac{r_0}{r} + (0.6 + 1.7\beta + 1.1\beta^2) \right)^{-1}$$

where $r_0 = 1\text{nm}$, and

$$f_L(r) = \exp \left(- \frac{r^2}{(0.37 \cdot r_{\max})^2} \right)$$

and

$$d = \frac{\beta}{2} \frac{hc}{2\pi\omega_r}$$

where:

$$\omega_r = 13\text{eV}$$

In a manner similar to that in Geiss's formula, the C_3 constant is taken to such value that $\rho \int_0^{r_{\max}} 2\pi r D(r) dr = L$ holds:

$$C_3 = \frac{\frac{L}{2\pi\rho} - C_1 \frac{z^{*2}}{\beta^2} \int_0^{r_{\max}} f_S(r) f_L(r) \frac{dr}{r}}{\int_0^{r_{\max}} \exp(-r/2d) \frac{dr}{r}}$$

Appendix B (Extended target calculations)

Knowing the formula for the dose $D(r)$ delivered by delta electrons at a point at a distance r from the ion track one may also write the formula for averaged dose $D_{\text{ext}}(t, a_0)$ delivered in a thin cylindrical volume of radius a_0 at a distance t from the ion track. We will refer to the circle S_t with radius a_0 , at a distance t from the ion track as the target. By neglecting volume thickness one may reduce this problem to 2-dimensional integration:

$$D_e(t, a_0) = \frac{1}{|S_t|} \iint_{S_t} D(x, y) dx dy$$

where $D(x, y)$ is the dose delivered to the point with coordinates (x, y) (due to rotational symmetry one could easily calculate it as $D(\sqrt{x^2 + y^2})$)

By changing coordinates from Cartesian to polar, obtains:

$$D_e(t, a_0) = \frac{1}{\pi a_0^2} \int_{t_{\min}}^{t_{\max}} D(r) \Phi(r, t, a_0) dr$$

Here $\Phi(r, t, a_0)$ denotes the length of an arc segment, centered around the ion track, of radius r , contained in a circle of radius a_0 at the distance t from the ion track. t_{\min} is the minimum distance of the ion track to the border of the target, which is equal to $t - a_0$ if the ion track is outside the target, or assumed to be 0 if ion track is inside or on the border of the target. t_{\max} is the maximum distance from the ion track to the border of the target, which is equal to $t + a_0$.

Φ could be calculated using following formula:

$$\Phi(r, t, a_0) = \begin{cases} 2 \arctan \sqrt{\frac{a_0^2 - (t-r)^2}{(r+t)^2 - a_0^2}} & \text{if } r > |t - a_0|, \\ \pi & \text{if } r \leq |t - a_0|. \end{cases}$$

Appendix C (Software)

The *libamtrack* library, as an open-source project, is available for download from the webpage libamtrack.dkfz.org. Detailed description of routines provided by the library is available in the reference manual provided on the project webpage. The libamtrack source codes, together with the set of scripts and database of the carbon ion beam spectra are also attached to this thesis and grouped in four folders:

libamtrack

The source code of the libamtrack library is provided in the libamtrack directory. It contains:

- compilation instructions
- `src` subdirectory with source files (*.c) containing definition of all routines
- `include` subdirectory with header files (*.h) containing declaration of all routines and documentation in doxygen format
- `example` subdirectory with two sample codes written in C, showing usage of the libamtrack library
- `wrapper` subdirectory with interface to the libamtrack library for Python language and R library

The *libamtrack* library does not provide any executable file, as it was designed as a library - a set of routines which can be invoked from any code provided by user. It can be compiled as a shared library under Linux and Windows operating system. Two sample codes are provided, which use the libamtrack library and can be compiled to an executable file: one shows how energy of the particle is calculated from its relative velocity beta and the second one produce an output which later can be used to prepare plots of electron range, radial dose distribution and stopping power for various configurations of the formulae used, particle and target material. The easiest way to get familiar with the library is to use the R package. After installation of R one may easily install the libamtrack plugin, which enables user to use selected set of functions from libamtrack in the R environment. A sample session showing the usage of the R plugin by calculation of the radial dose distribution and maximum energy transfer to the delta electron:

```
> library("libamtrack")
This is libamtrack 0.5.3 'Green Wombat' (2012-04-27).
```

```

Type '?libamtrack' for help.
> # Compute dose in several distances (from 1e-9 to 1e-4 m) of an 100 MeV/u
> # proton in water according to 'Cucinotta' distribution
> AT.D.RDD.Gy( r.m = 10^(-9:-4),
+ E.MeV.u = 100,
+ particle.no = 60012,
+ material.no = 1,
+ rdd.model = 7,
+ rdd.parameter = c(1e-10, 1e-10),
+ er.model = 5,
+ stopping.power.source.no = 1)$D.RDD.Gy
[1] 9.856050e+06 4.513804e+04 2.586443e+02 2.600422e+00 2.485355e-02
[6] 2.537419e-06
attr(,"Csingle")
[1] TRUE
> # maximum energy transferred to delta electron by a 100 MeV/amu particle
> AT.max.E.transfer.MeV(E.MeV.u=100)$max.E.transfer.MeV
[1] 0.2309850
attr(,"Csingle")
[1] TRUE

```

fitting-katz-cell-survival

The script which aids in finding Katz model free parameters for which model prediction fits data best. This script can be used by executing “find.py” file. The configuration is stored in the file “fit.cfg” and limited to the following items:

- input data folder with cell survival curves data
- radial dose distribution formula to be used in Katz model
- precision of the fitting algorithm

The output of the calculation will be stored in a separate directory, containing files with calculated parameters and data necessary to produce survival curve plots.

Codes performing necessary calculation are gathered in src directory.

Together with script example configuration and cell survival data is provided.

spc

“spc” folder contains sample files with energy-fluence spectra of the carbon ion beam

carbon-sobp

carbon-sobp contains scripts for finding coefficients of the linear combination of the Bragg peaks which gives certain dose or survival profile. This tool can be used by executing “plot.py” script. All necessary input parameters need to be provided in a setup.cfg configuration file (an example configuration file is provided together with codes): path to the folder with energy-fluence spectra files

- range on which given profile is to be obtained
- number of pristine Bragg peaks in the linear combination

-
- choice of desired profile: either dose or survival
 - coefficients of polynomial defining desired profile
 - Katz model parameters (needed if survival is calculated)
 - parameters of grid on which profile accuracy is calculated
 - precision of minimization algorithm

The output of the calculation will be stored in a separate directory, containing files with calculated coefficients and data necessary to produce plots of dose (or survival profiles).

Codes performing necessary calculation are gathered in the src directory.

Bibliography

- [Agostinelli et al., 2003] Agostinelli, S., Allison, J., Amako, K. e., Apostolakis, J., Araujo, H., Arce, P., Asai, M., Axen, D., Banerjee, S., Barrand, G., et al. (2003). Geant4-a simulation toolkit. *Nuclear instruments and methods in physics research section A: Accelerators, Spectrometers, Detectors and Associated Equipment*, 506(3):250–303.
- [Andersen and Ziegler, 1977] Andersen, H. and Ziegler, J. (1977). *Hydrogen stopping powers and ranges in all elements*. Stopping and ranges of ions in matter. Pergamon Press.
- [Attili et al., 2008] Attili, A., Russo, G., Marchetto, F., Bourhaleb, F., Ansarinejad, A., Cirio, R., Cirrone, P., Donetti, M., Garella, A., Givhchi, N., Giordanengo, S., Monaco, V., Pardo, J., Pecka, A., Peroni, C., Rinaldi, I., and Sacchi, R. (2008). Evaluation of radiobiological effects of carbon ion beams: Mixed particle fields and fragmentation. *Medical Physics*, 35:2935.
- [Barkas and Evans, 1963] Barkas, W. and Evans, D. (1963). *Nuclear Research Emulsions: Techniques and theory*. Pure and applied physics. Academic Press.
- [Bassler et al., 2010] Bassler, N., Jäkel, O., Søndergaard, C. S., and Petersen, J. B. (2010). Dose-and LET-painting with particle therapy. *Acta Oncologica*, 49(7):1170–1176.
- [Battistoni et al., 2007] Battistoni, G., Cerutti, F., Fassò, A., Ferrari, A., Muraro, S., Ranft, J., Roesler, S., and Sala, P. R. (2007). The FLUKA code: description and benchmarking. *AIP Conf.Proc.*, 896:31–49.
- [Berger et al., 2005] Berger, M. J., Coursey, J. S., Zucker, M. A., and Chang, J. (2005). ESTAR, PSTAR, and ASTAR: Computer Programs for Calculating Stopping-Power and Range Tables for Electrons, Protons, and Helium Ions (version 1.2.3). In *NISTIR 4999*. National Institute of Standards and Technology.
- [Beringer and others (Particle Data Group), 2012] Beringer, J. and others (Particle Data Group) (2012). Review of particle physics. *Phys. Rev. D*, 86:010001.
- [Bethe, 1932] Bethe, H. (1932). Bremsformel für elektronen relativistischer geschwindigkeit. *Zeitschrift für Physik*, 76:293–299.
- [Bethe, 1953] Bethe, H. A. (1953). Molière’s theory of multiple scattering. *Phys. Rev.*, 89:1256–1266.
- [Beuve, 2009] Beuve, M. (2009). Formalization and theoretical analysis of the local effect model. *Radiation research*, 172(3):394–402.
- [Butts and Katz, 1967] Butts, J. J. and Katz, R. (1967). Theory of RBE for heavy ion bombardment of dry enzymes and viruses. *Radiation Research*, 30:855–871.
- [Chwastowski et al., 2012] Chwastowski, J., Grzymkowski, R., Kruk, M., Nabozny, M., Natkaniec, Z., Olszewski, A., Sobocinska, Z., Sosnicki, T., Szostak, M., Syktus, P., et al. (2012). The CC1 project–system for private cloud computing. *Computer Science*, 13:2.

- [Cucinotta et al., 1997] Cucinotta, F., Wilson, J. W., Shavers, M. R., and Katz, R. (1997). Calculation of heavy ion inactivation and mutation rates in radial dose model of track structure. Technical report, NASA.
- [Cucinotta et al., 1999] Cucinotta, F. A., Nikjoo, H., and Goodhead, D. T. (1999). Applications of amorphous track models in radiation biology. *Radiation and environmental biophysics*, 38(2):81–92.
- [Douglas and Fowler, 1976] Douglas, B. and Fowler, J. (1976). The effect of multiple small doses of X rays on skin reactions in the mouse and a basic interpretation. *Radiat Res*, 66(2):401–26.
- [Elsässer et al., 2008] Elsässer, T., Krämer, M., and Scholz, M. (2008). Accuracy of the Local Effect Model for the prediction of biologic effects of carbon ion beams in vitro and in vivo. *International Journal of Radiation Oncology*Biology*Physics*, 71(3):866 – 872.
- [Elsässer and Scholz, 2007] Elsässer, T. and Scholz, M. (2007). Cluster effects within the local effect model. *Radiation Research*, 167:319–329.
- [Elsässer and Scholz, 2010] Elsässer, T. and Scholz, M. (2010). Comments on "Formalization and theoretical analysis of the local effect model" by Beuve (*Radiat. Res.* 172, 394-402, 2009). *Radiation research*, 173(6):855–856.
- [Elsässer et al., 2010] Elsässer, T., Weyrather, W. K., Friedrich, T., Durante, M., Iancu, G., Kramer, M., Kragl, G., Brons, S., Winter, M., Weber, K.-J., and Scholz, M. (2010). Quantification of the relative biological effectiveness for ion beam radiotherapy: Direct experimental comparison of proton and carbon ion beams and a novel approach for treatment planning. *International Journal of Radiation Oncology*Biology*Physics*, 78(4):1177 – 1183.
- [Fowler, 2010] Fowler, J. (2010). 21 years of biologically effective dose. *British Journal of Radiology*, 83(991):554–568.
- [Fowler, 1964] Fowler, J. F. (1964). Differences in survival curve shapes for formal multi-target and multi-hit models. *Physics in Medicine and Biology*, 9(2):177.
- [Fowler, 1989] Fowler, J. F. (1989). The linear-quadratic formula and progress in fractionated radiotherapy. *British Journal of Radiology*, 62(740):679–694.
- [Friedland et al., 1998] Friedland, W., Jacob, P., Paretzke, H. G., and Stork, T. (1998). Monte Carlo simulation of the production of short DNA fragments by low-linear energy transfer radiation using higher-order DNA models. *Radiation research*, 150(2):170–182.
- [Furusawa et al., 2000] Furusawa, Y., Fukutsu, K., Aoki, M., Itsukaichi, H., Eguchi-Kasai, K., Ohara, H., Yatagai, F., Kanai, T., and Ando, K. (2000). Inactivation of aerobic and hypoxic cells from three different cell lines by accelerated ^3He -, ^{12}C - and ^{20}Ne -ion beams. *Radiation research*, 154(5):485–496.
- [Geiss, 1997] Geiss, O. B. (1997). *TLDs in Teilchenstrahlen (in German)*. PhD thesis, Gesellschaft für Schwerionenforschung, Darmstadt, Germany.
- [Geiss et al., 1998] Geiss, O. B., Krämer, M., and Kraft, G. (1998). Efficiency of thermoluminescence detectors to heavy charged particles. *NIM B*, 142:592–598.
- [Goodhead, 1987] Goodhead, D. T. (1987). Relationship of microdosimetric techniques to applications in biological systems. *The dosimetry of ionizing radiation*, 2:1–89.
- [Greilich et al., 2010] Greilich, S., Grzanka, L., Bassler, N., Andersen, C., and Jäkel, O. (2010). Amorphous track models: A numerical comparison study. *Radiation Measurements*, 45(10):1406 – 1409.
- [Greilich et al., 2013] Greilich, S., Hahn, U., Kiderlen, M., Andersen, C., and Bassler, N. (2013). Efficient calculation of local dose distribution for response modelling in proton and ion beams. *arXiv preprint arXiv:1306.0185*.
- [Grzanka et al., 2011] Grzanka, L., Greilich, S., Korcyl, M., Jäkel, O., Waligórski, M., and

- Olko, P. (2011). The application of amorphous track models to study cell survival in heavy ions beams. *Radiation Protection Dosimetry*, 143(2-4):232–236.
- [Gudowska et al., 2004] Gudowska, I., Sobolevsky, N., Andreo, P., Belkic, D., and Brahme, A. (2004). Ion beam transport in tissue-like media using the Monte Carlo code SHIELD-HIT. *Physics in Medicine and Biology*, 49(10):1933.
- [Haettner, 2006] Haettner, E. (2006). *Experimental study on carbon ion fragmentation in water using GSI therapy beams*. PhD thesis, Kungliga tekniska hogskolan Stockholm, Sweden.
- [Hall and Giaccia, 2006] Hall, E. and Giaccia, A. (2006). *Radiobiology for the radiologist*. Lippincott Williams & Wilkins.
- [Hansen et al., 2012] Hansen, D. C., Lühr, A., Sobolevsky, N., and Bassler, N. (2012). Optimizing SHIELD-HIT for carbon ion treatment. *Physics in Medicine and Biology*, 57(8):2393.
- [Hauptner et al., 2006] Hauptner, A., Friedland, W., Dietzel, S., Drexler, G., Greubel, C., Hable, V., Strickfaden, H., Cremer, T., Friedl, A., Krücken, R., et al. (2006). Spatial distribution of DNA double-strand breaks from ion tracks. *Matematisk-fysiske Meddelelser*, 52:59–85.
- [Hawkins, 1998] Hawkins, R. B. (1998). A microdosimetric-kinetic theory of the dependence of the RBE for cell death on LET. *Medical Physics*, 25(7):1157–1170.
- [Herrmann et al., 2011] Herrmann, R., Greilich, S., Grzanka, L., and Bassler, N. (2011). Amorphous track predictions in libamtrack for alanine relative effectiveness in ion beams. *Radiation Measurements*, 46(12):1551 – 1553.
- [ICRU, 1983] ICRU (1983). *Microdosimetry*. Number 36 in ICRU report. International Commission on Radiation Units and Measurements.
- [ICRU, 1994] ICRU (1994). *Stopping Powers and Ranges for Protons and Alpha Particles*. Number 49 in ICRU report. International Commission on Radiation Units and Measurements.
- [ICRU, 2005] ICRU (2005). *Stopping of ions heavier than helium*. Number 73 in ICRU report. International Commission on Radiation Units and Measurements.
- [ICRU, 2011] ICRU (2011). *Fundamental quantities and units for ionizing radiation*. Number 85 in ICRU report. International Commission on Radiation Units and Measurements.
- [Janni, 1982] Janni, J. F. (1982). Proton Range-Energy Tables, 1 keV-10 GeV, Energy Loss, Range, Path Length, Time-of-Flight, Stragglng, Multiple Scattering, and Nuclear Interaction Probability. Part I. For 63 Compounds. *Atomic data and nuclear data tables*, 27:147.
- [Katz, 2003] Katz, R. (2003). The parameter-free track structure model of Scholz and Kraft for heavy-ion cross sections. *Radiation research*, 160(6):724–728.
- [Katz and Cucinotta, 1999] Katz, R. and Cucinotta, F. (1999). Tracks to therapy. *Radiation Measurements*, 31(1-6):379–388. Proceedings of the 19th International Conference on Nuclear Tracks in Solids.
- [Katz et al., 1971] Katz, R., Sharma, S., and Hamayoonfar, M. (1971). Cellular inactivation by heavy ions, neutrons, and pions. *Robert Katz Publications*, page 72.
- [Katz and Sharma, 1974] Katz, R. and Sharma, S. C. (1974). Heavy particles in therapy: an application of track theory. *Physics in Medicine and Biology*, 19(4):413.
- [Katz et al., 1972] Katz, R., Sharma, S. C., and Homayoonfar, M. (1972). The structure of particle tracks. In Attix, F. H., editor, *Topics in Radiation Dosimetry*, chapter 6, pages 317–383. Academic Press, New York.
- [Katz and Varma, 1992] Katz, R. and Varma, M. N. (1992). Radial distribution of dose.

- In *Physical and Chemical Mechanisms in Molecular Radiation Biology*, pages 163–180. Springer.
- [Katz et al., 1994] Katz, R., Zachariah, R., Cucinotta, F. A., and Zhang, C. (1994). Survey of cellular radiosensitivity parameters. *Radiation research*, 140(3):356–365.
- [Klein et al., 2011] Klein, F., Greilich, S., Andersen, C. E., Lindvold, L. R., and Jäkel, O. (2011). A thin layer fiber-coupled luminescence dosimeter based on $\text{Al}_2\text{O}_3\text{:C}$. *Radiation Measurements*, 46(12):1607–1609.
- [Kolb, 2010] Kolb, C. (2010). *Eine plattformunabhängige Benutzerschnittstelle für numerische Programmbibliotheken am Beispiel libamtrack*. Bachelor’s thesis, Hochschule Heilbronn.
- [Korcyl, 2012] Korcyl, M. (2012). *Track structure modelling for ion radiotherapy*. PhD thesis, Jagiellonian University, Cracow, Poland.
- [Korcyl et al., 2013] Korcyl, M., Grzanka, L., Olko, P., and Waligórski, M. (2013). On the scaling properties of the radial distribution of dose in katz’s track structure model applied to 1-hit detectors.
- [Korcyl and Waligórski, 2009] Korcyl, M. and Waligórski, M. P. (2009). Track structure effects in a study of cell killing in normal human skin fibroblasts. *International journal of radiation biology*, 85(12):1101–1113.
- [Krämer et al., 2000] Krämer, M., Jäkel, O., Haberer, T., Kraft, G., Scharadt, D., and Weber, U. (2000). Treatment planning for heavy-ion radiotherapy: physical beam model and dose optimization. *Physics in Medicine and Biology*, 45(11):3299.
- [Krämer and Scholz, 2000] Krämer, M. and Scholz, M. (2000). Treatment planning for heavy-ion radiotherapy: calculation and optimization of biologically effective dose. *Physics in Medicine and Biology*, 45(11):3319.
- [Krämer and Scholz, 2006] Krämer, M. and Scholz, M. (2006). Rapid calculation of biological effects in ion radiotherapy. *Physics in Medicine and Biology*, 51(8):1959.
- [Landau, 1944] Landau, L. (1944). On the energy loss of fast particles by ionization. *J.Phys.(USSR)*, 8:201–205.
- [Lühr et al., 2012] Lühr, A., Hansen, D. C., Teiwes, R., Sobolevsky, N., Jäkel, O., and Bassler, N. (2012). The impact of modeling nuclear fragmentation on delivered dose and radiobiology in ion therapy. *Physics in Medicine and Biology*, 57(16):5169.
- [Mairani et al., 2010] Mairani, A., Brons, S., Cerutti, F., Fasso, A., Ferrari, A., Krämer, M., Parodi, K., Scholz, M., and Sommerer, F. (2010). The FLUKA Monte Carlo code coupled with the local effect model for biological calculations in carbon ion therapy. *Physics in Medicine and Biology*, 55(15):4273.
- [Mitaroff et al., 1998] Mitaroff, A., Kraft-Weyrather, W., Geiss, O., and Kraft, G. (1998). Biological verification of heavy ion treatment planning. *Radiation and environmental biophysics*, 37(1):47–51.
- [Olko, 2002] Olko, P. (2002). *Microdosimetric Modelling of Physical and Biological Detectors*. Habilitation, Institute of Nuclear Physics, Kraków, Poland.
- [Paganetti and Goitein, 2001] Paganetti, H. and Goitein, M. (2001). Biophysical modeling of proton radiation effect based on amorphous track models. *Int J Radiat Biol*, 77(9):911–928.
- [Paretzke, 1987] Paretzke, H. (1987). Radiation track structure theory. *Kinetics of nonhomogeneous processes*, pages 89–170.
- [Paretzke et al., 1974] Paretzke, H., Leuthold, G., Burger, G., and Jacobi, W. (1974). Approaches to physical track structure calculations. In *Fourth Symposium on Microdosimetry*, pages 123–140.
- [Paretzke, 1973] Paretzke, H. G. (1973). Comparison of track structure calculations with experimental results. In *4th symposium on microdosimetry*.

- [Pirruciello and Tobias, 1980] Pirruciello, M. and Tobias, C. (1980). Biological and medical research with accelerated heavy ions at the bevelac. Report LBL-11220, Berkeley, CA: Lawrence Berkeley Laboratory.
- [Pshenichnov et al., 2005] Pshenichnov, I., Mishustin, I., and Greiner, W. (2005). Neutrons from fragmentation of light nuclei in tissue-like media: a study with the GEANT4 toolkit. *Physics in Medicine and Biology*, 50(23):5493.
- [Puck and Marcus, 1956] Puck, T. T. and Marcus, P. I. (1956). Action of X-rays on mammalian cells. *The Journal of experimental medicine*, 103(5):653–666.
- [Roth and Katz, 1980] Roth, R. A. and Katz, R. (1980). Heavy ion beam model for radiobiology. *Radiation Research*, 83(3):499–510.
- [Russo, 2007] Russo, G. (2007). *Effetti biologici dell'irraggiamento con ioni carbonio*. PhD thesis, Politecnico di Torino, Torino, Italy.
- [Scholz, 2001] Scholz, M. (2001). *Grundlagen der biologischen Bestrahlungsplanung für die Schwerionen-Tumorthérapie*. Habilitation, Ruprecht-Karls-Universität, Heidelberg, Germany.
- [Scholz and Kraft, 1994] Scholz, M. and Kraft, G. (1994). Calculation of heavy ion inactivation probabilities based on track structure, x ray sensitivity and target size. *Radiation Protection Dosimetry*, 52(1-4):29–33.
- [Scholz and Kraft, 2004] Scholz, M. and Kraft, G. (2004). The physical and radiobiological basis of the local effect model: A response to the commentary by R. Katz. *Radiation research*, 161(5):612–620.
- [Sørensen et al., 2011] Sørensen, B. S., Overgaard, J., and Bassler, N. (2011). In vitro RBE-LET dependence for multiple particle types. *Acta Oncologica*, 50(6):757–762.
- [Tabata et al., 1972] Tabata, T., Ito, R., and Okabe, S. (1972). Generalized semiempirical equations for the extrapolated range of electrons. *Nuclear Instruments and Methods*, 103(1):85 – 91.
- [Varma and Baum, 1980] Varma, M. N. and Baum, J. W. (1980). Energy Deposition in Nanometer Regions by 377 MeV/Nucleon 20 Ne Ions. *Radiation Research*, 81:355–363.
- [Vavilov, 1957] Vavilov, P. (1957). Ionization losses of high-energy heavy particles. *Sov.Phys.JETP*, 5:749–751.
- [Waligórski et al., 1986] Waligórski, M., Hamm, R., and Katz, R. (1986). The radial distribution of dose around the path of a heavy ion in liquid water. *International Journal of Radiation Applications and Instrumentation. Part D. Nuclear Tracks and Radiation Measurements*, 11(6):309 – 319.
- [Wambersie et al., 1994] Wambersie, A., Richard, F., and Breteau, N. (1994). Development of fast neutron therapy worldwide: Radiobiological, clinical and technical aspects. *Acta oncologica*, 33(3):261–274.
- [Weyrather et al., 1999] Weyrather, K., Ritter, S., Scholz, M., and Kraft, G. (1999). RBE for carbon track-segment irradiation in cell lines of differing repair capacity. *International Journal of Radiation Biology*, 75(11):1357–1364.
- [Weyrather and Kraft, 2004] Weyrather, W. and Kraft, G. (2004). RBE of carbon ions: Experimental data and the strategy of RBE calculation for treatment planning. *Radiotherapy and Oncology*, 73, Supplement 2(0):S161 – S169.
- [Wilson et al., 1946] Wilson, R. R. et al. (1946). Radiological use of fast protons. *Radiology*, 47(5):487–491.
- [Zhang et al., 1985] Zhang, C., Dunn, D., and Katz, R. (1985). Radial distribution of dose and cross-sections for the inactivation of dry enzymes and viruses. *Radiation Protection Dosimetry*, 13:215–218.
- [Zhu et al., 1997] Zhu, C., Byrd, R. H., Lu, P., and Nocedal, J. (1997). Algorithm 778:

L-BFGS-B: Fortran subroutines for large-scale bound-constrained optimization. *ACM Trans. Math. Softw.*, 23(4):550–560.

List of Tables

2.1	Energy-range formulae used to calculate the maximum range of delta-electrons, r_{\max} , implemented in the libamtrack library. For more details concerning the exponent α [Waligórski et al., 1986], and the function f [Tabata et al., 1972], Appendix A should be consulted. The units in which the electron or ion energy, denoted by ω or E are given, are keV or MeV, respectively.	27
2.2	Selected formulae describing the radial dose distribution, implemented in the libamtrack library. For further details, see Appendix A.	28
5.1	Cell survival corresponding to dose calculated at 1.5cm depth, using the Katz model and LEM.	72
5.2	Best-fitted parameters of the Katz model, representing aerobic and hypoxic V79 cells [Korcyl, 2012]	73

List of Figures

1	Relative depth-dose profiles of photons, protons and carbon ions. The Bragg peak of proton and carbon beams is clearly visible. Note that all dose profiles have been normalized to the same entrance dose. Reprinted from Haettner [Haettner, 2006].	5
2	Illustration of depth distributions of “physical dose” (or of depth-dose) and of “biological dose” (or of depth-cellular inactivation level) in spread-out carbon and proton beams, in a water phantom. The spreading-out of the Bragg peak is achieved by a suitable superposition of ion beams of different initial energies and fluences. Reprinted from http://totlxl.to.infn.it/ , Andrea Attili, INFN-TPS project resources.	6
3	Monte Carlo-calculated contribution to the dose from secondary fragments of a 330 MeV/amu carbon ion in water. The nominal range of this monoenergetic carbon beam is 200 mm. Reprinted from Pshenichnov et al. [Pshenichnov et al., 2005]	7
1.1	A two-dimensional representation of a 3-D track-segment of a 4-MeV α -particle in H ₂ O (water vapour normalised to density of 1 g/cm ³), simulated using the MOCA-14 Monte Carlo track structure code [Paretzke, 1987]. Dots denote the positions of individual ionisations. The value of Linear Energy Transfer, LET (Eq. 1.4) is calculated as the mean energy imparted to water by the 4 MeV ⁴ He ions (31 keV) divided by the length of the illustrated path length (0.3 μ m). The insert on the right shows the radial histogram of ionisations, corresponding to the radial dose distribution, $D(r)$. Figure adapted from Goodhead [Goodhead, 1987], and reprinted from Olko [Olko, 2002].	13
1.2	Stopping power of protons in liquid water based on PSTAR database [Berger et al., 2005] and on the Bethe formula 1.2, implemented in the libamtrack library. The range of ion energies (0.1 – 500 MeV) relevant to ion radiotherapy is shown by vertical lines	15
1.3	Depth-dose dependence, mean energy vs. depth, and fluence vs. depth of a pristine (non-modulated) proton beam. The entrance values (at 0 cm depth) are: energy: $E = 59.75$ MeV; dose: $D = 1.727$ Gy; and fluence: $F = 10^9$ ions/cm ² . Calculations made by the author, using the Geant4 package and the libamtrack library.	17

1.4	Survival of CHO cells irradiated with 1 MeV/u carbon ions or 250 kVp X-rays (reprinted from [Weyrather and Kraft, 2004]). For the carbon data, the best fitted value is $\alpha = 1.387 \text{ Gy}^{-1}$. For the X-ray data points, the best-fitted parameters of the LQ formula are: $\alpha = 0.227 \text{ Gy}^{-1}$, $\beta = 0.017 \text{ Gy}^{-2}$ (linear fit) or $\alpha = 0.224 \text{ Gy}^{-1}$ and, $\beta = 0.0185 \text{ Gy}^{-2}$ (fit to logarithms of data points). The best fitted parameters of the m-target formula to the X-ray data points are: $m=2.31$ and $D_0=1.69 \text{ Gy}$ (from a linear fit to a larger set of data, see also Fig. 3.4 and chapter 3.9).	20
1.5	Basic assumptions of the LEM model, reproduced from Attili [Attili et al., 2008]	22
2.1	Projected electron ranges vs. initial electron energy in liquid water. Experimental data are from Tabata [Tabata et al., 1972] (measurements in different materials, density-rescaled to liquid water). The ion energy range useful in ion beam radiotherapy is indicated by vertical lines. Experimental data and the respective electron energy-range relationships have been implemented in the libamtrack library.	26
2.2	Comparison of experimentally measured radial distribution of dose around 377 MeV/amu neon ions in tissue-equivalent gas [Varma and Baum, 1980] and $D(r)$ calculated using the formulae of Katz, Zhang, Geiss and Cucinotta. Experimental uncertainties were not provided by Varma et. al. The right-hand panel shows the same data and calculations, but on a semi-logarithmic plot where data points and results of versus of $D(r)$ calculations are multiplied by their respective r^2 values.	31
2.3	Upper plot: Ratio of the radially integrated $D(r)$ formulae of Katz and of Zhang ($\theta = 0$) and the values of LET versus proton energy The formulae of Geiss and Cucinotta on radial integration return the values of LET by definition. Lower plot: Proton LET (i.e. the result of radial integration of the formulae of Geiss and Cucinotta) and results of radial integration of the $D(r)$ formulae of Katz and of Zhang ($I = 0$) vs. proton energy. As the LET values, the proton stopping power values from the PSTAR database [Berger et al., 2005] are used. Author's calculation based on the libamtrack library.	33
3.1	Inactivation cross-sections normalized to their plateau values (σ_0), plotted as a function of LET (panel A) or z^{*2}/β^2 (panel B) for $m=2.5$, $D_0 = 1 \text{ Gy}$ or 10 Gy and $a_0 = 1 \mu\text{m}$ or $10 \mu\text{m}$. Each curve was plotted for ions with Z ranging from 1 to 100 and for relative ion speed β , from $\beta = 0.05$ to $\beta=0.99$. The radial dose distribution function of Zhang was used in these calculations. Figure reprinted from Korcyl [Korcyl, 2012]	40
3.2	Inactivation cross-sections, normalised to σ_0 vs. $z^{*2}/\kappa\beta^2$, based on the radial dose distribution function of Katz. Calculations were performed using the integration (green lines) and scaled (red lines) versions of the Katz model, for ions of $Z=1,2,3,5,10,50$ and 100 and energies $0.1 - 500 \text{ MeV/amu}$. Katz model parameters used: $m = 2$, $D_0 = 5 \text{ Gy}$, $a_0 = 1\mu\text{m}$, $\kappa = 1500$, $\sigma_0 = 1.2 \pi a_0^2$	45
3.3	Inactivation cross-sections, normalised to σ_0 vs. $z^{*2}/\kappa\beta^2$, based on the radial dose distribution function of Zhang. Calculations were performed using the integration (green lines) and scaled (red lines) versions of the Katz model, for ions of $Z=1,2,3,5,10,50$ and 100 and energies $0.1 - 500 \text{ MeV/amu}$. Katz model parameters used: $m = 2$, $D_0 = 5 \text{ Gy}$, $a_0 = 1 \mu\text{m}$, $\kappa = 2500$, $\sigma_0 = 1.2 \pi a_0^2$	46

3.4	Katz model-predicted CHO cell survival curves (based on best-fitted parameters) and experimentally measured data points for carbon beams (of energies 4.2, 11, 18, 76.9 and 266.4 MeV/amu) and for 250 kVp X-rays. The experimental data is from [Weyrather et al., 1999]. The Katz model parameters are: $m = 2.31$, $D_0 = 1.69 \text{ Gy}$, $\sigma_0 = 5.96 \cdot 10^{-11} \text{ m}^2$, $\kappa = 1692.8$ Calculations based on the libamtrack library.	48
4.1	Dose vs depth of a carbon beam of initial energy 270 MeV/amu in liquid water and of beam fragments. Data extracted from data sets available in the libamtrack library, were generated using the SHIELD-HIT10A code [Gudowska et al., 2004]. The entrance channel dose is 2 Gy. Upper panel: cumulative representation. Lower panel: individual depth-dose distributions of the primary beam and of secondary ion species. In the lower panel the 6-18 cm depth region is magnified to better visualise the individual dose contributions of secondary particles. Data beyond the depth of 20 cm have not been plotted.	53
4.2	Fluence vs depth of a carbon beam of initial energy 270 MeV/amu in liquid water and of beam fragments. Data extracted from data sets available in the libamtrack library, were generated using the SHIELD-HIT10A code [Gudowska et al., 2004]. The primary beam fluence in the entrance channel was adjusted to represent the beam entrance dose of 2 Gy, to conform with Fig. 4.1. Upper panel: cumulative representation. Lower panel: individual depth-fluence distributions of the primary beam and of secondary ion species. Data beyond the depth of 20 cm have not been plotted.	54
4.3	Fluences of primary and secondary ions primary carbon beam of initial energy 270 MeV/amu in liquid water, shown as a function of depth (along the x-axis) and energy (along the y-axis). The entrance carbon beam dose is 2 Gy. On each panel energy-fluence spectra are shown for each ion species (protons thru carbon). The fluence values for the different ions are represented by different colours: red is the highest (range: $5 \cdot 10^7 \text{ cm}^{-2}$ to $6 \cdot 10^5 \text{ cm}^{-2}$), green - intermediate values, white background - no ions (fluence=0).	56
4.4	Upper panel: A flat depth-dose distribution of 1 Gy over the depth range 8-12 cm, obtained by summing the contributions of Bragg peaks of 49 pristine carbon beams of different initial energies and fluences (see Fig. 4.5). Lower panel: Survival vs. depth of CHO cells irradiated by the carbon beam with flat dose distribution shown in the upper panel. Calculations of CHO cell survival vs. depth were performed using the scaled Katz model, where CHO cells were represented by model parameters $m = 2.31$, $D_0 = 1.69 \text{ Gy}$, $\sigma_0 = 5.966 \cdot 10^{-11} \text{ m}^2$, and $\kappa = 1692.8$ (see par. 3.9). All calculations were performed for liquid water, using the libamtrack library.	60
4.5	Initial energies and fluences of the 49 carbon ion beams required to achieve the flat dose profile presented in the upper panel of Fig. 4.4. Each bar corresponds to a single pristine Bragg peak of initial energy given on the abscissa. Calculations performed using the libamtrack library.	61
4.6	Convergence of the dose profile optimization algorithm. Points show the minimum and maximum dose values over the depth of the flat region (8-12 cm) after each iteration step. Calculations performed using the libamtrack library . .	61

5.1	Upper panel: Depth-dose profile of a sum of 49 pristine Bragg peaks with different initial energies and fluences yielding a flat profile of survival of CHO cells vs. depth at the survival level of 0.2 over depths between 8 and 12 cm, shown in the lower panel. CHO cells survival was calculated using Katz's scaled model. The model parameters representing CHO cell survival are: $m = 2.31$, $D_0 = 1.69$ Gy, $\sigma_0 = 5.96 \cdot 10^{-11} \text{m}^2$, and $\kappa = 1692.8$. A magnified inset of the flat survival region demonstrates small oscillations in the survival level, due to the sharpness of pristine Bragg peaks. Calculations performed in liquid water, using the libamtrack library.	67
5.2	Initial energies and fluences of the 49 carbon ion beams required to achieve the flat survival profile presented in the upper panel of Fig. 5.1. Each bar corresponds to a single pristine Bragg peak of initial energy given on the abscissa. Calculations performed in liquid water, using the libamtrack library. . .	68
5.3	Convergence of the dose profile optimization algorithm. Points show the minimum and maximum dose values over the depth of the flat region (8-12 cm) after each iteration step. Calculations performed using the libamtrack library . .	68
5.4	Survival of CHO cells vs depth: results of calculations using the survival optimization algorithm and the scaled Katz model, where CHO cells are represented by the model parameters: $m = 2.31$, $D_0 = 1.69$ Gy, $\sigma_0 = 5.96 \cdot 10^{-11} \text{m}^2$, and $\kappa = 1692.8$ (cf. Fig. 5.1, lower panel), calculations performed using the libamtrack library, compared with experimental data published by Mitaroff et al. [Mitaroff et al., 1998].	69
5.5	The depth-dose profile used in calculation of Kramer and Scholz [Krämer and Scholz, 2000] (green line) compared with depth dose profile calculated with the aid of the libamtrack library (red line). Profile marked with red line was adjusted to agree with Kramer's profile in depths range between 8 and 12 cm. Calculations performed using the libamtrack library.	70
5.6	Survival of CHO cells vs depth: results of calculations using the dose optimization algorithm (dose profile presented on figure 5.5) and the scaled Katz model, where CHO cells are represented by the model parameters: $m = 2.31$, $D_0 = 1.69$ Gy, $\sigma_0 = 5.96 \cdot 10^{-11} \text{m}^2$, and $\kappa = 1692.8$, calculations performed using the libamtrack library, compared with results of LEM calculations (reproduced from Kramer et al. [Krämer and Scholz, 2000]).	71
5.7	Variation of depth-survival profiles with beam entrance dose. A CHO survival vs. depth profile was designed to give a flat survival level of 0.5 between 8 and 12 cm depths (scaling factor, $f=1$, black full line). Next, the input energy-fluence spectrum of the beam was re-scaled by factors: 0.25, 0.5, 1.5 and 2, and the respective depth-survival profiles were re-calculated (coloured full lines). For the Katz model parameters representing CHO cells, used in these calculations, see Fig. 5.1. Calculations performed using the libamtrack library.	72
5.8	Cell survival depth-profiles calculated for aerobic and hypoxic V79 cells using Katz model (parameters listed in Table 5.2). For each case: aerobic and hypoxic two different beam configurations were used, each prepared in such way that the designed survival was equal to 0.5 over the interval between 8 and 12 cm. Calculations performed using the libamtrack library.	74
5.9	Dose depth-profiles related to cell survival profiles presented on figure 5.8. Calculations performed using the libamtrack library.	74
5.10	Initial energy-fluence spectra related to cell survival presented in figure 5.8. Calculations performed using the libamtrack library.	75

5.11 Cell survival depth-profiles calculated for aerobic and hypoxic V79 cells in two identical carbon ion beams. Initial beam configuration was prepared for the survival of hypoxic cells to be 50% (0.5) over the target region between 8 and 12 cm.	76
-----------------------------------------------------------------------------------------------------------------------------------------------------------------------------------------------------------------------------------------------------------------	----